



**UNIVERSITI PUTRA MALAYSIA**

**MINKOWSKI FRACTAL TAG ANTENNAS INTEGRATED WITH SPLIT RING  
RESONATORS AND COMPLEMENTARY SPLIT RING RESONATORS FOR  
RADIO FREQUENCY IDENTIFICATION APPLICATIONS**

**ALI SADEQ ABDULHADI JALAL**

**FK 2013 63**



**MINKOWSKI FRACTAL TAG ANTENNAS INTEGRATED WITH SPLIT  
RING RESONATORS AND COMPLEMENTARY SPLIT RING  
RESONATORS FOR RADIO FREQUENCY IDENTIFICATION  
APPLICATIONS**

**By**

**ALI SADEQ ABDULHADI JALAL**

**Thesis Submitted to the School Graduate Studies, Universiti Putra Malaysia, in  
Fulfilment of the Requirements for the Degree of Doctor of Philosophy**

**August 2013**

## **COPYRIGHT**

All material contained within the thesis, including without limitation text, logos, icons, photographs and all other artwork, is copyright material of Universiti Putra Malaysia unless otherwise stated. Use may be made of any material contained within the thesis for non-commercial purposes from the copyright holder. Commercial use of material may only be made with the express, prior, written permission of Universiti Putra Malaysia.

Copyright © Universiti Putra Malaysia



## DEDICATION

*To my altruistic and beloved wives...*

*To my lovely sons (Hussain and Mustafa)...*

*To my supportive siblings...*

*To every striving muhsin person who is constantly improving aspects of life...*

*To those who are compassionate towards achieving perfection (ihsaan)...*

*To the consistent pursuers of knowledge aiming for positive change...*

*A special contribution to my home country Iraq and to Malaysia;*

*With lots of gratitude...*

Abstract of thesis presented to the Senate of Universiti Putra Malaysia in fulfilment of the requirement for the degree of Doctor of Philosophy

**MINKOWSKI FRACTAL TAG ANTENNAS INTEGRATED WITH SPLIT RING RESONATORS AND COMPLEMENTARY SPLIT RING RESONATORS FOR RADIO FREQUENCY IDENTIFICATION APPLICATIONS**

By

**ALI SADEQ ABDULHADI JALAL**

**August 2013**

**Chairman: Assoc. Prof. Alyani Binti Ismail, PhD**

**Faculty: Engineering**

RFID stands for Radio Frequency Identification. The main goal of an RFID system is to carry data on a transponder (tag) that can be retrieved with a transceiver through a wireless connection. The contactless Identification (ID) system relies on data transmission via radio frequency electromagnetic (EM) signals, and consequently, the whole operation is non-line-of-sight and weather independent. These advantages overcome the limitations of optical barcodes, which are line-of-sight and weather dependent and need manual operation. Most RFID tags are comprised of an antenna and integrated circuit (IC). The IC performs all of the data processing and is powered by extracting power from the interrogation signal transmitted by the RFID reader. The tag antenna determines the amount of power transferred from the reader to the tag and back from the tag to the reader. Though there are no constraints on the physical parameters of the reader's antenna, such as

being planar or small in size, these constraints do apply on the tag's antenna. In fact, the tag miniaturizing is limited by the tag antenna size.

This thesis reports on the design, fabrication, and measurement of Ultra High Frequency (UHF) RFID tag antennas (860 to 960 MHz), which can be used in various applications. The proposed tag antennas are designed and fabricated to achieve low tagging costs, tagging of small objects at item level, as well as tagging metallic objects with miniaturized tags.

First, it presents three different types of planar fractal RFID tag antenna designs integrated with square Split Ring Resonators (SRR) in an attempt to improve their performance characteristics at low cost. Three fractal iterations are considered to perform size reduction. Each antenna design was etched on FR4 epoxy substrate with an evident compact size. The antenna sizes are:  $82 \times 88.59 \times 1.6 \text{ mm}^3$  for *AN1*;  $72 \times 78.59 \times 1.6 \text{ mm}^3$  for *AN2* and  $66.5 \times 73.09 \times 1.6 \text{ mm}^3$  for *AN3*. The modified Minkowski fractal structure has been adopted to perform size reduction in three different iteration designs. Return loss results show that the integration of SRRs with antennas performs a frequency down-shift of the antenna resonant frequency thereby achieving further size reduction over the original fractal structure that was aimed for size reduction. The impedance of the designed antennas were simulated then measured to validate the design. The experiment results showed that the maximum read range of the proposed tag antennas, *AN1*, *AN2* and *AN3* is about 2.10 m, 1.10 m and 0.75 m respectively with 4.0 W EIRP radiation power of the RFID reader. The proposed RFID Tag antennas are compact, low cost, and with good reading range

that make them suitable for RFID applications. They are used for tagging objects other than metals or liquids.

Second, two metal mount fractal tag antennas are designed and tested. The two antennas are integrated with square Complementary SRRs (CSRR) in a floating intermediate conductive copper layer. This floating layer achieves down shift to the antenna resonant frequency and enhances its gain due to the added capacitance from the CSRR structure. The size of the proposed tag antennas is  $36.7 \times 18.1 \times 3.165 \text{ mm}^3$  for antenna *N1* and  $35.3 \times 17.4 \times 3.165 \text{ mm}^3$  for antenna *N2*. Very small and compact tag antennas are achieved with good agreement between measured and simulated impedance results. The read range measurements showed that the maximum read range of *N1*, and *N2* is about 0.82 m and 0.48 m respectively, obtained when the two tags are placed on a square metallic sheet. The proposed RFID tag antennas offer attractive design for metallic objects identification such as gas cylinders and oil barrels tagging in petrol refineries.

Abstrak tesis yang dikemukakan kepada Senat Universiti Putra Malaysia sebagai memenuhi keperluan untuk ijazah Doktor Falsafah

**ANTENA LABEL PECAHAN MINKOWSKI BERSEPADU DENGAN  
PENYALUN GELANG-BELAH DAN PENYALUN PELENGKAP GELANG-  
BELAH UNTUK APLIKASI PENGENALAN FREKUENSI RADIO**

Oleh

**ALI SADEQ ABDULHADI JALAL**

**Ogos 2013**

**Pengerusi: Prof. Madya Alyani Binti Ismail, PhD**

**Fakulti: Kejuruteraan**

RFID adalah singkatan kepada *Radio Frequency Identification* iaitu sistem pengenalan identiti menggunakan frekuensi gelombang radio. Tujuan utama sistem RFID ini adalah untuk membawa data pada transponder (Label) supaya ia dapat diperolehi semula menggunakan alat pemancar-penerima melalui hubungan tanpa wayar. Sistem ID tanpa sentuhan ini bergantung kepada penghantaran data melalui isyarat frekuensi radio elektromagnetik (EM) dan ini bermakna, seluruh operasi adalah bukan secara garis lurus dan bebas dipengaruhi cuaca. Kelebihan-kelebihan tersebut mampu mengatasi kelemahan dari kod bar optik di mana sistem tersebut memerlukan penghantaran isyarat secara garis lurus dan mudah dipengaruhi cuaca serta perlu dilaksanakan secara manual. Kebanyakan label RFID terdiri daripada antena dan litar bersepadu (IC). IC melaksanakan semua pemprosesan data dan dikuasakan dengan menyaring kuasa daripada oleh isyarat yang dipancarkan oleh



pembaca RFID. Manakala antena label menentukan jumlah kuasa yang dihantar daripada pembaca ke label dan kembali kepada pembaca dari label. Walaupun tiada sebarang kekangan pada parameter fizikal antenna pembaca, seperti berbentuk satah ataupun bersaiz kecil, kekangan ini nyata digunakan pada rekabentuk antena. Bahkan, pengecilan label adalah terhad berikutan saiz antena tersebut.

Tesis ini melaporkan kaedah rekabentuk, proses fabrikasi dan pengukuran terhadap label antena berfrekuensi ultra tinggi (UHF) (860 sehingga 960 MHz) di mana ia boleh digunakan untuk pelbagai aplikasi. Label antena yang dicadangkan telah direkabentuk dan difabrikasi untuk mendapatkan kos yang rendah, melabelkan objek-objek kecil pada aras barangan, dan juga melabelkan objek logam dengan label yang telah dikesilkan.

Pertama sekali, tesis ini akan menerangkan tiga jenis rekabentuk antena label RFID bersepadu dengan penyalun segiempat sama gelang –belah sebagai satu kaedah untuk membaiki ciri-ciri prestasi antena tersebut. Tiga lelaran akan diambil kira sebagai percubaan untuk pengecilan saiz antena. Setiap rekabentuk antena telah dipunarkan pada substratum epoksi FR4 dengan saiz yang lebih kompak. Saiz setiap antena adalah seperti berikut:  $82 \times 88.59 \times 1.6 \text{ mm}^3$  untuk AN1;  $72 \times 78.59 \times 1.6 \text{ mm}^3$  untuk AN2 and  $66.5 \times 73.09 \times 1.6 \text{ mm}^3$  untuk AN3. Struktur Pecahan Minkowski terubahsuai telah diguna pakai untuk melaksanakan pengecilan saiz terhadap rekabentuk tiga lelaran yang berbeza. Hasil dari kehilangan kembali menunjukkan bahawa antena bersepadu dengan penyalun segiempat sama gelang-belah (SRR) memberikan anjakan penurunan frekuensi pada frekuensi salun antena mengakibatkan pengecilan saiz berbanding dengan struktur pecahan yang asal

dimana tujuan utama adalah untuk mendapatkan saiz yang lebih kecil. Anjakan penurunan frekuensi daripada SRR berlaku ekoran daripada penambahan regangan daripada SRR tersebut terhadap galangan antenna yang asal. Seterusnya, galangan antenna telah disimulasi dan diukur untuk pengesahan rekabentuk. Hasil eksperimen menunjukkan julat bacaan maksima untuk antenna label yang dicadangkan, AN1, AN2, dan AN3 adalah pada 2.10m, 1.10m and 0.75m dengan kuasa radiasi EIRP sebanyak 4.0W pada pembaca RFID. Antena Label RFID yang dicadangkan adalah kompak, kos yang lebih rendah serta julat bacaan yang baik membuatkan antenna ini sesuai untuk aplikasi RFID. Antena ini boleh digunakan untuk melabel objek-objek selain besi atau cecair.

Seterusnya, dua jenis antenna label pecahan bercagak logam telah direka dan diuji. Kedua-dua antenna tersebut disepadukan dengan penyalun pelengkap gelang –belah (CSRR) pada lapisan pertengahan beraliran kuprum yang terapung. Lapisan terapung ini dapat mencapai anjakan penurunan terhadap frekuensi salun antenna dan juga mampu meningkatkan gandaan antenna kerana penambahan kemuatan daripada struktur CSRR. Berikut merupakan saiz untuk antenna label yang dicadangkan:  $36.7 \times 18.1 \times 3.165 \text{ mm}^3$  untuk antenna N1 dan  $35.3 \times 17.4 \times 3.165 \text{ mm}^3$  untuk antenna N2. Antena label yang sangat kecil dan kompak telah dicapai dengan kesepadanan galangan hasil daripada keputusan simulasi dan juga ujikaji. Pengukuran julat bacaan diperolehi apabila dua label diletakkan pada kepingan segiempat logam dan ia menunjukkan julat bacaan maksima bagi N1 adalah 0.82, dan N2 ialah 0.48m. Antena Label RFID yang dicadangkan ini mampu memberikan rekabentuk yang menarik untuk pengenalan objek logam seperti penanda untuk gas silinder dan tong minyak dalam industri petroleum.

## ACKNOWLEDGEMENTS

Of all that exists in the entire universe, my sheer gratitude is dedicated to no other than the Most Compassionate Allah S.W.T. Who had Generously Bestowed me a golden chance to further my doctorate degree in Universiti Putra Malaysia.

I am too touched being fated an ardently obliging beloved family members who are incessantly empowering my drive towards completing the painstaking processes throughout the tribulations of the study. In addition to the dynamic spur of enthusiasm, which is inexplicably bursting from the fierce love I deeply feel for my lovely sons – towards the betterment of our future life. So goes to other inspiring family members.

Anyhow, all the way through, I am truly indebted to my flexible but efficient supervisor: Associate Professor Dr. Alyani binti Ismail for her clear-cut style of supervision yet promoting students' freedom of ideas expression to stand upright with her securing offer of unwavering support – really, I am among the lucky few. In addition, I wish to express my appreciation to the members of my committee, Professor Dr. Mohamad Adzir Bin Mahdi, Professor Dr. Nor Kamariah Noordin, and Associate Professor Dr. Mohamad Fadlee A. Rasid for offering their valuable time and comments. I would also like to thank the SENSTECH SDN BHD (728289-X), Kuala Lumpur, Malaysia, and those others that have helped in the thesis work directly or indirectly.

I certify that a Thesis Examination Committee has met on 23 August 2013 to conduct the final examination of Ali Sadeq Abdulhadi Jalal on his thesis entitled "Minkowski Fractal Tag Antennas Integrated with Split Ring Resonators and Complementary Split Ring Resonators for Radio Frequency Identification Applications" in accordance with the Universities and University Colleges Act 1971 and the Constitution of the Universiti Putra Malaysia [P.U.(A) 106] 15 March 1998. The Committee recommends that the student be awarded the Doctor of Philosophy.

Members of the Thesis Examination Committee were as follows:

**M. Iqbal bin Saripan, PhD**

Associate Professor  
Faculty of Engineering  
Universiti Putra Malaysia  
(Chairman)

**Roslina binti Mohd Sidek, PhD**

Associate Professor  
Faculty of Engineering  
Universiti Putra Malaysia  
(Internal Examiner)

**Borhanuddin bin Mohd Ali, PhD**

Professor  
Faculty of Engineering  
Universiti Putra Malaysia  
(Internal Examiner)

**Hussain Al-Rizzo, PhD**

Professor  
University of Arkansas at Little Rock  
United States  
(External Examiner)



---

**NORITAH OMAR, PhD**

Associate Professor and Deputy Dean  
School of Graduate Studies  
Universiti Putra Malaysia

Date: 19 September 2013

This thesis was submitted to the Senate of Universiti Putra Malaysia and has been accepted as fulfilment of the requirement for the degree of Doctor of Philosophy. The members of the Supervisory Committee were as follows:

**Alyani Binti Ismail, PhD**

Associate Professor  
Faculty of Engineering  
Universiti Putra Malaysia  
(Chairman)

**Mohamad Adzir Bin Mahdi, PhD**

Professor  
Faculty of Engineering  
Universiti Putra Malaysia  
(Member)

**Nor Kamariah Noordin, PhD**

Professor  
Faculty of Engineering  
Universiti Putra Malaysia  
(Member)

**Mohamad Fadlee A. Rasid, PhD**

Associate Professor  
Faculty of Engineering  
Universiti Putra Malaysia  
(Member)

---

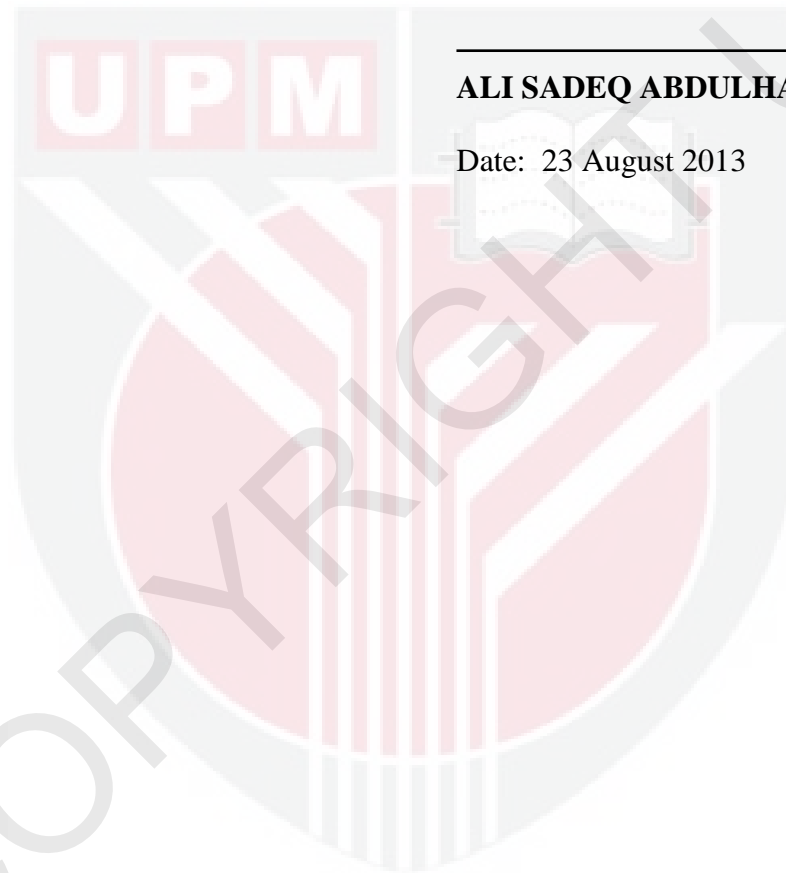
**BUJANG BIN KIM HUAT, PhD**

Professor and Dean  
School of Graduate Studies  
Universiti Putra Malaysia

Date:

## DECLARATION

I declare that the thesis is my original work except for quotations and citations which have been duly acknowledged. I also declare that it has not been previously, and is not concurrently, submitted for any other degree at Universiti Putra Malaysia or at any other institution.



**ALI SADEQ ABDULHADI JALAL**

Date: 23 August 2013

## TABLE OF CONTENTS

	<b>Page</b>
<b>ABSTRACT</b>	iii
<b>ABSTRAK</b>	vi
<b>ACKNOWLEDGEMENTS</b>	ix
<b>APPROVAL</b>	x
<b>DECLARATION</b>	xii
<b>LIST OF TABLES</b>	xv
<b>LIST OF FIGURES</b>	xvi
<b>LIST OF ABBREVIATIONS</b>	xx
<b>CHAPTER</b>	
<b>1 INTRODUCTION</b>	
1.1 Background	1
1.2 Problem Statement and Motivation	1
1.3 Research Aim and Objectives	5
1.4 Scope of Research	5
1.5 Overview of Research Methodology	6
1.6 Organization of the Thesis	9
<b>2 LITERATURE REVIEW</b>	
2.1 Introduction	11
2.2 Background of RFID	11
2.3 Brief History of RFID	12
2.4 RFID Tag Types and Classification	13
2.4.1 RFID Tag Types Based on Power Supply	13
2.4.2 RFID Tags Operating Frequencies	16
2.4.3 RFID Tags Classes	18
2.5 RFID Tag Antenna Design Considerations	19
2.5.1 Antenna Size and Shape	19
2.5.2 Bandwidth	20
2.5.3 Radiation Pattern	21
2.5.4 Directivity and Gain	22
2.5.5 Polarization	25
2.5.6 Impedance Matching	26
2.5.7 Read Range	29
2.5.8 Deformation	31
2.5.9 Fabrication Materials and Process	31
2.5.10 Proximity to Objects	32
2.6 Impedance Measurement of RFID Tag Antenna	33
2.7 Overview of RFID Tag Antennas	39
2.7.1 Three to Two Curve Fractal Folded Dipole	40
2.7.2 Fractal Dipole Antenna for 915MHz and 2.4GHz	41
2.7.3 Dual-Band Dipole Antenna	41
2.7.4 Minkowski Fractal Microstrip Antenna for RFID Tags	42

2.7.5	Fractal Loop Antenna for Passive UHF RFID Tags Applications	43
2.7.6	Low-Profile PIFA Array Antennas	44
2.7.7	A Miniature RFID Tag Antenna Design for Metallic Objects Application	45
2.7.8	Dual Band Tag with AMC Ground Plane	46
2.7.9	Metal Antenna on a Compact HIS Substrate	47
2.7.10	Metal Mount Meandered Patch Antennas	48
2.8	Summary of Previous Work	49
2.9	Summary	51
<b>3</b>	<b>METHODOLOGY</b>	
3.1	Introduction	52
3.2	Minkowski Fractal Structure	54
3.2.1	Modified Minkowski Fractal Structure Design	55
3.2.2	Design Parameters	58
3.3	SRR and CSRR Design	60
3.4	Summary	63
<b>4</b>	<b>MINKOWSKI FRACTAL ASYMMETRICAL RFID ANTENNA WITH SPLIT RING RESONATOR</b>	
4.1	Introduction	64
4.2	Antennas Design	64
4.2.1	Asymmetrical Antenna 1 ( AN1)	66
4.2.2	Asymmetrical Antenna 2 ( AN2)	71
4.2.3	Asymmetrical Antenna 3 ( AN3)	75
4.3	Results and Discussion	80
4.4	Summary	90
<b>5</b>	<b>MINIATURIZED METAL MOUNT MINKOWSKI FRACTAL RFID TAG ANTENNAS WITH COMPLEMENTARY SPLIT RING RESONATOR</b>	
5.1	Introduction	92
5.2	Antennas Design	92
5.2.1	Antenna N1	95
5.2.2	Antenna N2	100
5.3	Simulation and Measurement Results	105
5.4	Summary	113
<b>6</b>	<b>SUMMARY, CONCLUSIONS, CONTRIBUTIONS AND FUTURE WORK</b>	
6.1	Summary and Conclusions	115
6.2	Contributions	117
6.3	Recommendations for Future Work	118
	<b>REFERENCES</b>	119
	<b>APPENDICES</b>	126
	<b>BIODATA OF STUDENT</b>	129
	<b>LIST OF PUBLICATIONS</b>	130



## LIST OF TABLES

Table		Page
2.1	RFID tag operating frequencies	17
2.2	Summary of the reviewed work on RFID tag antenna designs	50
4.1	Dimensions of antenna <i>AN1</i>	68
4.2	Dimensions of antenna <i>AN2</i>	72
4.3	Dimensions of antenna <i>AN3</i>	77
4.4	Simulated and measured antenna impedances	85
4.5	Simulated and measured half-power bandwidths of the three antennas	88
4.6	Calculated and measured read range of the three antennas	90
5.1	Antenna <i>N1</i> dimensions	96
5.2	Antenna <i>N2</i> dimensions	102
5.3	Simulated and measured antenna impedances	109
5.4	Simulated and measured half-power bandwidths of the two antennas	110
5.5	Variation of maximum read range for different values of metal sheet size	112

## LIST OF FIGURES

Figure		Page
1.1	Scope of Research	6
1.2	Methodology Design Flow of RFID Tag Antennas	8
2.1	RFID System Block Diagram	12
2.2	Passive UHF RFID Tag Block Diagram	16
2.3	Field Regions Around an Antenna	22
2.4	The Equivalent Circuit of an RFID Tag	27
2.5	Antenna Impedance, Chip Impedance and Range Versus Frequency for a Typical RFID Tag	28
2.6	Two-Port Impedance Model of an Antenna and Feed	35
2.7	Schematic Representation of a Dipole Antenna and its Impedances	36
2.8	Photograph of the Proposed Two-Port Measurement Jig	37
2.9	Connections Using the Proposed Two-Port Jig to Measure the Impedance of a Dipole	37
2.10	Fabricated $3/2$ Fractal Dipole Antenna	40
2.11	Fabricated Fractal Dipole Antenna	41
2.12	Geometry of the Proposed Dipole Antenna	42
2.13	Photograph of Manufactured Antenna with a Modified Minkowski Fractal Curve	43
2.14	(a) Layout of Fractal Loop Antenna and (b) Its Photograph	44
2.15	Geometry of the Proposed: (a) First PIFA Array Antenna, and (b) Second PIFA Array Antenna	45
2.16	Fabricated Metal Tag Antenna	46
2.17	Photograph of (a) the Fabricated Cavity with the AMC Ground Plane, and (b) Bowtie Tag Antenna	47

2.18	Photograph of RFID tag Antenna. (a) Dipole Antenna and HIS. (b) The whole Antenna with an RFID Chip	48
2.19	Photograph of the Meandered Patch Antenna	49
3.1	Flow Chart of Minkowski Fractal Tag Antenna Design Process Integrated with SRR or CSRR	53
3.2	The Iterative Generation of a Minkowski fractal: (a) the Generator, (b) Square Patch, (Initiator), (c) The 1 <sup>st</sup> Iteration and (d) The 2 <sup>nd</sup> Iteration	55
3.3	Construction of the Modified Minkowski fractal structure: (a) the Generator, (b) Square Patch (the Initiator), (c) 1 <sup>st</sup> Iteration, (d) 2 <sup>nd</sup> Iteration and (e) 3 <sup>rd</sup> Iteration	56
3.4	(a) Basic layout of the SRR and (b) its Equivalent Lumped-Circuit Model	61
3.5	(a) Basic layout of the CSRR and (b) its Equivalent Lumped-Circuit Model	62
4.1	Layout of the Square SRR Design	65
4.2	Lumped-Element Circuit Model of (a) Proposed Tag Antenna, (b) Proposed Tag Antenna with SRR Layer and (c) the Proposed RFID Tag Antenna Overall Equivalent Lumped-Element Model	66
4.3	(a) Layout of Antenna AN1, (b) its Photograph with Tag Chip and (c) Photograph of SRR <sub>1</sub>	67
4.4	Simulation Results of Antenna AN1 Input Impedances with Different Values of: (a) Fractal Patch Length $L_1$ , (b) Indentation Factor $a_2$ and (c) SRR Outer Square Side Length ( $SRR_1$ ) ( $L_1$ and $SRR_1$ are as Denoted in Figure 4.3)	70
4.5	(a) Layout of Antenna AN2, (b) its Photograph with Tag Chip and (c) Photograph of SRR <sub>2</sub>	72
4.6	Simulation Results of Antenna AN2 Input Impedances with Different Values of: (a) Fractal Patch Length $L_2$ , (b) Indentation Factor $a_2$ and (c) SRR Outer Square Side Length ( $SRR_2$ ) ( $L_2$ and $SRR_2$ are as Denoted in Figure 4.5)	75
4.7	(a) Layout of Antenna AN3, (b) its Photograph with Tag Chip and (c) Photograph of SRR <sub>3</sub>	76

4.8	Simulation Results of Antenna $AN3$ Input Impedances with Different Values of: (a) Fractal Patch Length $L_3$ , (b) Indentation Factor $a_2$ and (c) SRR Outer Square Side Length ( $SRR_3$ ) ( $L_3$ and $SRR_3$ are as Denoted in Figure 4.7)	79
4.9	Simulated Return Loss of the Three Antennas with and without SRR for: (a) Antenna $AN1$ , (b) Antenna $AN2$ and (c) Antenna $AN3$	81
4.10	Simulated Far Field Radiation Patterns for: (a) Antenna $AN1$ , (b) antenna $AN2$ and (c) Antenna $AN3$	83
4.11	(a) Differential Probe, (b) Open-Ended Side of Semirigid Cables, (c) Measurement Setup of Antenna $N1$ and (d) Measurement Setup of Antenna $N2$	84
4.12	Impedance Simulation and Measurement Results of the Proposed Antennas: (a) Antenna $AN1$ , (b) Antenna $AN2$ and (c) Antenna $AN3$	87
4.13	Simulated and Measured PRC of the Proposed Tag Antennas: (a) Antenna $AN1$ , (b) Antenna $AN2$ and (c) Antenna $AN3$	89
5.1	Layout of the Two Square CSRR Design	93
5.2	Lumped-Element Circuit Model of (a) Proposed Tag Antenna, (b) Proposed Tag Antenna with an Inter-CSRR Layer and (c) the Proposed RFID Tag Antenna Overall Equivalent Lumped-Element Model	94
5.3	Design Arrangement of the Proposed 1 <sup>st</sup> Iteration ( $N1$ ) Fractal RFID Tag Antenna: (a) Top Layer, (b) Inter-CSRR Layer, (c) Bottom Layer and (d) Cross Section	95
5.4	(a) Photograph of the Three Layers of the Proposed 1 <sup>st</sup> Iteration ( $N1$ ) Fractal RFID Tag Antenna and (b) Photograph of the Assembled RFID Tag	97
5.5	Simulation Results of Antenna $N1$ Input Impedances with Different Values of: (a) Fractal Patch Length $L_1$ , (b) Indentation Factor $a_2$ and (c) CSRR Outer Square Side Length ( $CSRR_1$ ) ( $L_1$ and $CSRR_1$ are as Denoted in Figure 5.3)	99
5.6	Design Arrangement of the Proposed 2 <sup>nd</sup> Iteration ( $N2$ ) Fractal RFID Tag Antenna: (a) Top Layer, (b) Inter-CSRR Layer, (c) Bottom Layer, and (d) Cross Section	100
5.7	(a) Photograph of the Three Layers of the Proposed 2 <sup>nd</sup> Iteration ( $N2$ ) Fractal RFID Tag Antenna and (b) Photograph of the Assembled RFID Tag	101

5.8	Simulation Results of Antenna $N2$ Input Impedances with Different Values of: (a) Fractal Patch Length $L_2$ , (b) Indentation Factor $a_2$ and (c) CSRR Outer Square Side Length ( $CSRR_2$ ) ( $L_2$ and $CSRR_2$ are as Denoted in Figure 5.6)	104
5.9	Simulated Return Loss for: (a) Antenna $N1$ and (b) Antenna $N2$	106
5.10	Simulated Far Field Radiation Patterns: (a) for Antenna $N1$ and (b) for antenna $N2$	107
5.11	Measurement Setup for Metal Mount Tag Antenna	108
5.12	Impedance Simulation and Measurement Results of the Proposed Tag Antennas for: (a) Antenna $N1$ and (b) Antenna $N2$	109
5.13	Simulated and Measured PRC of the Proposed Tag Antennas: (a) for Antenna $N1$ and (b) for Antenna $N2$	111
5.14	Simulation Results of Antenna Radiation Patterns with Different Values of Metal Sheet Side Length for: (a) Antenna $N1$ and (b) Antenna $N2$	113

## LIST OF ABBREVIATIONS

AIDC	Auto Identification and Data Capture
AUT	Antenna Under Test
AMC	Artificial Magnetic Conductor
ASIC	Application Specific Integrated Circuit
$BW_p$	Percentage Bandwidth
$BW_r$	Ratio Bandwidth
CSRRs	Complementary Split Ring Resonators
CST	Computer Simulation Technology
EAS	Electronic Article Surveillance
EIRP	Equivalent Isotropic Radiated Power
EM	Electromagnetic
EPC	Electronic Product Code
ERP	Effective Radiated Power
GHz	Gigahertz
HDPE	High Density Polyethylene
HF	High Frequency
HFSS	High Frequency Structure Simulator
HIS	High Impedance Surface
HPBW	Half-Power Beamwidths
IC	Integrated Circuit
ID	Identification
IFF	Identification of Friend or Foe
ISM	Industrial Scientific and Medical

LF	Low Frequency
MHz	Megahertz
PBG	Photonic Band Gap
PCB	Printed Circuit Board
PIFA	Planar Inverted F Antenna
PP	Polypropylene
PRC	Power Reflection Coefficient
PTC	Power Transmission Coefficient
RF	Radio Frequency
RFID	Radio Frequency Identification
SAW	Surface Acoustic Wave
SHF	Super High Frequency
SMA	Sub Miniature version A
SRD	Short Range Devices
SRRs	Split Ring Resonators
UWB	Ultra-Wideband
VNA	Vector Network Analyzer

# CHAPTER 1

## INTRODUCTION

### 1.1 Background

Radio Frequency Identification (RFID) involves sending of a radio frequency query signal from a remote reader to a tag or transponder and receiving the modulated signal scattered back from the tag. The tag contains information regarding the object it is attached to. The reader then decodes the received signal, and sends the information of the object to a central processing unit. This unit might be receiving information from nearby readers, placed at other locations communicating with nearby tags. Thus a communication system is constructed by which items, located at different places of a retail-store or a warehouse can be tracked and identified. The antennas used in such a system, on the tag and on the reader for signal/power transfer, constitute the back-bone of the system. The antennas determine the amount of power transferred from the reader to the tag and back from the tag to the reader. Though there are no constraints on the physical parameters of the reader antenna, such as being planar or small in size, these constraints do apply on the tag antenna design. In fact, the tag miniaturizing is limited by the antenna size.

### 1.2 Problem Statement and Motivation

RFID is a technology that has existed for many years, but it is only recently that it has experienced rapid growth that has arisen from application of this technology in various supply chains. The catalyst to the growth of RFID came after the



introduction of the Electronic Product Code (EPC) concept whereby each tagged object can have its information stored in a database elsewhere instead of in the tags attached to them. With each of the tagged objects having a unique identity (due to the unique EPC in each tag) and having its information stored in a database, information associated with each of the physical objects can be accessed and updated anytime and anywhere, hence allowing easy track and trace of physical objects throughout supply chains. In addition, since large memories are not required to store object information, the cost of tags is low. All these factors open the possibility of wide implementation of RFID technology by tagging and identifying every single physical object (or product) in supply chains for total visibility within those supply chains. Hence, there is a vision to extend the RFID technology to item level tagging by giving each specific item a unique identity rather than pallet and case level tagging (Sarma et al., 2001).

From inventory management to theft detection, RFID has been applied in many areas such as in the automotive industry and logistics, as well as in warehouses and retail stores (Smith et al., 2003; Wilding et al., 2004; Angeles, 2005; Loebbecke, 2005; Ngai et al., 2007). Passive RFID technology is increasingly adopted in many contexts, even quite far from the canonical ones basically related to logistics. Identification of goods containing liquid or made of metal (Kwon et al., 2005; Yu et al., 2007; Chen et al., 2009; Catarinucci et al., 2010; Catarinucci et al., 2011), RFID-based sensor data transmission (Yeager et al., 2008; Catarinucci et al., 2008; Vaz et al., 2010; Occhiuzzi et al., 2011), platform tolerant tags (Catarinucci et al., 2008; Esposito et al., 2010), are only a few of the many possible examples where tags customized for specific applications are needed. This necessity has been

acknowledged by the electromagnetic scientific community which, over the last few years, has put a great deal of effort into RFID projects. The consequent rapid proliferation of scientific works on tag design and optimization is a matter of fact (Rao et al., 2005b; Kwon et al., 2005; Yu et al., 2007; Hidayath et al., 2007; Yeager et al., 2008; Marrocco et al., 2008; Catarinucci et al., 2008; Chen et al., 2009; Monti et al., 2009; Or et al., 2009; Monti et al., 2010; Catarinucci et al., 2010; Vaz et al., 2010; Catarinucci et al., 2011; Congedo et al., 2011; Occhiuzzi et al., 2011; Catarinucci et al., 2012; Marrocco et al., 2012).

Although RFID brings forward the benefit of efficient supply chain management, many challenges are posed due to the increasing implementation of RFID technology. Among the major challenges are:

1. Degradation of RFID system performance and reliability due to the presence of metals
2. RFID tagging costs
3. Tagging smaller objects at item level
4. Impedance matching between antenna and chip

Overview discussions on RFID challenges can be found in the literature such as in (Wu et al., 2006; Roberts et al., 2006; Mitra, 2007; Uddin et al., 2010).

To allow a thorough and full deployment of RFID, and to bring into realization the vision of tagging objects down to item level, feasible solutions must be drawn to meet these RFID challenges from all aspects. In this thesis, the main focus is on tackling the first challenge listed above, with the complex material of concern being metallic objects and structures. One of the major RFID implementation problem is

its performance degradation when tagging metallic objects or operating in an environment containing metallic structures. The tagging of objects at pallet, case, and even item levels will most likely involve metallic objects.

While tackling the first challenge, the research reported in this thesis also places emphasis on meeting the second and third challenges listed above (concerning cost and size respectively), which become especially important when item level tagging is involved. This means that tags must be made from inexpensive materials and simple to manufacture, in order to lower its cost in comparison to the item to be tagged on. However, ohmic losses of an antenna increase as the antenna size gets smaller (Cole et al., 2002), and hence the antenna efficiency will decrease. Therefore, maintaining a balance between the tag size, cost and performance is a challenging task. Modified Minkowski fractal structures have been adopted throughout this thesis work for the purpose of size reduction. Further size reduction is achieved by integrating Split Ring Resonators (SRR) and Complementary SRRs (CSRR) with designed fractal antenna structures. The designed antennas are fabricated at low cost using Flame Retardant (FR4) substrate.

This thesis also elaborates on the fourth challenge listed above which is of a paramount importance for proper tag antenna design. Chips vendors produce a variety of Application Specific Integrated Circuits (ASIC) that are available in the market with different impedance values. Antenna designers should stick to these values, where in most cases; they are not free to choose the desired antenna size to achieve the desired task. With good impedance matching, the tag ensures maximum power transfer between its antenna and the chip maximizing the read range.

### **1.3 Research Aim and Objectives**

The primary goal of this study is to design different structures of modified Minkowski fractal tag antennas integrated with Split Ring Resonators (SRRs) and Complementary Split Ring Resonators (CSRRs) for RFID applications. The design is aimed for both; nonmetallic and metallic objects tagging.

The research is focused on the following four main objectives:

1. To design dipole RFID tag antennas and investigate fractal shapes for size reduction,
2. To design a miniaturized loop RFID tag antenna for metallic objects identification,
3. To study the effect of integrating SRRs and CSRRs on the design performance of these tag antennas, and
4. To validate the performance of the designed tag antennas via measurements of their complex impedance and read range.

### **1.4 Scope of Research**

The scope of this thesis is to design new miniaturized fractal antennas for RFID applications integrated with SRRs and CSRRs to enhance their performance characteristics. The modified Minkowski fractal structure is used in two types of antenna designs: dipole and loop integrated with SRRs and CSRRs, where they are newly used for RFID applications. The flow of this study is illustrated in Figure 1.1.

The continuous-lines represent the direction followed in this thesis to achieve the objectives, while the dashed-lines are referring to other related research areas that are outside the scope of this work.

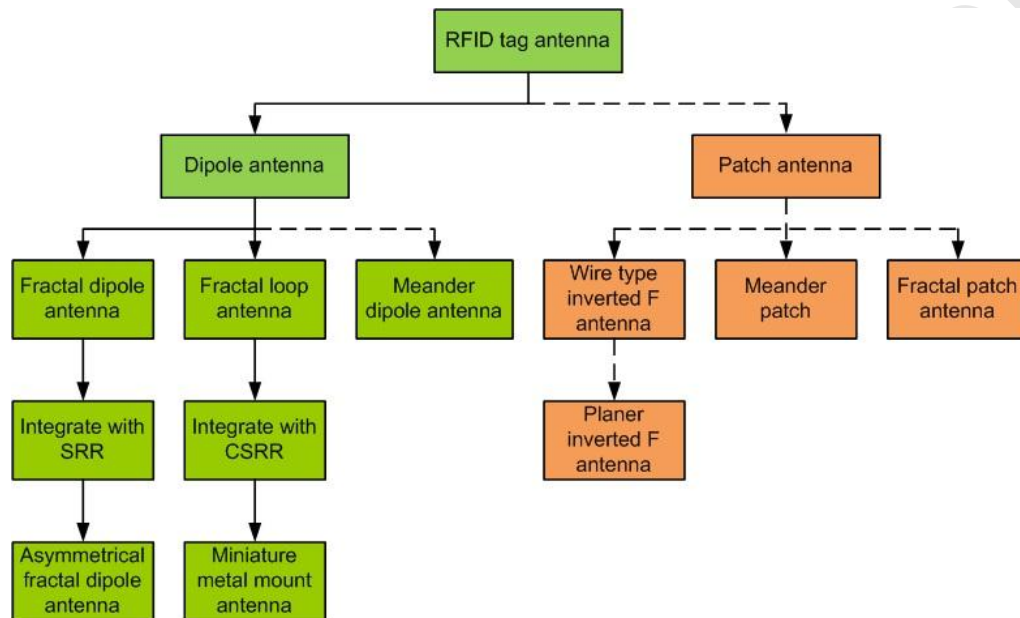


**Figure 1.1. Scope of Research**

## 1.5 Overview of Research Methodology

Firstly, to achieve the objectives of this work, extensive research on RFID tag antennas, SRRs and their CSRRs was carried out to understand their fundamentals and how these types of materials can be integrated with antennas. Next, inexpensive materials are determined for antenna construction with suitable chips after identifying antenna parameters and obtaining used chip impedance. Then, a 3D full-wave electromagnetic simulator (CST Microwave Studio, Version 2010) was used to simulate the structures. Afterwards, unique methods of integration have been applied

between the SRRs and CSRRs with tag antennas after it was successfully designed for RFID applications. Finally, measurements have been performed on the RFID tag antennas to validate the design methods. The developed methodology for designing RFID tag antennas is illustrated in the flow chart depicted in Figure 1.2.



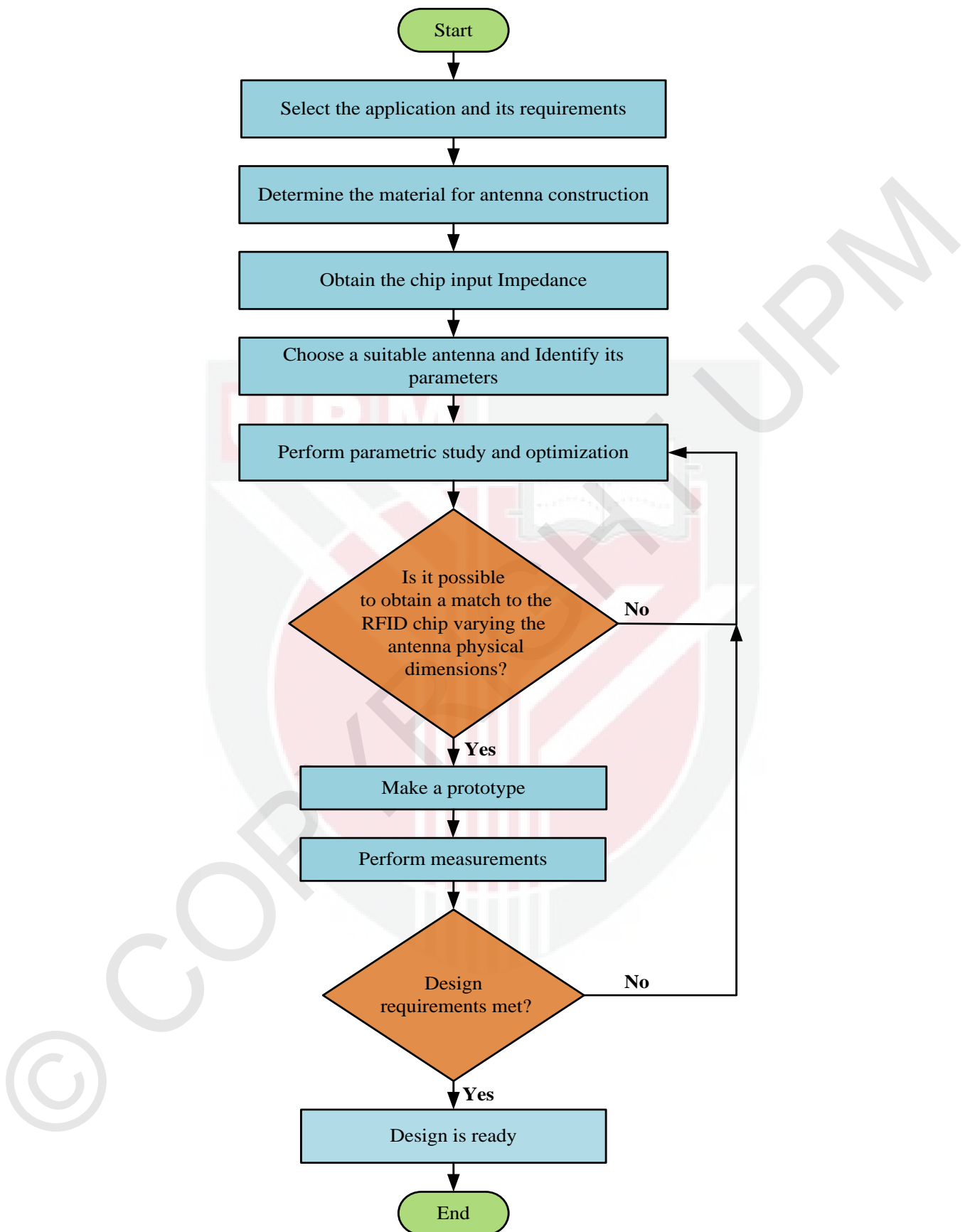


**Figure 1.2. Methodology Design Flow of RFID Tag Antennas**

## 1.6 Organization of the Thesis

This thesis is organized into six chapters, which are summarized as follows:

Chapter 1 provides a general introduction to the research area, and identifies the current problems in designing RFID tag antennas that motivated this research. It also introduces the goal, objectives, methodology, scope of research as well as the organization of thesis writing.

Chapter 2 presents a literature review on RFID system and RFID tag antennas. It first provides a background and history of RFID technology and some details about their classes and types. Then some details are provided about RFID tag antenna design considerations as well as some recent designs and applications. Finally, a summary ends the chapter.

Chapter 3 describes the methodology used to design the modified Minkowski fractal structures that are used in antenna designs in Chapters 4 and 5 in an attempt for antenna miniaturization. The performance of the SRRs and CSRRs behaviors are investigated in terms of their lumped element equivalent circuits, and discuss effects of integrating these elements on antenna resonant frequency and other performance metrics. Parameters affecting fractal structures, SRRs, and CSRRs are also included in this chapter. Methodology is finally summarized.

Chapter 4 contains a description on new design of three compact single-layered asymmetrical RFID tag antennas based on the modified Minkowski structure. Some



antenna parameters are studied showing their effects on antenna self-resonant frequency. The antennas are integrated with a square SRR on their back planes to achieve further miniaturization over the use of the fractal structure. Content is reviewed at the end of the chapter.

Chapter 5 elaborates on a novel design of two miniaturized metal mount double-layered symmetrical RFID tag antennas. Each antenna is integrated with a CSRR as a floating intermediate layer to enhance the performance characteristics in terms of return loss, gain, and lowered resonance frequency. Parametric study is also shown for different antenna parameters. Comprehensive analyses were done throughout the chapter concerning theoretical and simulation validation as well as the design techniques adopted. Finally, a summary on the chapter is reviewed at the end.

In Chapter 6, the entire thesis is summarized and concluded, followed by discussion of the major contributions of the work. Eventually, potential ideas for future work are suggested.

## **CHAPTER 2**

### **LITERATURE REVIEW**

#### **2.1 Introduction**

This chapter reviews literature relevant to the main themes of this thesis. It first presents the background and a brief history of RFIDs. Then some details on RFID tag classification and challenges in their antenna design are presented. A brief review for the state-of-the-art antenna designs for RFID tags is also provided. Lastly, summary and conclusions are given by the end of the chapter.

#### **2.2 Background of RFID**

A typical RFID system is composed of several different parts; as shown in Figure 2.1. These parts include; the RFID tag; or transponder, an RFID interrogator; or reader; and the application software that is needed in order to act as an interface between the RFID system and its' users. The transponder carries the ID data, the reader extracts the data from the transponder; or tag; and the software helps this all happen more smoothly. RFID technology utilizes radio waves in order to transmit data back and forth between the reader and the tag. The reader transmits out radio waves, and in return it receives modulated return echoes; which are processed by the reader. After the tag modulates the electromagnetic wave and transmits the resulting data back to the reader, it is processed for things such as asset tracking, real-time identification, security surveillance, and a broad variety of other authentication and managerial purposes.

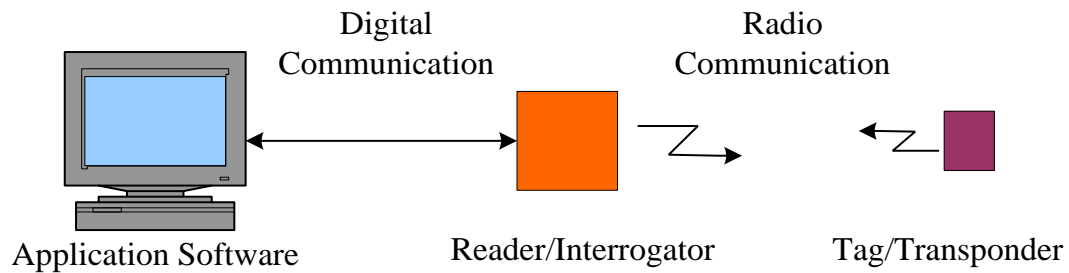


**Figure 2.1. RFID System Block Diagram**

### 2.3 Brief History of RFID

The application of the basic principle of RFID was first used in World War II. In 1935, the radar was discovered, and was used by the Germans, the Japanese, the Americans, and the British to alert them of approaching planes from a distance. However, identification between the enemy's planes and that of the country's own pilot became an issue. The Germans then found out that reflected radio signals apparently change whenever pilots roll their planes. This made them identify which is an ally and which is not. Concurrently, the British developed a system whereby a transponder was installed in the aircraft and in return an ally and a non-ally plane would then be distinguishable. This coded radar scheme is termed Identification of Friend or For (IFF) (Landt, 2001), (Roberti, 2006). In connection to this, Harry Stockman began exploring RFID in October 1948 (Stockman, 1948). According to Stockman, solutions for the remaining issues in reflected-power communication and the exploration of useful application of this technology would only be achieved through a substantial research and development work. His vision has prospered soon after the developments in transistor, integrated circuit, microprocessor, and the communication networks transpired. RFID's success had to wait for a period of time (Roberti, 2006). RFID actually uses similar principle as the former. Transponder

would receive a signal which would either reflect or broadcast it. Since then, using RFID as an Auto Identification and Data Capture (AIDC) technology has drastically rose. At this moment, RFID is already being widely used in different fields like chain managements, credit card security system, toll systems, and for animal tracking and identification and many more.

## **2.4 RFID Tag Types and Classification**

### **2.4.1 RFID Tags Types Based on Power Supply**

There are three classifications of RFID tags based on power supplies:

1. Active tags: These tags are battery assisted and in order for the data to be transmitted back to the reader, they make use of the battery to amplify the interrogating signal. Therefore, RF interrogating signal does not need to be used to energize the tag. As such, these tags can be read at much greater distances. Another way to differentiate active tags is through their digital section. The ID code is provided by the digital section besides the embedded security protocols and encryption techniques. Since processors carry out both the processing of data and implementation of protocols, performing the encryption and data processing instructions has to use additional coprocessors at times. Also, because of the presence of the built-in power supply in active tags, and its non-dependency on the reader's interrogation signal, passive tags process and store lesser data than the former. The first object to be engaged in the transmission of data is the *tag*. Since it is not necessary for an interrogating RF signal to energize

the latter, an active tag can continuously transmit data without the reader's assistance. This type of communication between the reader and the tag is called transponder driven. Even with the on-board power supply of active tags, supplementary techniques were put in place to maximize the use of the battery. This additional technique was in the form of sleep modes. Active tags which are not interrogated by a reader go into sleep mode, and as a result, they conserve power (Kossel et al., 1999). The active RFID tags most notable advantage is that they can be programmed again, thus, they can be repetitively utilized in various applications up until the battery life is drained.

2. **Semiactive tags:** Semiactive tags differ from active tags as the formers are catered by an on-board power-supply for the purpose of minor signal processing tasks. However, they are not used to amplify received and transmitted signals. With that being said, semiactive tag's power consumption from the on-board battery is less which makes its life longer than that of the active tag. The next notable difference is that they have shorter reading range in comparison with the active tag as allocation of the power is solely for the signal processing unit. Thus, this tag can be termed as a mid-way approach in comparison with the fully active tag and a fully passive tag with no battery. During the interrogation, an acknowledgement signal must be sent by the tag prior to a response; this is known as interrogator driven. Moreover, with the availability of very-low powered yet highly efficient microprocessors in the market today, some semiactive tags can still perform complicated tasks like processing and encrypting of data and they can attain reading ranges almost as good as the fully active tags.

3. Passive tags: Unlike the active tags, passive tags do not have internal power supply and thus, they solely rely on the RF interrogating power sent by the reader for data processing and transmission. Apparently, there are a number of passive tags which can carry through data processing, but others cannot. In addition to this, passive tags are normally in the form of Electronic Article Surveillance (EAS) tags which are typically available in the market for safety and security purposes or what is known to be Surface Acoustic Wave (SAW) tags. Due to the fact that passive tags have simple designs, most of them promote low power consumption and low cost. As for the design, all of them ought to have a Radio Frequency (RF) front end, an analog circuit, and a digital circuit which is tailor-fit to their data processing techniques; after all they only rely on the reader's interrogating RF signal for the energy needed for operation.

Figure 2.2 shows the block diagram of a passive RFID tag which uses backscatter modulation. It mainly consists of tag antenna and tag chip. The tag chip contains a RF-analog front end, a digital control block, and a non-volatile memory (Turuc, 2009).

Considering that the new IC design and manufacturing is a large and costly venture, RFID tag antennas specifically designed for a certain ASIC which can be found in the market today. Therefore, proper impedance matching between the antenna and chip is highly important. On the other hand, cost and fabrication issues made it prohibitive in RFID tags to add an external matching network. To solve this matter, ASIC, which has complex impedance varying with the frequency and input power applied to the chip, can be directly matched to the antenna (Seshagiri et al., 2005).

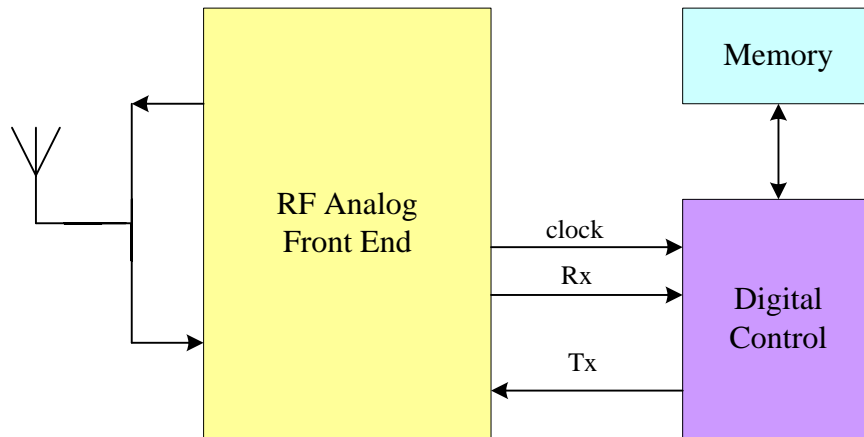


**Figure 2.2. Passive UHF RFID Tag Block Diagram**  
(Source: Turuc, 2009)

#### 2.4.2 RFID Tags Operating Frequencies

RFID systems are designed to operate with Low Frequency (LF) up to Super High Frequency (SHF); the allocation of certain frequency bands is to prevent interference from other electromagnetic (EM) devices. In addition, the type of communication between the reader and the tag is determined by the operational frequency band designated to the RFID systems, may it be induction-based or radiation-based. Practically, systems with LF and HF utilize the inductive-based. The read range for such systems lies between a few centimeters up to a meter. Low frequency RFID has a wide range of use such as identifying a vehicle and accessing parking lot. Meanwhile, contact-less smart cards, credit cards, passports and access control systems are just a few of the primary applications of HF systems. The radiation-based, on the other hand, is being used by UHF RFID systems. The latter are useful for various applications- from supply chain to inventory management to product tracking. The read range is also quite large which extends up to 10 meters. Surface Acoustic Wave (SAW) systems are categorized as the chip-less tags. Chip-less tags

may not contain an integrated chip, but the data reflected back to the reader is encoded in a unique pattern. Surface Acoustic Wave tags can operate at different temperature ranging from cryogenic to several hundred degrees. Also, they can endure x-rays with high energy or even gamma ray which would make semiconductor devices of no use. In theory, the read range of these systems reaches up to a hundred meters (Plessky et al., 2010). The unlicensed Industrial Scientific and Medical (ISM) and Short Range Devices (SRD) frequency bands that are used for RFID are illustrated in table 2.1 (Finkenzeller, 2003).

**Table 2.1. RFID tag operating frequencies**  
(Source: Finkenzeller, 2003)

<b>Frequency Rang</b>	<b>Description</b>
<b>&lt; 135 kHz</b>	Low frequency
<b>6.765 - 6.795 MHz</b>	High frequency (ISM)
<b>7.400 - 8.800 MHz</b>	High frequency, used for EAS
<b>13.553 - 13.567 MHz</b>	High frequency (13.56 MHz, ISM – contact less smartcards, credit cards, passports, access control systems, security, and several other applications)
<b>26.957- 27.283 MHz</b>	High frequency
<b>433 MHz</b>	UHF (ISM) rarely used for RFID
<b>868-870 MHz</b>	UHF (SRD) used for RFID
<b>902 - 928 MHz</b>	UHF (SRD) widely used for RFID
<b>2.400 - 2.483 GHz</b>	SHF (ISM), (2.45 GHz SAW), vehicle identification
<b>5.725 - 5.875 GHz</b>	SHF (ISM), rarely used for passive RFID, active tags commonly use these frequencies



### 2.4.3 RFID Tags Classes

The Auto ID Center (Sarma et al., 2003) has classified the UHF RFID tags according to the way they operate and function. They are divided into 6 classes as stated below:

- Class 0 is for passive read only tags. In order to communicate to the reader, they use out-of-band signaling (Powell, 2003) and backscatter technique.
- Class 1 is for passive read only tags as well, but they are programmed only once which can either be done by the manufacturer or by the user. They utilize band signaling and back scattering as a method of communication (Powell, 2003).
- Class 2 is for passive tags which have the capability of storing and encrypting. They make use of backscattering to communicate with the reader.
- Class 3 is for semiactive tags which use a battery supply to make the internal circuitry operational. Backscattering is also used to communicate with the reader.
- Class 4 tags have a transmitter and a battery source to energize the internal circuitry. They also have the capability of communicating with other tags of the same technology.
- Class 5 tags are also active. They are capable of successfully energizing other Integrated Circuits (IC) of the same class and of lower classes. A two way communication with Class 4 tags is also feasible. RFID readers may be categorized under this class.

## 2.5 RFID Tag Antenna Design Considerations

### 2.5.1 Antenna Size and Shape

In terms of antenna design, there are a couple of things to be considered. First, the tag *size*. As for this criterion, it is better to use a tag that can be embedded or attached to objects like cardboard boxes, airline baggage strips, and the alike. For that reason, it is commendable to use small tags. On the contrary, greater power supplied to ASIC and larger scatter aperture is provided by large tag antennas as more power is reflected back to the reader. To put it differently, increasing antenna gain requires larger tags. Evidently, tag size and gain should be compromised.

Antenna complex impedance depends on the size and shape of the antenna. A modification in the antenna size to adjust the impedance is impractical because it might change both resistance and reactance. Hence, adjusting the impedance by changing the shape is more advisable.

The resistive-capacitive behavior of the ASIC's impedance requires an inductive antenna to attain a conjugate match. If a matching network is to be used for antenna impedance modification, it has to be embedded within the antenna due to the limitations on its size. The modifications in different antenna parameters in terms of length and location may perform amendments of inductive-resistive characteristics.

Typically, antenna sizes are approximately one-fourth wavelengths of the lowest operating frequency, i.e.  $\lambda/4$ . Normally, antenna directivity ranges from 1.5 dBi to

1.9 dBi in the main direction (Stutzman et al., 1981; Kraus et al., 2001; Balanis, 2005; Drabowitch et al., 2005). A standard reference  $\lambda/4$  wavelength dipole offers a directivity of 2.14 dBi.

The most vital stage of tag design is the antenna design as the overall performance for specific requisites is determined.

### 2.5.2 Bandwidth

The *bandwidth* is the antenna operating frequency band within which the antenna performs as preferred. In the event that the radiation patterns do not change within the said band, the bandwidth could be related to the antenna matching band. In fact, this is the case of small antennas where a fundamental limit is related to its bandwidth, and its efficiency. Antenna bandwidth can be defined in various ways. Ratio Bandwidth (BW) (Stutzman et al., 1981; Kraus et al., 2001; Balanis, 2005; Drabowitch et al., 2005) is defined in Equation 2.1 as:

$$BW_r = \frac{f_U}{f_L} \quad (2.1)$$

where  $f_U$  and  $f_L$  are the upper and lower frequency of the band, respectively. The other definition is that of the percentage bandwidth ( $WB_p$ ) and it is related to the ratio bandwidth as in Equation 2.2 (Stutzman et al., 1981; Kraus et al., 2001; Balanis, 2005; Drabowitch et al., 2005):

$$BW_p = 200 \frac{f_U - f_L}{f_U + f_L} \% = 200 \frac{BW_r - 1}{BW_r + 1} \% \quad (2.2)$$

### 2.5.3 Radiation Pattern

The *radiation pattern* of the antenna is a graphical representation of the strength of its power density in space. Theoretically, an isotropic antenna has a spherical radiation pattern which does not physically exist. In each RFID antenna, there are two types of radiation patterns which are: E-plane and H-plane.

Energy in antenna is not radiated equally in all directions. The *radiation power pattern* is the power density's spatial variation along a constant radius. Most of the time, the far field region determines the radiation pattern which is considered in terms of the directional coordinates. As shown in Figure 2.3 (Stutzman et al., 1981; Kraus et al., 2001; Balanis, 2005; Drabowitch et al., 2005), there are three regions surrounding an antenna:

- (a) Reactive near-field  $0 < R_1 < 0.62\sqrt{D^3/\lambda}$
- (b) Radiating near-field (Fresnel)  $0.62\sqrt{D^3/\lambda} < R_2 < 2D^2/\lambda$
- (c) Far-field (Fraunhofer)  $2D^2 / \lambda < R < \infty$

where  $R$  is the field radius,  $D$  is the antenna's largest linear dimension and  $\lambda$  is the wavelength. The variation in distance from the reactive near field to the far field, cause changes in antenna's amplitude and phase patterns.

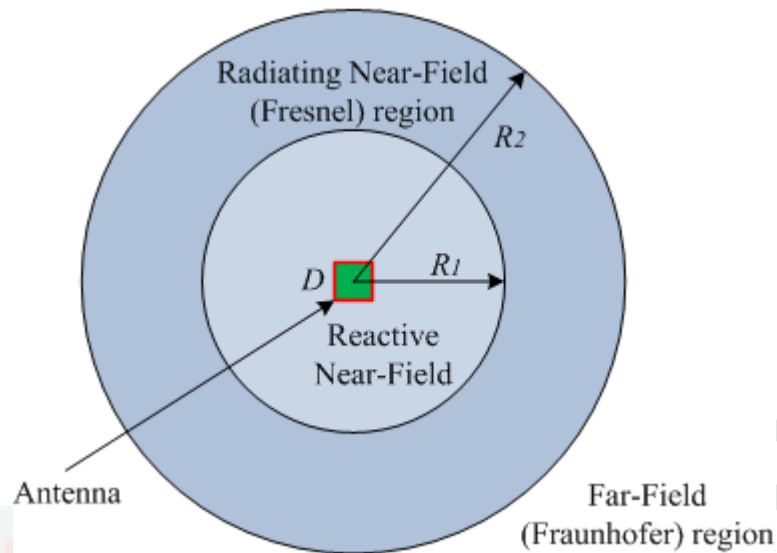


**Figure 2.3. Field Regions Around an Antenna**  
 (Source: Stutzman et al., 1981; Balanis, 2005)

#### 2.5.4 Directivity and Gain

By definition, the *directivity* of an antenna is “*the ratio of the radiation intensity in a given direction from the antenna to the radiation intensity averaged over all directions.*” As demonstrated in Equation 2.3, the directivity of a nonisotropic source is equivalent to the ratio of its radiation intensity in a given direction (Balanis, 2005):

$$D = \frac{U}{U_i} = \frac{4\pi U}{P_r} \quad (2.3)$$

where the directivity of the antenna is represented by  $D$ ;  $U$  symbolizes the radiation intensity of the antenna;  $U_i$  is the isotropic source’s radiation intensity; and  $P_r$  is the total power radiated.

Whenever the direction of the directivity is unspecified, the maximum radiation intensity's direction is implied and the maximum directivity is given as evident in Equation 2.4 (Stutzman et al., 1981; Kraus et al., 2001; Balanis, 2005; Drabowitch et al., 2005):

$$D_{max} = \frac{U_{max}}{U_i} = \frac{4\pi U_{max}}{P_r} \quad (2.4)$$

where  $D_{max}$  is the maximum directivity and  $U_{max}$  is the maximum radiation intensity.

Meanwhile, *gain*, is a parameter which focuses on the directionality of a particular antenna. An isotropic antenna emits radiation of the same power in all directions, while a directive antenna preferentially radiates in specific direction. Categorically, gain, directive gain, or power gain of an antenna are prescribed as the ratio of the (power per unit surface) radiation intensity of the antenna in a specific direction over the intensity of the radiation emitted at the same distance by a hypothetical isotropic lossless antenna as illustrated in Equation 2.5 (Stutzman et al., 1981; Kraus et al., 2001; Balanic, 2005; Drabowitch et al., 2005):

$$G = \frac{4\pi U}{P_{in}} \quad (2.5)$$

Even though the antenna gain is correlated to its directivity, it measures the efficiency and the directional capabilities of an antenna. Contrary to gain, directivity is a measure which only has regard to the property of antenna directionality, and as a result it is only affected by its pattern. Practically, the directivity of an antenna is

always larger than that of its gain (Stutzman et al., 1981; Kraus et al., 2001; Balanis, 2005; Drabowitch et al., 2005), as shown in Equation 2.6:

$$G = \frac{4\pi U}{P_{in}} = e_{cd} \frac{4\pi U}{P_r} = e_{cd} D \quad (2.6)$$

The antenna gain and directivity are related by Equation 2.6, where  $e_{cd}$  is the radiation efficiency factor of the antenna,  $D$  is the directivity, and  $G$  is the gain. Relative gain is normally dealt with, and as such, it is specified by the ratio of antenna power gain in a given direction to the ratio of a reference antenna power gain in the same direction, as exemplified in Equation 2.7. While performing this kind of measurement, input power must be identical for both antennas. The power gain of a reference antenna should be already known. A reference antenna might be a dipole, horn, or any other type of well-calibrated antenna (Stutzman et al., 1981; Kraus et al., 2001; Balanis, 2005; Drabowitch et al., 2005).

$$G = G_{ref} \frac{P_{max}}{P_{max}|_{ref}} \quad (2.7)$$

Should the radiation direction is not specified; the calculation of the power gain is always in the direction of maximum radiation. An actual antenna's maximum directivity can change from 1.76 dB to 50 dB for a short dipole and large dish antenna respectively. As for the maximum gain, doesn't have a lower bound and is more often - 10 dB or lower for electrically small antennas.

In national UHF frequency regulations, radiated power is defined with different terms in the different countries. The two most common terms are EIRP and ERP.

The Equivalent Isotropic Radiated Power (EIRP) is primarily used in Asia and in the USA, while the Effective Radiated Power (ERP) is mainly used in Europe. Equation 2.8 below shows the relationship between EIRP and the ERP (Stutzman et al., 1981; Kraus et al., 2001; Balanis, 2005; Drabowitch et al., 2005):

$$EIRP = ERP \cdot 1.64 \quad (2.8)$$

### 2.5.5 Polarization

To increase the range, tag antenna *polarization* is ought to be compatible with antenna's reader. By using a circularly polarized reader antenna with linearly polarized tag gets rid of the sensitivity to polarization, but causes them an additional 3 dB loss. Some tags also have circular polarization (Imping Monza RFID Products). They make use of two orthogonal dipoles. The  $\lambda/4$  *delay* line affixed to the feed of the two dipoles produces the ninety degree out-of phase. Even though the majority of the RFID tags available in the market are linearly polarized, a lot of RFID reader systems still use circularly polarized antennas to make sure that tags are read in any position (Nikitin, et al., 2008). Up-to-date readers have four RF input/output ports which are operated in a sequential manner. The antennas connected to these ports are positioned in a way that the field will be illuminated to various angles and/or to perpendicular directions. In this manner, a configuration to the reading zone takes place to reduce the communication losses with tags regardless of their orientation.



Similar polarization sense and axial ratio must be achieved in order for them to transfer greatest possible power from a transmitting and receiving antennas. If the antennas are not properly aligned or aren't in the same polarization, the transfer of power between two antennas will be lowered. As a result, the overall efficiency and performance of the system will be reduced. However, when the transmitting and receiving antennas are linearly polarized, misaligned antennas will cause a mismatch loss in polarization. This, in turn, can be determined by using the formula in Equation 2.9 (Stutzman et al., 1981; Kraus et al., 2001; Balanis, 2005; Drabowitch et al., 2005):

$$\text{Loss (dB)} = 20 \log(\cos\theta) \quad (2.9)$$

where  $\theta$  is the difference in alignment angle between two antennas. Approximately 0.3 dB is lost for 15°, 1.25 dB for 30°, 3 dB for 45° and an infinite loss for 90°. In other words, the higher the polarization mismatch is, the higher the actual loss will be.

### 2.5.6 Impedance Matching

A proper impedance matching between the antenna and the chip directly affects the performance characteristics of RFID, for example, the tag's reading range: the greatest distance at which information can be read or written by the reader. Therefore, it is evident that proper impedance match is crucial in RFID.

In RFID tags, there is usually a direct connection between the antenna and the chip, as demonstrated in Figure 2.4, where  $Z_a = R_a + jX_a$  is the complex antenna impedance

and  $Z_c = R_c + jX_c$  is the complex chip (load) impedance. The voltage source shown in Figure 2.4 represents an open circuit RF voltage which is induced on terminals of the receiver (antenna).  $Z_a$  and  $Z_c$  both change with frequency. Lastly,  $Z_c$  may vary as it is based on the power the chip absorbs.

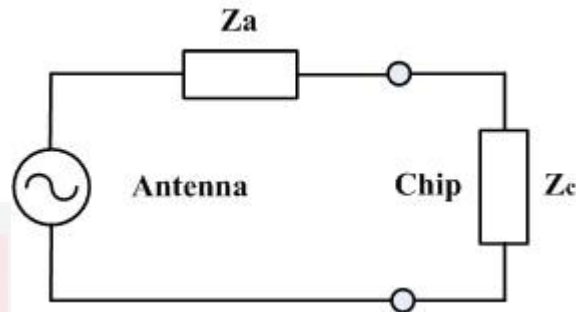


**Figure 2.4. The Equivalent Circuit of an RFID Tag**

Apparently, an RFID chip is a nonlinear load in which complex impedance in each state may vary in terms of frequency and input power. A specified minimum voltage is required to turn the chip circuitry on. The said threshold, and the dependence of the impedance on the input power, is gauged by the details of the chip's RF front end, and the energy consumed by the specific chip (De Vita et al., 2005). The dependence of the impedance on frequency is mainly identified by the chip's parasitic and packaging effects.

The performance of the tag can be strongly affected by the variation of the chip's impedance with power and frequency. In order to increase the tag's range, the antenna is normally matched to the impedance of the chip at a minimum power level needed for the chip to function. For the majority of the tag application cases, the tag continuously operates whenever it is in proximity to the RFID reader antenna, where in there is a higher power incident on the tag. Even so, a situation where a

substantial variation of the chip's impedance with a greater input power leads to a severe mismatch on tag impedance. Also, this may cause dead spots within the tag's operational range. Equation 2.10 (Rao et al., 2005b) shows the amount of power ( $P_c$ ) which the chip can absorb from the antenna:

$$P_c = P_a \tau \quad (2.10)$$

where  $P_a$  is antenna's maximum available power and  $\tau$  is the Power Transmission Coefficient (PTC).  $P_a$  is the power that may be delivered to the chip when  $Z_a = Z_c^*$ . Equation 2.11 illustrates the power transmission coefficient ( $\tau$ ) (Rao et al., 2005):

$$\tau = \frac{4R_c R_a}{|Z_a + Z_c|^2}, \quad 0 \leq \tau \leq 1 \quad (2.11)$$

The degree of impedance matching between the chip and the antenna is directly defined by the power transmission coefficient ( $\tau$ ).

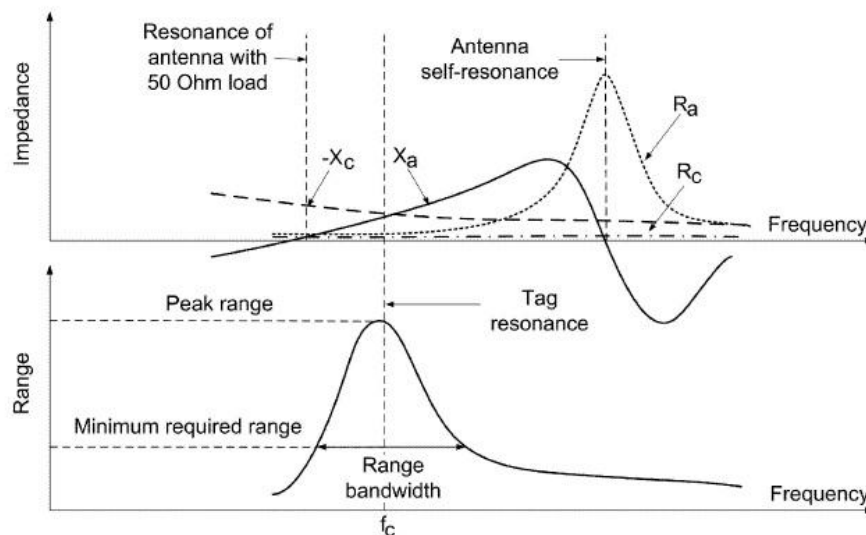


**Figure 2.5. Antenna Impedance, Chip Impedance and Range versus Frequency for a Typical RFID Tag**

(Source: Rao et al., 2005b)

Figure 2.5 demonstrates the qualitative behavior of the antenna and chip impedance and the read range as a function of frequency for a regular RFID tag (Rao et al.,

2005). The tag resonance is at the peak range ( $f_c$ ). Generally,  $\tau$  (Equation 2.11) dominates the frequency dependence and mainly identifies the tag resonance that occurs at the frequency of the best impedance match between chip and antenna. The said frequency is not the same as the antenna self-resonance and the resonant frequency of a 50 Ohm loaded antenna.

Kurokawa introduced the following definition given in Equation 2.12 for the power wave reflection coefficient  $s$  after describing a concept of power waves travelling between a generator and load (Kurokawa, 1965):

$$s = \frac{Z_a - Z_c^*}{Z_a + Z_c} \quad (2.12)$$

To attain the most suitable match between the antenna and the IC, reducing the power reflection coefficient  $|s|^2$  as in Equation 2.13 is recommended (Nikitin et al., 2005):

$$|s|^2 = \left| \frac{Z_a - Z_c^*}{Z_a + Z_c} \right|^2, \quad 0 \leq |s|^2 \leq 1 \quad (2.13)$$

The power reflection coefficient  $|s|^2$  is the complement of the power transmission coefficient  $\tau$  ( $|s|^2 = 1 - \tau$ ) and provides what fraction of the maximum power available from the generator is not delivered to the load.

### 2.5.7 Read Range

*Read range* is one of the most important performance parameters of RFID tags. One of the limitations of read range is the maximum distance at which the tag receives enough power to be turned on and scatter back. The other one is the maximum distance where the scattered signal can still be detected by the reader. Typically, the

smaller of the two distances is considered to be the read range. In general, the read range is determined by the former distance since the reader sensitivity is high enough (Nikitin et al., 2005).

As illustrated in Equation 2.14, the power collected by an RFID antenna can be computed with the use of Friis free-space transmission formula. (Balanis, 2005):

$$P_a = \frac{P_t G_t G_r \lambda^2}{(4\pi r)^2} \quad (2.14)$$

where  $P_t$  represents the power transmitted by the reader,  $G_t$  is the reader's antenna gain,  $G_r$  is the gain of the receiving tag antenna,  $\lambda$  is the wavelength, and  $r$  is the distance between the reader and the tag. The product ( $P_t G_t$ ) is the EIRP.

Should the minimum threshold power required to turn on the chip is  $P_{th}$ , then read range  $r$  can be computed as in Equation 2.15 (Balanis, 2005):

$$r = \frac{\lambda}{4\pi} \sqrt{\frac{P_t G_t G_r \tau}{P_{th}}} \quad (2.15)$$

The tag range bandwidth shown in Figure 2.5 by definition is the frequency band in which an acceptable minimum read range is offered by the tag over that band. The maximum possible read range  $r_{max}$  if the tag is perfectly matched to the chip ( $\tau = 1$ ) is given in Equation 2.16:

$$r_{max} = \frac{\lambda}{4\pi} \sqrt{\frac{P_t G_t G_r}{P_{th}}} \quad (2.16)$$

### 2.5.8 Deformation

The design of tag antennas are often made suitable for flat surfaces. Recently, developments of flexible tag antennas were massively produced at low cost. Affixing these tag antennas to non-flat surfaces would highly affect the radiation properties due to deformation.

Furthermore, de-tuning is caused by the distortion of the geometry of antenna which in turn leads to performance degradation. In fact, the antenna resonates at a different frequency because of impedance mismatch and de-tuning. Proper usage of the tag to products moderates this undesirable effect.

### 2.5.9 Fabrication Materials and Process

Printed antenna design has two requirements: a good conductor such as copper or conductive ink and substrate like High Density Polyethylene (HDPE) or Polypropylene (PP).

Dielectric constant ( $\epsilon_r$ ), loss tangent ( $\tan \delta$ ) and thickness are the three main design parameters of the substrate. The effective wavelength is reduced with the use of any dielectric constant substrate. Moreover, it lowers the resonant frequency and narrows the bandwidth. A substrate with high loss tangent ( $\tan \delta$ ) increases the

operating bandwidth and reduces the radiated power. The effect of the above mentioned parameters can be avoided by using high thickness substrates.

Using conductive adhesive to connect the ASIC to the antenna is a preferable method in terms of low temperature process and low cost. Yet, even with additional costs, nickel compounds can be used to coat the connection terminals of copper or aluminum antenna to avoid oxidation.

The traditional thick or thin-film technology using expensive metal ink is another method to print or deposit the antenna traces. Printing long fine traces may lead to conductivity variation along the trace which is one of the disadvantages of this method. The read-write distance is reduced due to this conductivity variation. For this reason, thick film technology is favorable for the 915 MHz and 2.45 GHz RFID tags because of their simple shape and large traces.

#### **2.5.10 Proximity to Objects**

When objects are placed in proximity ( $0.01\lambda$ ), the RFID tag antenna electromagnetic properties may be modified. Plastics and water are considered as objects with high loss dielectric constants leading to tag detuning and radiation efficiency reduction, while an increase in the radiation resistance of an antenna is caused by proximity to conductive objects leading to inefficient power transfer. For a specific object, a tag antenna can be designed or tuned to achieve optimum performance.

## 2.6 Impedance Measurement of RFID Tag Antenna

In the recent years, UHF RFID system has dominated in supply-chain industry for logistic purposes. In comparison with other RFID technologies which use LF and HF band, UHF RFID offers three advantages: data rate is higher, reading range is longer and material cost is lower. Loop antenna, dipole antenna, or patch antenna with ground plane are some of the UHF RFID tag antenna forms used for various applications (Marrocco, 2008). To achieve maximum power transfer, conjugate matching is compulsory between tag antenna impedance and tag chip impedance disregarding the different antenna designs (Rao et al., 2005a).

Antenna simulation software is the most popular tool used for antenna design, such as High Frequency Structure Simulator (HFSS), Computer Simulation Technology (CST) and IE3D. Its design cycle is actually an empirical process, i.e. simulation is the first step for antenna design after identifying the specific design requirements, then prototype fabrication is next, afterwards the design requirement is to be validated by measurements. If the design requirement is not met, the design should be refined. Practically, the process of antenna design is recursive until the required specifications are met.

Accuracy in impedance measurement is very important in RFID tag antenna design. Symmetrical dipole and loop antenna structures are mostly utilized in UHF RFID tag antenna designs (Marrocco, 2008). A differential input signals feeds these antennas with virtual ground. By using a conventional single-ended, two-port Vector



Network Analyzer (VNA), identifying the input impedance of the antenna would not be accurately obtained (Meys et al., 1998).

Several research groups have proposed different methods to measure the input impedance of a balanced antenna, which is the most common RFID antenna configuration. By utilizing a balun or imaging method, the impedance of a balanced antenna can be extracted (Dobkin et al., 2005; Leong et al., 2007). Nevertheless, accuracy depends mainly on the characteristic of the balun and the size of the ground plane. Alternative methods involving the use of measured  $S$ -parameter have been proposed recently by connecting microstrip lines or coaxial cables as test fixtures (Palmer et al., 2006; Kuo et al., 2008; Qing et al., 2009; Zhu et al., 2010; Konya et al., 2011; Sasamori et al., 2012).

A detailed overview on the impedance measurement of balanced loads using a network analyzer, proposed by (Palmer et al., 2006), and meticulously validated in the RFID context in (Kuo et al., 2008) is demonstrated in this section. This method is going to be adopted for impedance measurements of antennas designed in this thesis.

Figure 2.6 shows the model proposed by Palmer for the impedances. The differential and common mode excitation voltages are represented by  $V_d$  and  $V_c$  respectively. Antenna feed terminals are nodes A and B, and  $Z_a$ ,  $Z_b$ , and  $Z_c$  represent the antenna impedances where typically,  $Z_a = Z_b$  and are positioned between nodes A and B (antenna terminals) and ground, while  $Z_c$  is the impedance between A and B.  $Z_{common}$

$= Z_a // Z_b$  is the common mode impedance and  $Z_{diff} = Z_c // (Z_a + Z_b)$  is the differential mode input impedance (see the Appendix A for derivation).

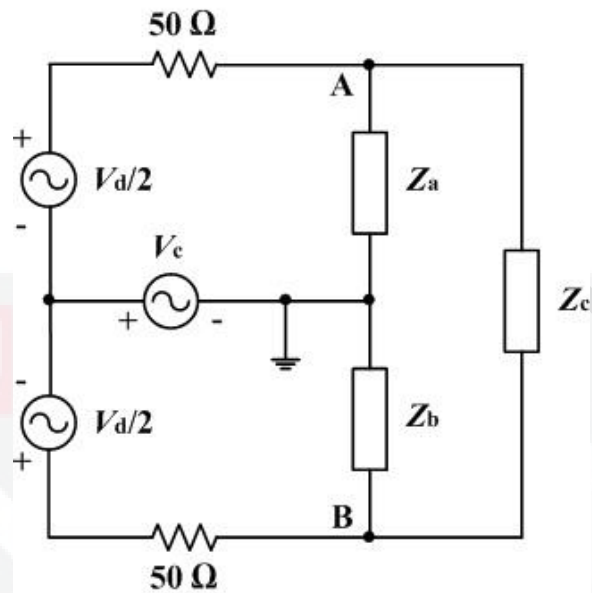


**Figure 2.6. Two-Port Impedance Model of an Antenna and Feed**  
(Source: Palmer et al., 2006)

The load or symmetrical antenna to be tested is simulated as a device with three terminals. In case of a dipole antenna, one arm is connected to node A and the other to node B. The ground of the transmission lines is the same as the ground feeding the dipole arms. This two-port dipole network connection is shown in Figure 2.7. The network analyzer ports connect to each arm of the dipole in the shown order. The dipole impedances are also shown in a schematic manner.

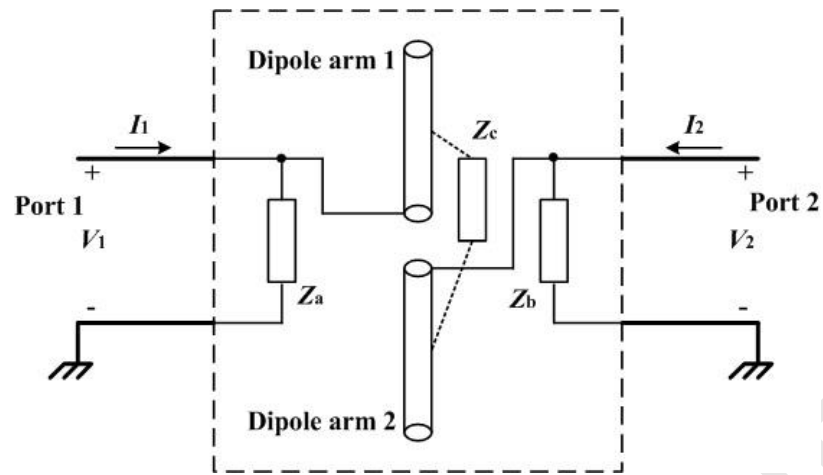


**Figure 2.7. Schematic Representation of a Dipole Antenna and its Impedances**  
(Source: Palmer et al., 2006)

A photograph of the proposed jig by (Palmer et al., 2006) to measure balanced loads is illustrated in Figure 2.8, while Figure 2.9 explains how the jig would be connected to obtain a dipole measurement. Here, the VNA is evident where each port is connected through test cables to one of the semirigid cables, respectively. The two semirigid cables are soldered together on their outer conductors, while their inner conductors are partially extended to place the feeding points closer to the terminals of the antenna under test.

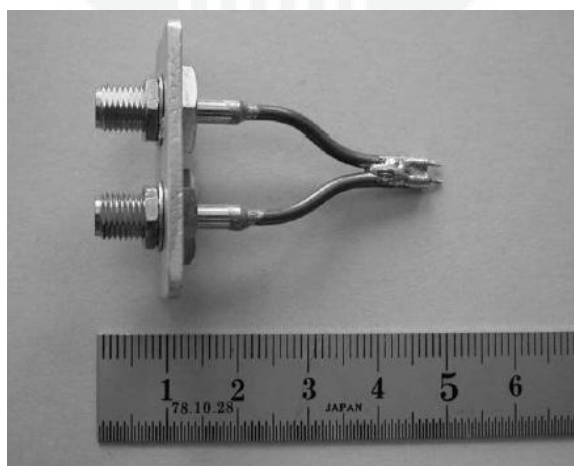


**Figure 2.8. Photograph of the Two-Port Measurement Jig**  
(Source: Palmer et al., 2006)

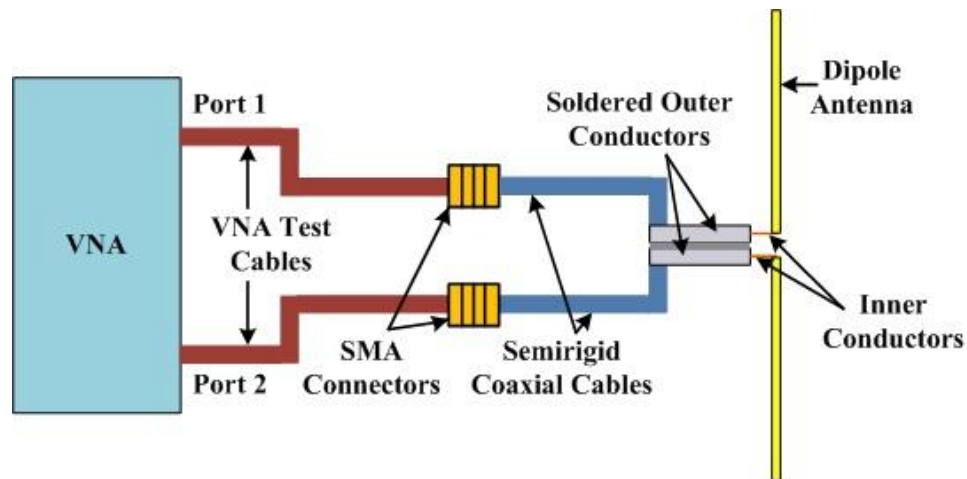


**Figure 2.9. Connections Using the Proposed Two-Port Jig to Measure the Impedance of a Dipole**

(Source: Palmer et al., 2006)

Five steps are followed to obtain the measurement of the antenna:

1. The VNA is calibrated at the Sub-Miniature version A (SMA) (Appendix B) connectors by making use of the supplied standards of the manufacturer.
2. The two semirigid cables' parameters are determined from a short circuit measurement (will be discussed later).
3. The antenna is placed and its two-port S-parameters are measured.
4. By deembedding the effect of the semirigid coaxial cables from the S-parameters at the SMA connectors, the antenna S-parameters are obtained.
5. The antenna impedances are derived from the S-parameters.

Characterization of the semirigid cables of the jig is performed during step 2 of the measurement. To simplify, each cable is considered as a transmission line with attenuation  $\alpha$  and phase delay  $\beta$ . For the measurement of these values, a short to ground is set at the end of the semirigid cables to obtain their complex input reflection coefficients.  $\beta l$  is obtained from this phase measurement which is double

the electrical length of the cable and also a 180° phase reversal because of the short placed at both ends, while  $\alpha l$ , the line attenuation, is obtained when the measured magnitude (in nepers) of the reflection coefficient is divided by 2.

Equation 2.17 shows how to obtain the ABCD-parameters with  $\alpha$  and  $\beta$  known (Temes et al., 1977):

$$\begin{bmatrix} \cosh(\alpha + j\beta) l & Z_0 \sinh(\alpha + j\beta) l \\ \frac{1}{Z_0} \sinh(\alpha + j\beta) l & \cosh(\alpha + j\beta) l \end{bmatrix} \quad (2.17)$$

where  $Z_0$  is normalized to 1.

It should be pointed out that the connections at the SMA connectors are presumed by the model to be of no reflection. Normally, the measurement of the reflection is -20 dB or lower and is not important for antenna measurement cases.

It is now possible to measure the full two-port S-Parameters having the antenna affixed to the jig since the two semirigid cables' parameters are identified. The antenna impedances,  $Z_{diff}$  and  $Z_{common}$ , are desirable at this point since the parameters,  $S_{11}$ ,  $S_{21}$ ,  $S_{12}$ , and  $S_{22}$  are already known. The following steps were done to come up with these impedances: First of all, the S-parameters were used to get the ABCD-parameters of the full measurement (Frickey, 1994). Next, an isolation of the antenna's ABCD-parameters is performed. This was performed by eliminating the effect of the semirigid cables from the full measurement, which required the pre- and post-multiplication of the ABCD-parameters of the full measurement with the inverse ABCD-parameters of the two semirigid cables. Then, the obtained antenna ABCD-parameters are converted into Y-parameters. Thus, by making use of the Y-

parameters, the impedances  $Z_a$ ,  $Z_b$ , and  $Z_c$  are obtained (the derivation is shown in Appendix A). Lastly, Equations 2.18 and 2.19 shows the impedances  $Z_{diff}$  and  $Z_{common}$  respectively:

$$Z_{diff} = \frac{Z_c(Z_a + Z_b)}{Z_a + Z_b + Z_c} \quad (2.18)$$

$$Z_{common} = \frac{Z_a Z_b}{Z_a + Z_b} \quad (2.19)$$

where  $Z_a$ ,  $Z_b$ , and  $Z_c$  are the impedances as shown in Figure 2.6.

## 2.7 Overview of RFID Tag Antennas

To date, several types of RFID tag antenna structures have been proposed and fabricated in the UHF band frequency range promising potential for producing highly-efficient tag antennas in terms of size, gain, read range and metallic objects identification. This section is a succinct review of some different types of RFID tag antenna structure designs.

### 2.7.1 Three to Two Curve Fractal Folded Dipole Antenna

A 3/2 curve fractal was introduced by (Zhou et al., 2010) which is better than other fractals in terms of multiband features. Furthermore, lowering the resonant frequency of antenna can be done without the need of having more space, while the radiation pattern remained the same to that of conventional square patch (Sadat et al., 2005). On the contrary, mirror compensation structure and Photonic Band Gap (PBG) have been proven beneficial for the enhancement of antenna's bandwidth and radiation properties (Qian et al. 1999; Wei et al., 2008; Lin et al. 2008). The layout

of the antenna is as follows: a dielectric board of 0.8 mm thickness and dielectric constant  $\epsilon_r = 5$  with dimensions of  $24 \times 7 \times 0.8 \text{ mm}^3$ . So based on dipole antenna, an innovative  $2/3$  curve fractal antenna is designed for dual-frequency. A photograph of the fabricated  $3/2$  fractal dipole antenna is shown in Figure 2.10, in which it is evident that 50 ohm is the basis for its design and measurement.

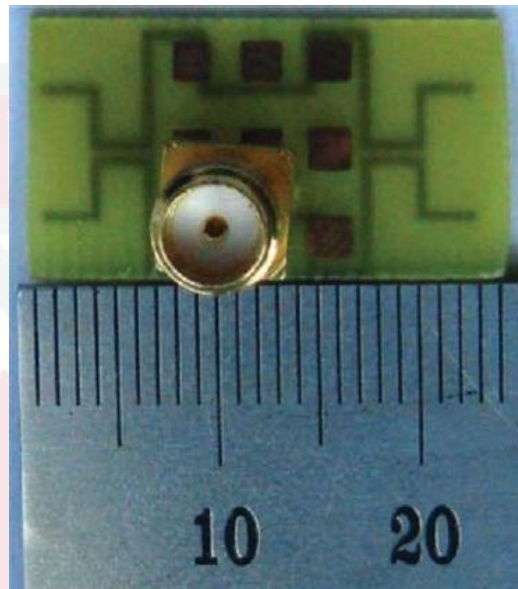


**Figure 2.10. Fabricated  $3/2$  Fractal Dipole Antenna**  
(Source: Zhou et al., 2010)

### **2.7.2 Fractal Dipole Antenna for 915MHz and 2.4GHz**

A compact printed dipole antenna using fractal shape for RFID is presented by (Kimouche et al., 2011). The proposed antenna consists of a third iteration fractal tree structure with the aim of reducing the antenna size. The antenna has been designed and optimized to cover the bi-band for passive RFID tag at 915MHz and 2.4 GHz. The Fractal antenna is optimized to be matched with a commercial tag (EPC GEN 2), which has input impedance of  $(14 - j144)$  at 915MHz and  $(14 - j650)$

at 2.4 GHz. The threshold power of the chip is  $P_{th} = -10$  dBm. The tag presents a reading distance of about 5m at 915MHz band, and 4.5m at 2.4 GHz. The antenna dimensions are  $78 \times 30 \times 1.58$  mm<sup>3</sup>. Figure 2.11 shows a photograph of the fabricated antenna.

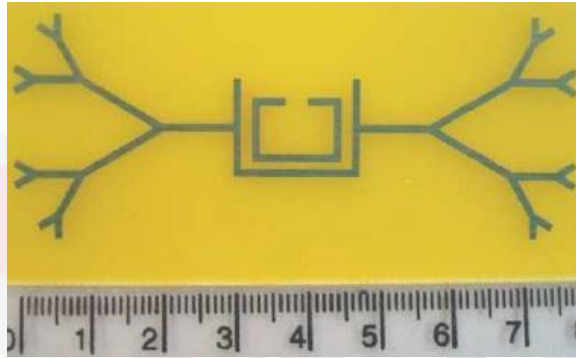


**Figure 2.11. Fabricated Fractal Dipole Antenna**  
(Source: Kimouche et al., 2011)

### 2.7.3 Dual-Band Dipole Antenna

A dipole antenna, introduced by (Lee et al., 2008), has a rectangular fractal shape radiator element with two operating bands for RFID. The antenna structure uses FR4 substrate having relative permittivity 4.4 and has a size of  $107.4 \times 33.2 \times 1.6$  mm<sup>2</sup>. The quantified gain of the suggested antenna ranged from -5.6 dBi to -1.8 dBi within UHF band and from 3.3dBi to 5.7dBi within microwave operation frequency band. However, this particular antenna was not measured for specific chip impedance neither for validation of reading range.



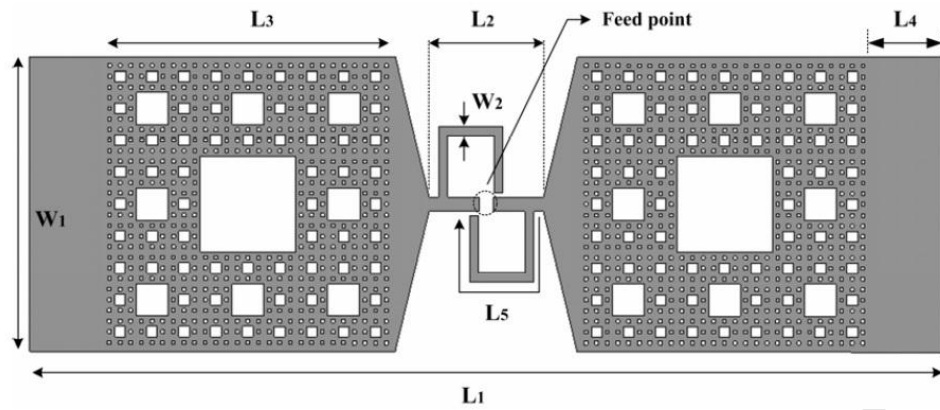


**Figure 2.12. Geometry of the Dipole Antenna**  
(Source: Lee et al., 2008)

#### 2.7.4 Minkowski Fractal Microstrip Antenna for RFID Tags

A one loop Minkowski fractal tag antenna is designed for size reduction by (Rusu et al., 2008) as shown in Figure 2.13. The antenna was fabricated by printing a copper trace (35  $\mu\text{m}$  thick, 0.5 mm wide) on a 3 mm thick Rogers Duroid (4003) substrate with a uniform ground plane on the other side of the substrate (35  $\mu\text{m}$  thick). Measurement was done by connecting the coaxial cables' ground to the antenna ground plane, and the signal wire was connected through the substrate to the port of a network analyzer. The Atmel Tagidu chip was utilized with  $P_{\text{th}} = 16\mu\text{W}$ . Lower gain and out of tuned operating frequency (875 MHz) is evident, which does not negatively affect its applicability. The antenna dimensions are  $30 \times 30 \times 3 \text{ mm}^3$ . The best simulated design after fabrication and measurement is obtained at 868MHz with a 0.5 meters reading distance.

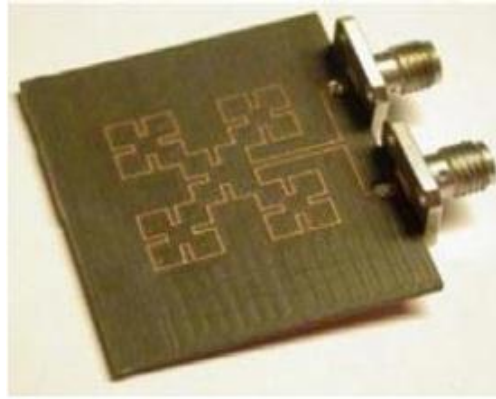


**Figure 2.13. Photograph of Manufactured Antenna with a Modified Minkowski Fractal Curve**

(Source: Rusu et al., 2008)

### 2.7.5 Fractal Loop Antenna for Passive UHF RFID Tags Applications

(Salama et al., 2008) illustrated and enhanced a fractal loop antenna, for UHF RFID tags at 900 MHz, based on the second iteration process of a Minkowski fractal curve as demonstrated in Figure 2.14. The dimension of the antenna is  $90.66 \times 77.5 \times 1.59$  mm<sup>3</sup>. For balanced currents to be obtained, a  $50\Omega$  coaxial cable type RG58/U and BNC connector is affixed to the manufactured antenna by means of a Bazooka Balun. As stated by the author, the values for the antenna gain and read range are 1.97 dBi and 6.5 m respectively.

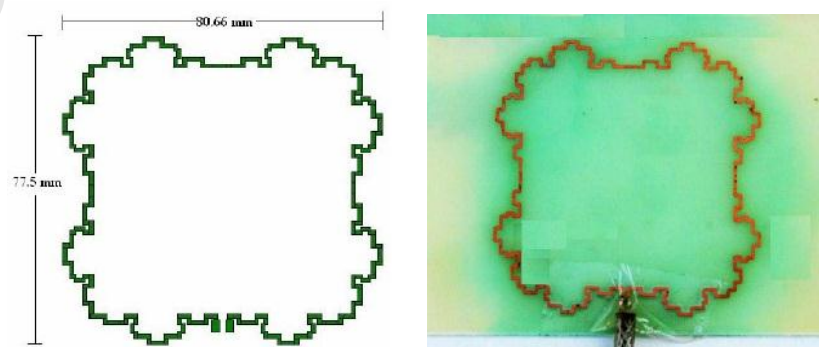
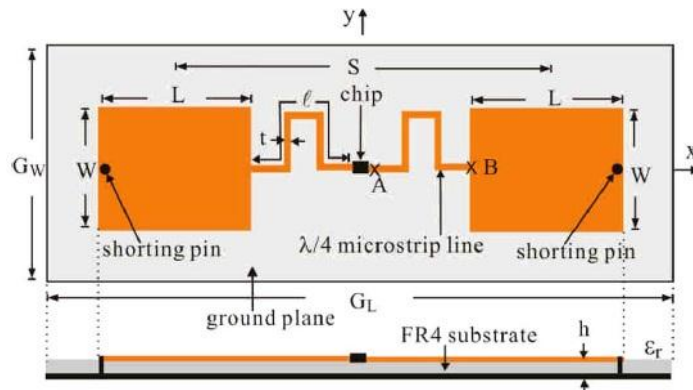


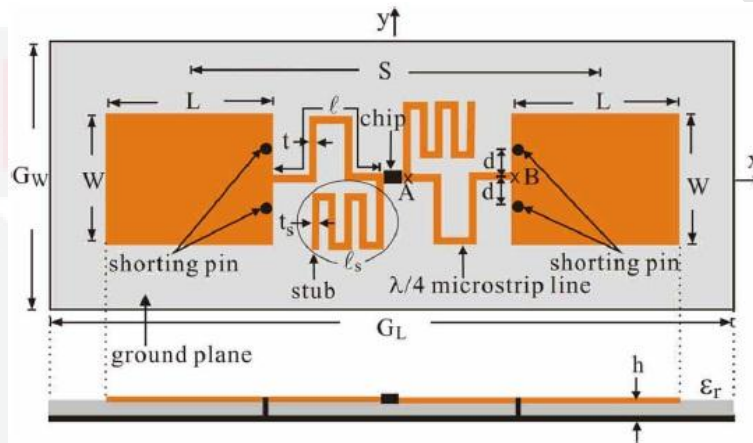
**Figure 2.14. (a) Layout of Fractal Loop Antenna and (b) Its Photograph**  
(Source: Salama et al., 2008)

### 2.7.6 Low-Profile PIFA Array Antennas

(Chen et al., 2010b) presented two Planer Inverted F array Antennas (PIFA) which are made for metallic objects identification. These antennas are fabricated on a 0.8 mm-thick substrate. Two quarter-wavelength microstrip lines feed the 1<sup>st</sup> array that has shorting pins set at the outer edges of the PIFAs. The main advantage of the array is that it has an uncomplicated feeding structure. A broad bandwidth is offered from the second array which has shorting pins situated at the inner edges of PIFAs, and integrating additional matching stubs into the quarter-wavelength microstrip lines to achieve complex impedance matching. An improved antenna gain and a quality reading-range performance can be attained for both array antennas through a proper selection of spacing within PIFAs. Furthermore, many metallic plates with different sizes are used to test these two antenna arrays. It is discovered then that the metal-plate size has no effect on the reading range for the second array antenna, which is better than the first array. Figure 2.15(a) and (b) shows the geometry of the two PIFA array antennas. The dimensions of the first PIFA array antenna illustrated in Figure 2.15(a) are  $65 \times 45 \times 0.8 \text{ mm}^3$ , while the second one depicted in Figure 2.15(b) has dimensions of  $127 \times 52 \times 0.8 \text{ mm}^3$ .



(a)



(b)

**Figure 2.15. Geometry of (a) First PIFA Array Antenna, and (b) Second PIFA Array Antenna**  
(Source: Chen et al., 2010b)

### 2.7.7 A Miniature RFID Tag Antenna Design for Metallic Objects Application

A proposition made by (Chen, 2009) is a layout of a miniature metal mount RFID tag antenna. The structure of the antenna comprises of two rectangular patches which are connected electrically by the means of vias to the ground plane and an unconnected inter-conductive layer to create a tag antenna that is fit for metallic objects tagging. Maximization of the antenna capacitive reactance is attained by inserting a conductive layer into the antenna structure. This will lower the self-

resonant frequency of the proposed antenna; thus, even with a small sized RFID tag antenna, antenna impedance's high imaginary part can be realized. The antenna is made for Alien H2 RFID chip. It is encased in a strap package in which has an input impedance of  $Z_c=19-j119 \Omega$  at 925 MHz. The sensitivity of the RFID strap is -14 dBm. The maximum read range of the prototype set on a metallic object is approximately 1.5 meters and the antenna size is  $33 \times 18 \times 3.2 \text{ mm}^3$ . Figure 2.16 illustrates a photograph of the metal tag antenna.

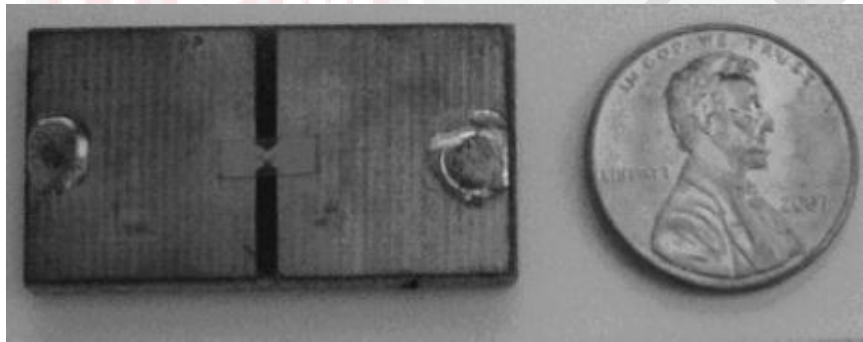


**Figure 2.16. Fabricated Metal Tag Antenna**  
(Source: Chen, 2009)

### 2.7.8 Dual Band Tag with AMC Ground Plane

A dual-band passive radio frequency identification (RFID) tag antenna applicable for a recessed cavity in metallic objects such as heavy equipment, vehicles, aircraft, and containers with long read range designed by using an Artificial Magnetic Conductor (AMC) ground plane is proposed in (Kim et al., 2012). The proposed tag antenna consists of a bowtie antenna and a recessed cavity with the AMC ground plane installed on the bottom side of the cavity. Figure 2.17 presents the fabricated cavity with the AMC ground plane and the bowtie antenna. The realized gain of the proposed antenna is 6.74 dBi at 869 MHz and 6.46 dBi at 913 MHz, respectively.

The antenna has a large size of  $140 \times 80 \times 50 \text{ mm}^3$  because it has a cavity that is supposed to be embedded into heavy metallic objects.

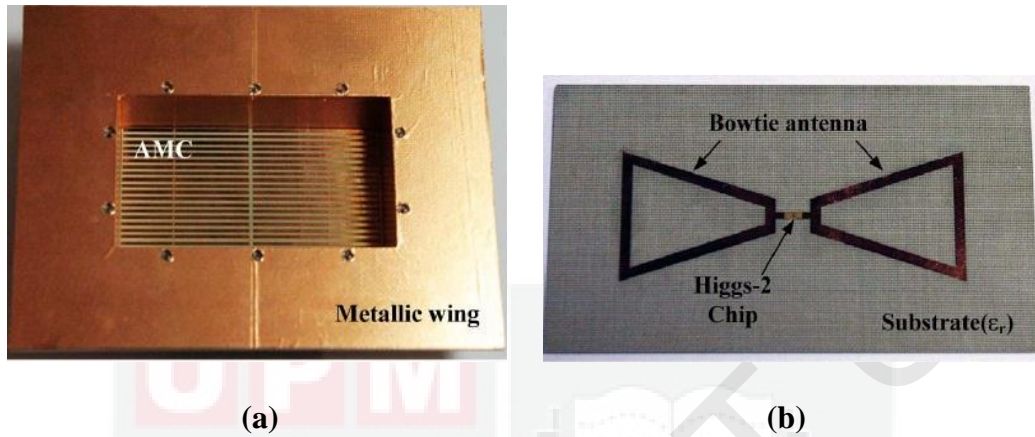


**Figure 2.17. Photograph of (a) the Fabricated Cavity with the AMC Ground Plane and (b) Bowtie Tag Antenna**  
(Source: Kim et al., 2012)

### 2.7.9 Metal Antenna on a Compact HIS Substrate

A radio frequency identification tag antenna working at 920MHz for metallic ground is proposed by (Liu et al., 2010) utilizing the special physical characteristic of a High Impedance Surface (HIS). A meandering structure was employed to reduce the size of a half-wave dipole as a top layer, HIS intermediate layer consisting of periodic metallic pattern patches etched on dielectric substrate, and the back of the substrate is metal ground plane as a bottom layer. The three layers are electrically disconnected. The author claims that the size of such a structure is larger than the one with vias at the same resonant frequency. The HIS not only solves problems which are caused by a metallic mounting structure, but also increases the gain of antenna. The antenna is designed for RFIC chip with an input impedance of about  $20-j121 \Omega$ . The measured maximum reading distance is 3.1 m, when the RFID tag



antenna is attached to a finite metal plane of size 43 mm×129 mm. Figure 2.18 shows a photograph of the fabricated antenna. The dielectric board employed is 1.52 mm in thickness with relative permittivity  $\epsilon_r$  of 10.02. The size of this antenna is 129×43×3.52 mm<sup>3</sup>.

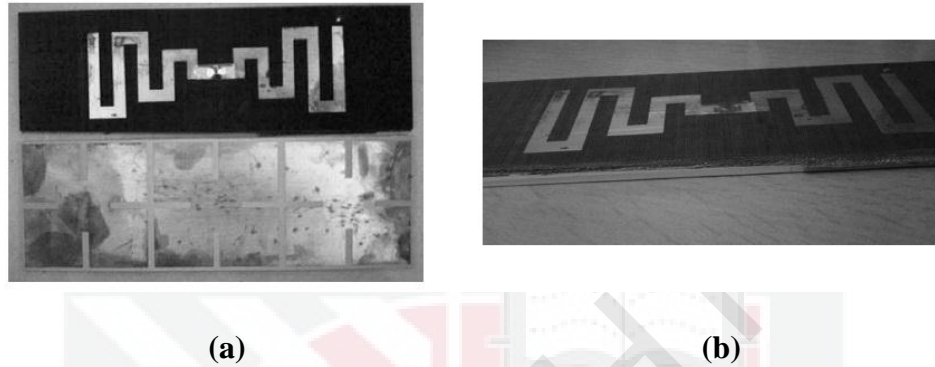


**Figure 2.18. Photograph of RFID tag Antenna. (a) Dipole Antenna and HIS. (b) The whole Antenna with an RFID Chip**  
(Source: Liu et al., 2010)

#### 2.7.10 Metal Mount Meandered Patch Antennas

Different meandered patch antennas are introduced by (Chen et al., 2010a) for UHF band RFID tags attached on metallic objects. With this layout, a long patch is curved to a number of half-wavelength radiating elements, the surface currents of all radiating elements becomes in phase and therefore achieves an improved gain and a good reading range performance. In addition, it is shown that higher the radiating elements are the higher the gain is. In this design, tag chip used Alien Higgs in strap package that possesses an impedance of  $13-j111 \Omega$  at the frequency of 915 MHz. The measured read range is 3.4 meters on metallic objects. A photograph of the meandered patch antenna is shown in Figure 2.19 and the size of this antenna is 100×50×0.8 mm<sup>3</sup>.

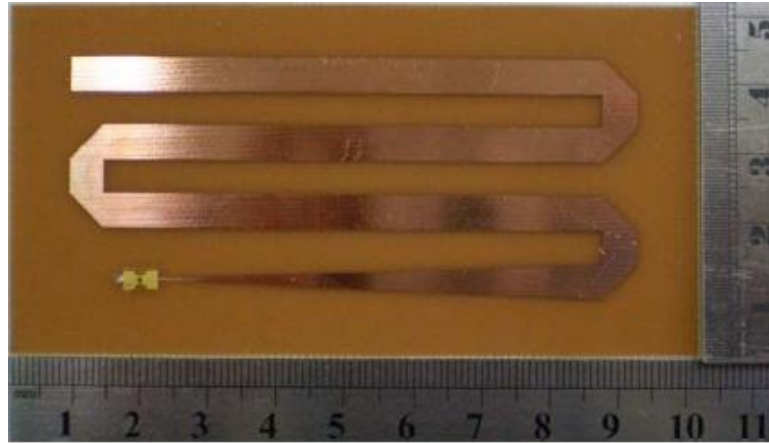


**Figure 2.19. Photograph of the Meandered Patch Antenna**  
(Source: Chen et al., 2010a)

## 2.8 Summary of Previous Work

Table 2.2 provides a summary of RFID tag antenna designs reviewed in Section 2.7. These antenna designs were reviewed in order to compare with antennas designed and measured in this thesis work. The table is classified by the design type, dimensions and some comments are provided for each design. The first five antenna structures discussed in Table 2.2 are used for objects tagging other than metals, while the rest of the table are for metallic objects identification. Some of the antenna types reviewed in the table belongs to the Minkowski fractal structure. There is burgeoning research conducted in this area actually but Table 2.2 is mainly intended to provide a general idea about the related RFID tag antenna designs rather than a complete review of the field.



**Table 2.2. Summary of the reviewed work on RFID tag antenna designs**

Reference	Design Method	Dimensions in mm <sup>3</sup>	Comments
Zhou et al. (2010)	Fractal folded dipole	24×7×0.8	Fractal design is aimed for size reduction and dual microwave frequencies resonance (2.4 and 5.8 GHz). It is simulated with 50 Ohm basis. PBG structure is integrated at the back plane to enhance return loss.
Kimouche et al. (2011)	Fractal dipole	78×30×1.58	Fractal design is aimed for size reduction. Designed and simulated with chip impedance having $P_{th}=-10$ dBm. Read range is around 5m.
Lee et al., (2008)	Fractal dipole	107.4×33.2×1.6	Two fractal patches dipole antenna with dual band operation. Design is 50 Ohm based according to results. Size is rather large.
Rusu et al. (2008)	Minkowski fractal loop	30 × 30 × 3	Minkowski fractal loop designed based on 50 Ohm. Gain is low because of small size, and the read range is 0.5 m even with high threshold chip ( $P_{th}=-18$ dBm).
Salama et al. (2008)	Minkowski fractal loop	90.66×77.5×1.59	A large size Minkowski fractal loop yielding good gain of 1.97 dBi and read range of 6.5 m. Chip threshold is not mentioned.
Chen et al. (2010b)	First PIFA array	65×45×0.8	Metal mount, designed without matching stub. Read range = 3.1 m. Large size.
Chen et al. (2010b)	Second PIFA array	127×52×0.8	Metal mount, designed with matching stub. Read range = 2.5 m. Very large size.
Chen (2009)	Loop	37×18×3.2	Metal mount, two layers antenna. Small size. Read range = 1.5 m with chip threshold $P_{th}=-14$ dBm.
Kim et al. (2012)	Bowtie dipole with AMC cavity	140×80×50	Long-range tag antenna for a recessed volume in metallic objects such as heavy equipment, vehicles, aircraft, and large-sized Containers. Very large size

			yielding very good gain of 6.47 dBi and long reading range of 23.74 m at 910 MHz. Chip threshold used is not mentioned.
<b>Liu et al. (2010)</b>	Meandered dipole with Minkowski fractal HIS	129×43×3.52	Metal mount two layered, one meandered dipole and the other is HIS. Size is very large. Reading range is 3.1 m. Chip threshold used is not mentioned.
<b>Chen et al., 2010a</b>	Meandered patch	100×50×0.8	Metal mount meandered patch. Large in size with reading range of 3.4 m. No information on threshold of used Chip.

## 2.9 Summary

In sum, this chapter is a general review of RFID tags covering their history, basic classifications, properties, and reported applications. In addition, this review summarizes studies of RFID tag antennas relevant to this thesis. These studies were summarized in a table for comparison purposes. The most important performance parameters for tag antenna design are the size and the reading range. According to Friis free-space transmission formula (Equation 2.16), the read range depends mainly on the antenna gain ( $G_r$ ) and the threshold power ( $P_{th}$ ) of the used RFID chip. The antenna size is a tradeoff with its gain and bandwidth. Concluding the chapter, the author of this thesis believes that there is still high potential for improving RFID antenna designs with better performance.

## CHAPTER 3

### METHODOLOGY

#### 3.1 Introduction

This chapter demonstrates the methodology used to design the RFID tag antennas presented in Chapters 4 and 5. It first presents the background and a brief history of Minkowski fractal structures. Secondly, it shows some details on the modified Minkowski fractal structure design used for RFID tag antennas in this thesis work, as well as the design parameters. Then a study on SRRs and CSRRs is conducted in terms of design structure and equivalent lumped circuit models, which are going to be integrated with RFID tag antenna designs. Lastly, a summary is given by the end of the chapter. The developed method for designing Minkowski fractal RFID tag antennas is illustrated in a flow chart shown in Figure 3.1.

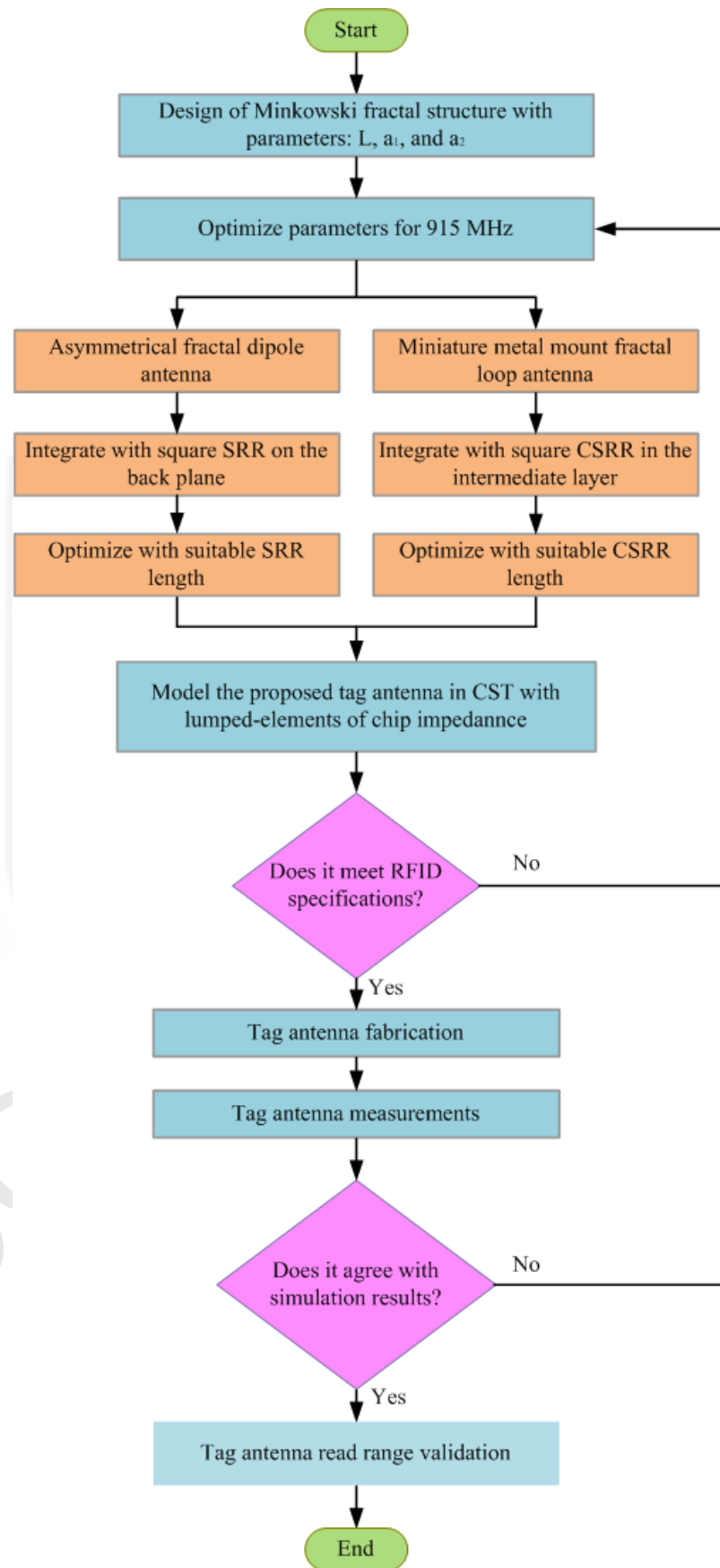


**Figure 3.1. Flow Chart of Minkowski Fractal Tag Antenna Design Process Integrated with SRR or CSRR**

### 3.2 Minkowski Fractal Structure

A fractal is a recursively generated object having a fractional dimension. The term fractal, which means broken or irregular fragments, was originally coined by (Mandelbort, 1983) to describe a family of complex shapes that possess an inherent self-similarity in their geometrical structures. Since then, a wide variety of applications for fractals has been found in many areas of science and engineering. One of the most promising areas of fractal electrodynamics research is its application to the antenna design.

After the original work of Mandelbrot, there emerged a wide variety of new shapes such as Sierpinski Gasket, Minkowski, Hilbert curve, Koch curve, Tree structure, fractal arrays, ...etc. More structures and applications for fractals can be found (Gianvittorio et al., 2002; Libbrecht, 2003; Werner et al., 2003). The self-similar design used in fractal antenna may increase the length or perimeter of the radiating element within a given surface area or volume. Fractal space filling contours means electrically large structures that can fit into small area. Since the electrical lengths play an important role in antenna design, this feature can be used as a viable miniaturization technique. The key aspect lies in their repetition of a motif over two or more size scaling, or 'iterations'. The space filling property of fractals tends to fill the area occupied by the antenna as the order of iteration is increased (Vinoy et al., 2010). Higher order fractal antennas exploit the space-filling property and enable miniaturization of antennas.

Figure 3.2(a) shows the original geometry which generates the Minkowski fractal structures. It is constructed by making  $a$  and  $b$  equal to one third of the horizontal line ( $L$ ), which is defined as the generator. If this contour is applied to the sides of the square patch (initiator) shown in Figure 3.2(b), by removing part of its area, one obtains 1<sup>st</sup> iteration as can be seen in Figure 3.2(c). The 1<sup>st</sup> iterated structure is used as the building block for the 2<sup>nd</sup> iteration and similar idea is used for further iterations. Figure 3.2(d) shows the 2<sup>nd</sup> iteration by applying the same criterion to each of the outer four squares of the 1<sup>st</sup> iteration structure.

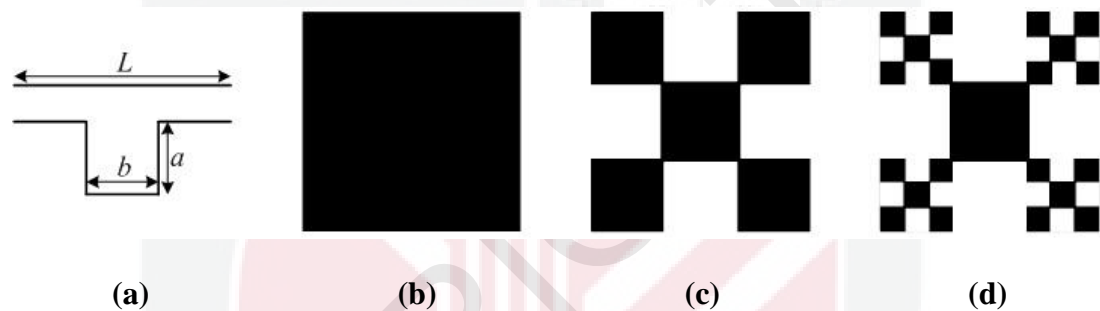


**Figure 3.2. The Iterative Generation of a Minkowski Fractal: (a) The Generator, (b) Square Patch, (Initiator), (c) The 1<sup>st</sup> Iteration and (d) The 2<sup>nd</sup> Iteration**  
 (Source: Mandelbort, 1983)

### 3.2.1 Modified Minkowski Fractal Structure Design

In this section, a modified Minkowski fractal structure is adopted. The modification on the previous structure is done by no more making  $a$  and  $b$  (Figure 3.2(a)) equal to each other neither equal to one third of the horizontal line  $L$ . Figure 3.3(a) shows the generator of this structure where in this case,  $b$  is done very small and assigned as  $W_1$ , while  $a$  might take any other value which usually does not exceed  $0.4L_0$  and

assigned as  $W_2$ . Generation steps of these fractal structures are illustrated in Figure 3.3 (Ali, 2007; Jalal, 2008).

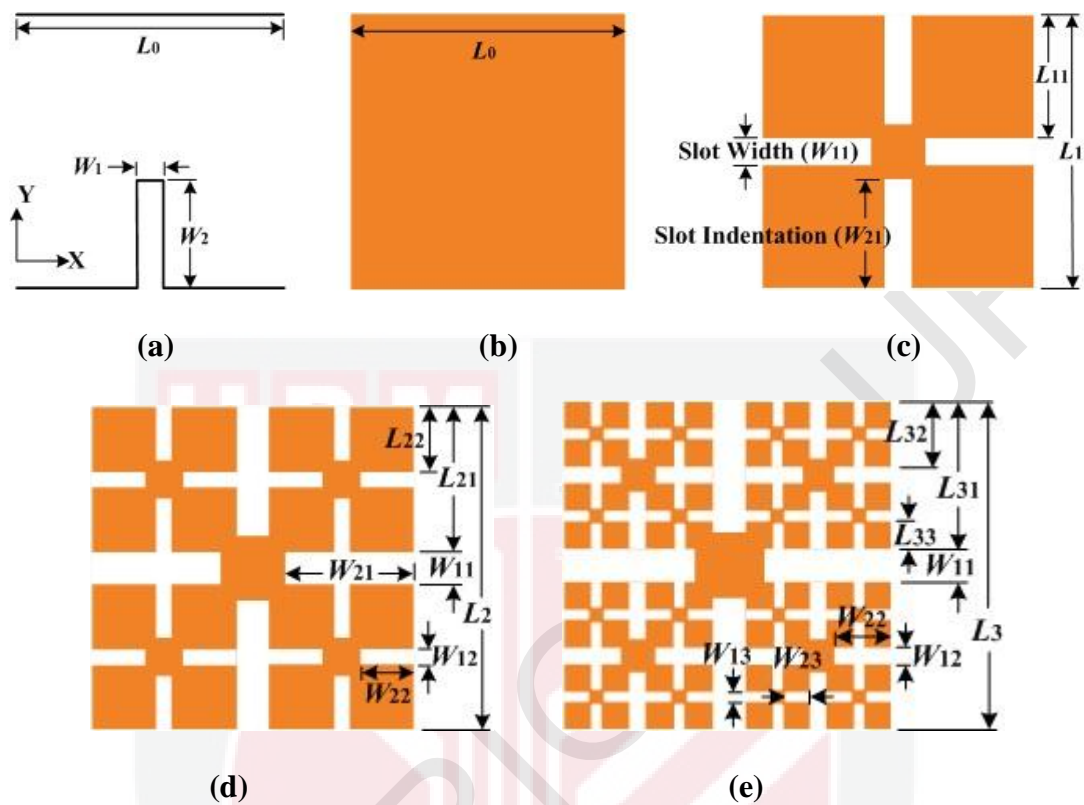


**Figure 3.3. Construction of the Modified Minkowski fractal Structure: (a) the Generator, (b) Square Patch (the Initiator), (c) 1<sup>st</sup> Iteration, (d) 2<sup>nd</sup> Iteration and (e) 3<sup>rd</sup> Iteration**  
(Source: Ali, 2007; Jalal, 2008)

By applying the generator structure of Figure 3.3(a) on the square patch of Figure 3.3(b), 1<sup>st</sup> iteration of the modified Minkowski fractal structure is obtained as shown in Figure 3.3(c). This 1<sup>st</sup> iteration structure contains two pairs of orthogonal rectangular slots. Each slot has a width ( $W_{11}$ ) and indentation ( $W_{21}$ ). The slot width and slot indentation are abbreviated as  $W_{xy}$ , where x stands for the width or indentation and takes the value of 1 or 2 respectively, while y stands for the iteration's number. The magnitudes of  $W_{11}$  and  $W_{21}$  are determined after choosing a suitable value of the slot width factor  $a_1$  and slot indentation factor  $a_2$  respectively where

$$a_1 = \frac{W_{11}}{L_1} \quad (3.1)$$

and

$$a_2 = \frac{W_{21}}{L_1} \quad (3.2)$$

To obtain the 2<sup>nd</sup> iteration of the modified Minkowski fractal structure, the generation criteria used in the 1<sup>st</sup> iteration process is applied on each of the four squares having side lengths of  $L_{11}$  in the 1<sup>st</sup> iteration structure shown in Figure 3.3(c), such that the 2<sup>nd</sup> iteration is constructed as shown in Figure 3.3(d). More orthogonal slots are obtained here which are smaller than those of the 1<sup>st</sup> iteration having smaller values of width and indentation according to Equation 3.3 as:

$$a_1 = \frac{W_{11}}{L_2} = \frac{W_{12}}{L_{21}} \quad (3.3)$$

and Equation 3.4 as:

$$a_2 = \frac{W_{21}}{L_2} = \frac{W_{22}}{L_{21}} \quad (3.4)$$

The 3<sup>rd</sup> iteration structure shown in Figure 3.3(e) is obtained by repeating the same procedure done to produce the 2<sup>nd</sup> iteration on the sixteen squares having side length of  $L_{22}$ , where in this case

$$a_1 = \frac{W_{11}}{L_3} = \frac{W_{12}}{L_{31}} = \frac{W_{13}}{L_{32}} \quad (3.5)$$

and

$$a_2 = \frac{W_{21}}{L_3} = \frac{W_{22}}{L_{31}} = \frac{W_{23}}{L_{32}} \quad (3.6)$$

According to (Falconer, 2003), since the generator used to develop the proposed modified Minkowski structure involves similarity transformations of more than one ratio;  $a_1$  and  $a_2$ , its dimension can be obtained from the solution of Equation 3.7:



$$2 \left[ \frac{1}{2} (1 - a_1) \right]^D + 2a_2^D + a_1^D = 1 \quad (3.7)$$

Where  $D$  represents the dimension,  $a_1$  and  $a_2$  are as denoted in Equations (3.1) to (3.6). The perimeter,  $P_n$  of the  $n^{\text{th}}$  iteration modified Minkowski fractal structure, is then calculated using (Ali et al., 2007) shown in Equation 3.8 as:

$$P_n = (1 + 2a_2)P_{n-1} \quad (3.8)$$

This modified Minkowski fractal structure is going to be considered for RFID tag antenna designs later in Chapters 4 and 5. In Chapter 4, the design is added with a T-shaped ground plane on the same side of the patch and a square SRR on the other side of the substrate; while in Chapter 5, two fractal patches are used as a top layer connected to a full-copper bottom layer through vias and inserted by a floating CSRR intermediate layer.

Since there are no general formulas that connect fractal geometry and antenna behavior, it was found for each design configuration some regularity that was used to guide our simulations. After a large number of simulations and measurements on modified Minkowski based configurations, the best ones are presented in Chapters 4 and 5.

### 3.2.2 Design Parameters

#### 1. The Effect of Square Patch Side Length ( $L$ ):

The square patch shown in Figure 3.3(b) (the initiator) has a certain side length value that determines the resonance frequency of a microstrip antenna designed with it. Calculations of the microstrip antenna length are based on

the transmission line model (Derneryd, 1976; Pozar, 1984; Ammam, 1997).

The length  $L_0$  is slightly less than a half wavelength in the dielectric.

Therefore, the main parameter affecting the resonance frequency is  $L_0$ .

## 2. The Effect of Slot Indentation Factor ( $a_2$ ):

Introducing a modified Minkowski fractal structure to the square patch (initiator) shown in Figure 3.3(b), will add more length to the perimeter of the original patch. This added length is due to the indentation factor ( $a_2$ ) added from the fractal structure slot. The perimeter of a square patch is calculated as in Equation 3.9:

$$P_0 = 4L_0 \quad (3.9)$$

When two pairs of perpendicular slots are constructed on the initiator to obtain the 1<sup>st</sup> iteration of the modified Minkowski fractal structure, the new structure will have a perimeter as shown in Equation 3.10 below:

$$P_1 = 4(L_0 + 2a_2L_0) \quad (3.10)$$

or

$$P_1 = 4L_0(1 + 2a_2) \quad (3.11)$$

Substituting 3.9 in 3.11,  $P_1$  will be as shown in Equation 3.12:

$$P_1 = P_0(1 + 2a_2) \quad (3.12)$$

This is actually the same as equation 3.8. Hence, by increasing the perimeter, the current path will increase yielding to lower resonant frequency. In order to keep the resonant frequency of the 1<sup>st</sup> iteration fractal structure equal to that of the original square patch (initiator), the side length ( $L_1$  in this case) should be decreased, thereby reducing the fractal patch size.

### 3.3 SRR and CSRR Design

An extensive analysis of the electromagnetic properties of SRRs and CSRRs is already presented in (Pendry et al., 1999; Smith et al., 2000; Marques et al., 2002; Gay-Balmaz et al., 2002; Marques et al., 2003). This analysis shows that SRRs behave as an LC resonator that can be excited by an external magnetic flux, exhibiting a strong diamagnetism above their first resonance. SRRs also exhibit cross-polarization effects (magneto-electric coupling) (Marques et al., 2002) so that excitation by a properly polarized time-varying external electric field is also possible. Figure 3.4 shows the basic topology of the SRR, as well as the equivalent lumped-circuit model proposed in (Marques et al., 2003). It is made of two concentric rings, each disconnected by a small gap. This gap strongly decreases the resonance frequency of the system. For this reason, it is possible to obtain a resonant structure with dimensions only a tenth of the corresponding wavelength, compared to a quarter of a wavelength for a closed ring (Gay-Balmaz et al., 2002). In Figure 3.4,  $C_o$  stands for the total capacitance between the rings as shown in Equation 3.13:

$$C_o = 2\pi r_o C_{pul} \quad (3.13)$$

where  $C_{pul}$  is the per unit length capacitance between the rings and  $r_o$  is the average radius of the two rings. The resonance frequency of the SRR is given by Equation 3.14 as:

$$f_o = \frac{1}{2\pi\sqrt{L_s C_s}} \quad (3.14)$$

where  $C_s$  is the series capacitance of the upper and lower halves of the SRR. The inductance  $L_s$  can be approximated by that of a single ring with radius  $r_o$  and width  $c$  (Marques et al., 2003).

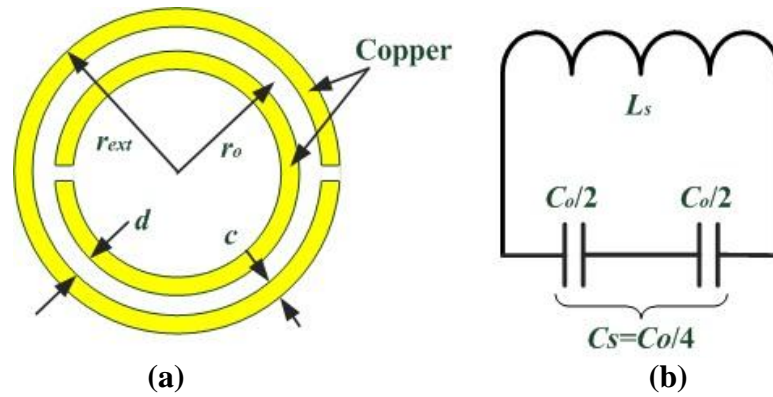


**Figure 3.4. (a) Basic layout of the SRR and (b) its Equivalent Lumped-Circuit Model**

(Source: Marques et al., 2003)

The aforementioned SRR structure is integrated in its square form with the modified Minkowski fractal structure discussed in section 3.2.1 to design three asymmetrical dipole antennas for RFID applications discussed later in Chapter 4. The added reactance from the SRR (due to  $C_s$  and  $L_s$ ) to the original antenna reactance shifts down the antenna resonance frequency thereby achieving further size reduction over that obtained from the fractal structure. The magnitude of the added reactance depends on the size of SRR. The SRR's size is considered as one of the antenna design parameters. Details of this antenna design and the SRR integration will be presented later in Chapter 4.

(Falcone et al., 2004) have shown that the complementary structures of SRRs have dual properties, if the effect of the metal thickness and losses of the dielectric substrate are neglected. Thus, when exciting the SRR by an axial magnetic field, it might be considered as a resonant magnetic dipole (Marques et al., 2003; Baena et al., 2005). Similarly, the CSRR essentially behaves as an electric dipole (with the same resonance frequency of its dual SRR) that can be excited by an axial electric

field. The basic structure of the CSRR, as well as the lumped-circuit model proposed in (Marques et al., 2003; Falcone et al., 2004) is shown in Figures 3.5(a) and (b).

The resonance frequency of the CSRR is given by Equation 3.15 as:

$$f_o = \frac{1}{2\pi\sqrt{L_c C_c}} \quad (3.15)$$

where  $C_c$  stands for the capacitance of a disk of radius  $r_o - c/2$  surrounded by a ground plane at a distance  $c$  of its edge, and  $L_c$  - is the parallel combination of the two inductances connecting the inner disk to the ground.

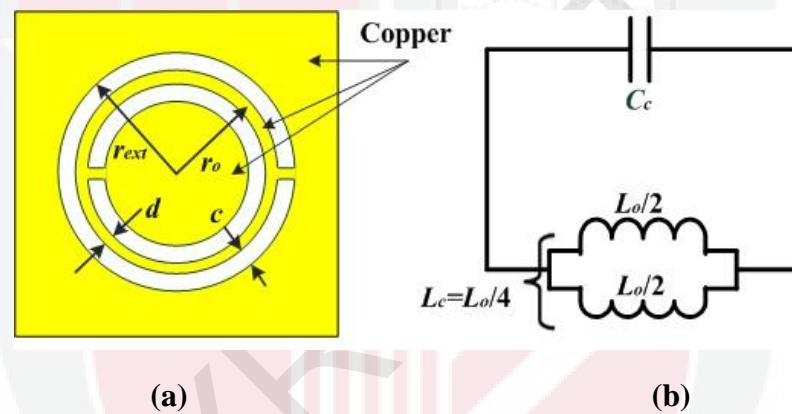


**Figure 3.5. (a) Basic Layout of the CSRR and (b) its Equivalent Lumped-Circuit Model**  
(Source: Marques et al., 2003; Falcone et al., 2004)

The above CSRR structure is integrated in its square form with the modified Minkowski fractal structure discussed in section 3.2.1 to design two metal mount loop antennas for RFID applications discussed later in Chapter 5. The added capacitance from the CSRR ( $C_c$  in this case) to the original antenna reactance shifts down the antenna resonance frequency thereby achieving further size reduction over that obtained from the fractal structure. The magnitude of the added reactance depends on the size of CSRR. The CSRR's size is considered as one of the antenna

design parameters. This antenna design together with CSRR integration is discussed in details later in Chapter 5.

### 3.4. Summary

In this chapter, the design methodology of two different types of RFID tag antennas for item level tagging, one integrated with SRRs and the other with CSRRs, based on the modified Minkowski fractal structure is presented. It has been shown that the fractal structures can be used for size reduction by increasing the fractal patch perimeter ( $P_n$ ). The perimeter is either increased by increasing the fractal patch length ( $L_n$ ), or by increasing the slot indentation factor ( $a_2$ ). The slot width factor has no effect on the perimeter. In addition, the integration of SRRs and CSRRs may offer further size reduction due to the added reactance. Parameters affecting antennas design in terms of resonant frequency and return loss has also been discussed which are: length ( $L$ ), indentation factor ( $a_2$ ), and SRR / CSRR size. The effect of variation of these parameters will be discussed in Chapters 4 and 5.

## CHAPTER 4

### MINKOWSKI FRACTAL ASYMMETRICAL RFID TAG ANTENNAS WITH SPLIT RING RESONATOR

#### 4.1 Introduction

Three antennas are proposed utilizing first, second, and third order iterations of modified Minkowski fractal structure with the aim of reducing the antenna size. The three antennas are loaded with a square Split Ring Resonator (SRR) on their back planes to achieve further size reduction. The antennas are designed and tuned to operate at 915 MHz frequency for passive RFID tags in the UHF band. The antennas were simulated and measured to verify their conjugate matching with chip impedance. The results of experimental tests showed that the three proposed RFID tags offer a maximum read range of 2.10 m, 1.10 m and 0.75 m. Details of antennas design and measurement results are presented and discussed. Measurement results are in good agreement with simulated results.

#### 4.2 Antennas Design

In this chapter, the modified Minkowski fractal geometry is used to design three asymmetrical fractal microstrip dipole antennas operating in the 915 MHz frequency band for UHF RFID applications. The three antenna designs are based on the 1<sup>st</sup>, 2<sup>nd</sup> and 3<sup>rd</sup> iteration of the modified Minkowski fractal shape shown in Figures 3.3 (c), (d) and (e) respectively, discussed earlier in Chapter 3. The three antenna structures consists of the modified Minkowski microstrip patch as a signal metallization and a

T-shaped microstrip ground plane on the same side of an FR4 substrate. The T-shaped structure is used to achieve excitation of the fractal patch near its center, since the foot print of the RFID chip used is only 0.5 mm (Murata MAGICSTRAP® Application Note, 2012).

The antennas were then loaded with a square SRR on their back planes to achieve their resonance shift to the desired frequency and enhance their performance in terms of return loss. The integration of the square SRRs performs a decrease in the resonant frequency because of its capacitance  $C_s$  and inductance  $L_s$  (as discussed in Chapter 3, section 3.3). The square SRR structure is shown in Figure 4.1. It consists of two concentric square rings with opposite splits,  $g$  of 1 mm, in the  $x$ - $y$  plane. Both rings have equal line widths and spacing of  $g$  which is also 1 mm, and a copper thickness of 0.035 mm. The side length of the outer square is assigned as  $SRR$ . The length of  $SRR$  for each antenna is tuned such that it gives a better return loss than the antenna without SRR as well as the shift of resonant frequency due to the added reactance. The three antenna designs were simulated and measured with and without the SRR to show its effect.

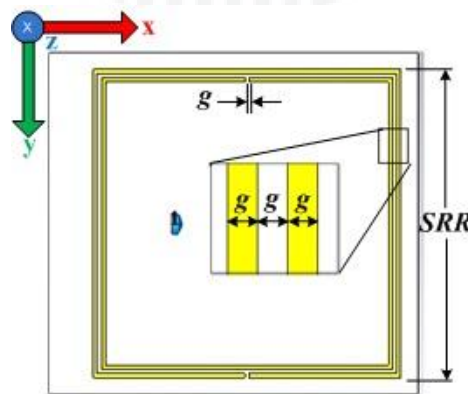


**Figure 4.1. Layout of the Square SRR Design**



Figure 4.2(a) and (b) depicts the lumped-element circuit diagrams of the proposed RFID tag antenna with and without SRR layer. Figure 4.2(b) illustrates the added capacitance ( $C_s$ ) considered in the model as well as the inductance  $L_s$ . Figure 4.2(c) illustrates the complete circuit model of the tag antenna. The lumped-element circuit model given in Figure 4.2 applies to the three asymmetrical fractal dipole antenna designs in this chapter. The only difference between SRRs used for each antenna is the size of the outer square ring. Each size of which gives a little bit different inductance and capacitance.

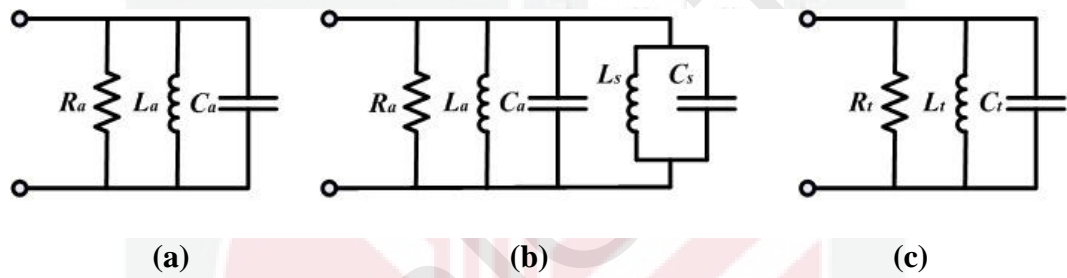


**Figure 4.2. Lumped-Element Circuit Model of (a) Proposed Tag Antenna, (b) Proposed Tag Antenna with SRR Layer and (c) the Proposed RFID Tag Antenna Overall Equivalent Lumped-Element Model**

#### 4.2.1 Asymmetrical Antenna 1 (ANI)

The first asymmetrical antenna is designed using the 1<sup>st</sup> iteration as shown in Figure 4.3(a). This asymmetrical tag antenna design is named as (ANI). The antenna structure consists of a microstrip fractal patch as a signal metallization and a T-shaped microstrip ground plane on the same side of an FR4 substrate. The antenna size is  $82 \times 88.59 \times 1.6 \text{ mm}^3$ .

Dimensions labeled on Figures 4.3(a) and (c) are given in Table 4.1. The design was based on setting  $a_1$  and  $a_2$  to be equal to 0.1 and 0.3 respectively for best antenna performance. Photograph of the assembled RFID tag antenna  $ANI$  is shown in Figure 4.3(b).

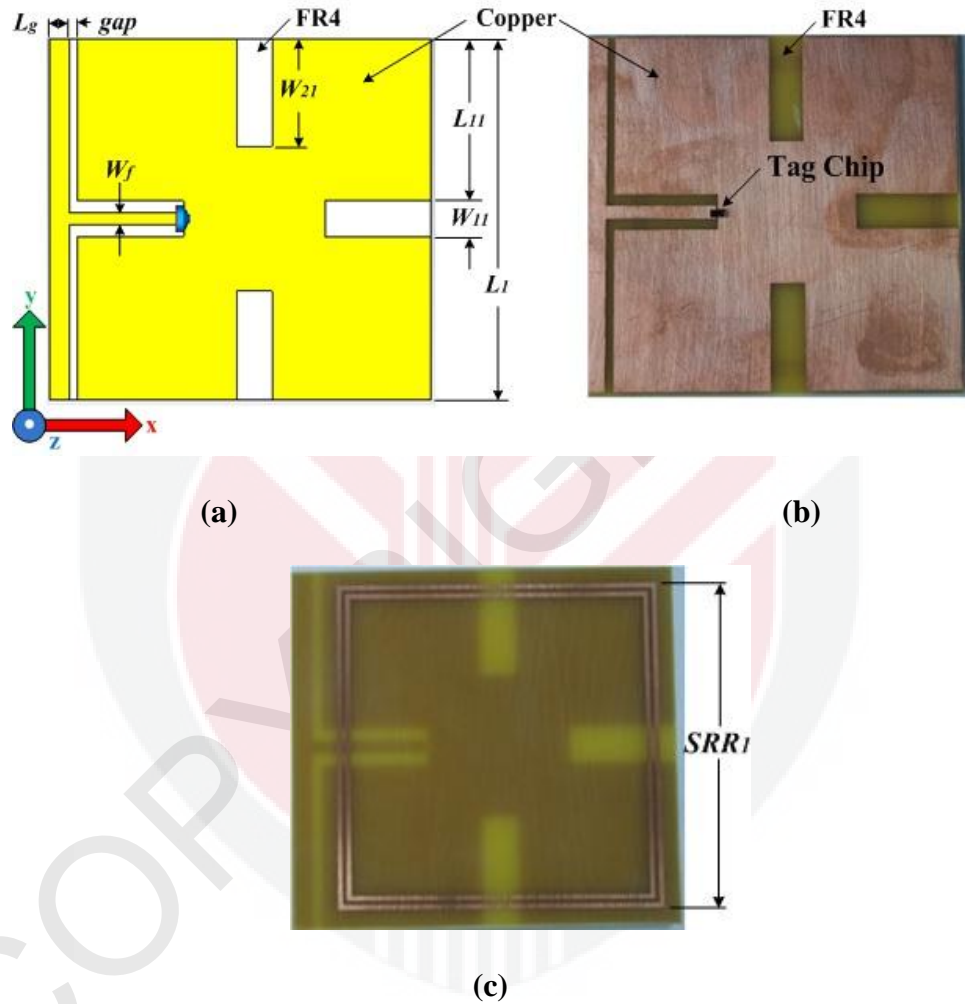


**Figure 4.3. (a) Layout of Antenna ANI, (b) its Photograph with Tag Chip and (c) Photograph of  $SRR_1$**

**Table 4.1: Dimensions of antenna ANI**

Parameter	Dimension (mm)
Total square side length ( $L_I$ )	82
First iteration square side length ( $L_{I1}$ )	36.9
First iteration slot width ( $W_{I1}$ )	8.2
First iteration slot indentation ( $W_{2I}$ )	24.6
Gap between T-shape and fractal shape ( $gap$ )	2
Feed element width ( $W_f$ )	3
T-shape length ( $L_g$ )	4.59
SRR outer square side length ( $SRR_I$ )	74

Figures 4.4 (a), (b) and (c) shows the simulated responses of the input impedances of ANI with different values fractal patch lengths ( $L_I$ ), indentation factor ( $a_2$ ) and the SRR outer square side length ( $SRR_I$ ). Figure 4.4(a) clearly shows that the larger length of patch results in lower resonant frequency of the RFID tag antenna. This is because of the well known feature of antenna design in terms of the relation between size and resonant frequency. Figure 4.4(b) shows the antenna impedance simulation results for different values of indentation factor ( $a_2$ ). It is clear that by increasing  $a_2$ , the fractal patch perimeter ( $P_n$ ) increases too as discussed in Chapter 3, Section 3.2.2. Hence, by considering first a square patch of length  $L_0=82$  mm without fractalation, its perimeter will be as shown in Equation 4.2:

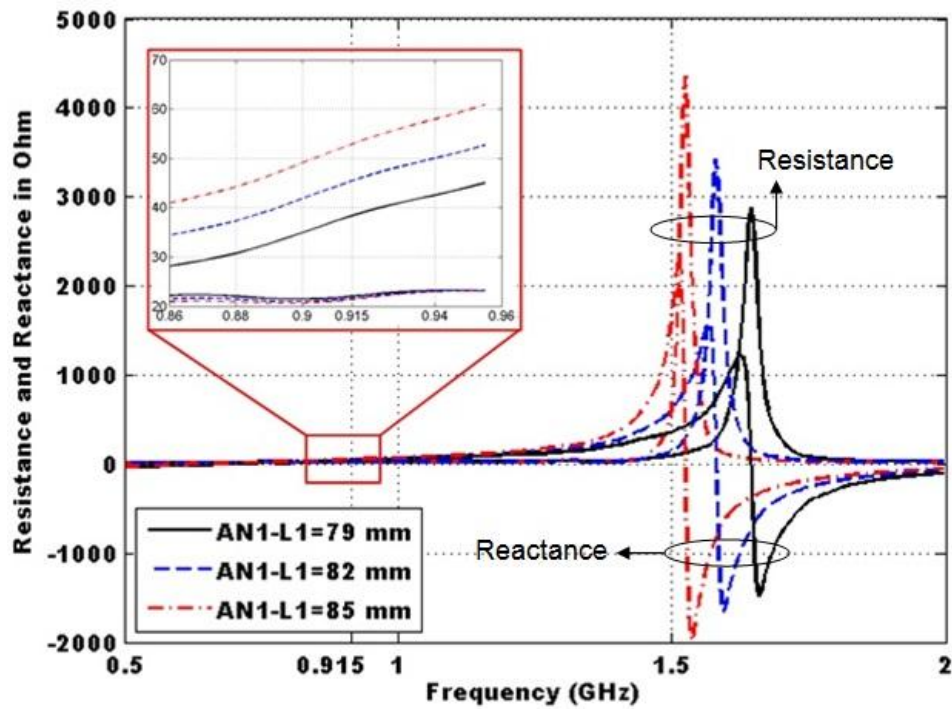
$$P_0 = 4L_0 = 4 \times 82 = 336 \text{ mm} \quad (4.1)$$

By applying the 1<sup>st</sup> iteration of the modified Minkowski fractal structure and using Equation 3.8, the new perimeter will be as shown in Equation 4.3:

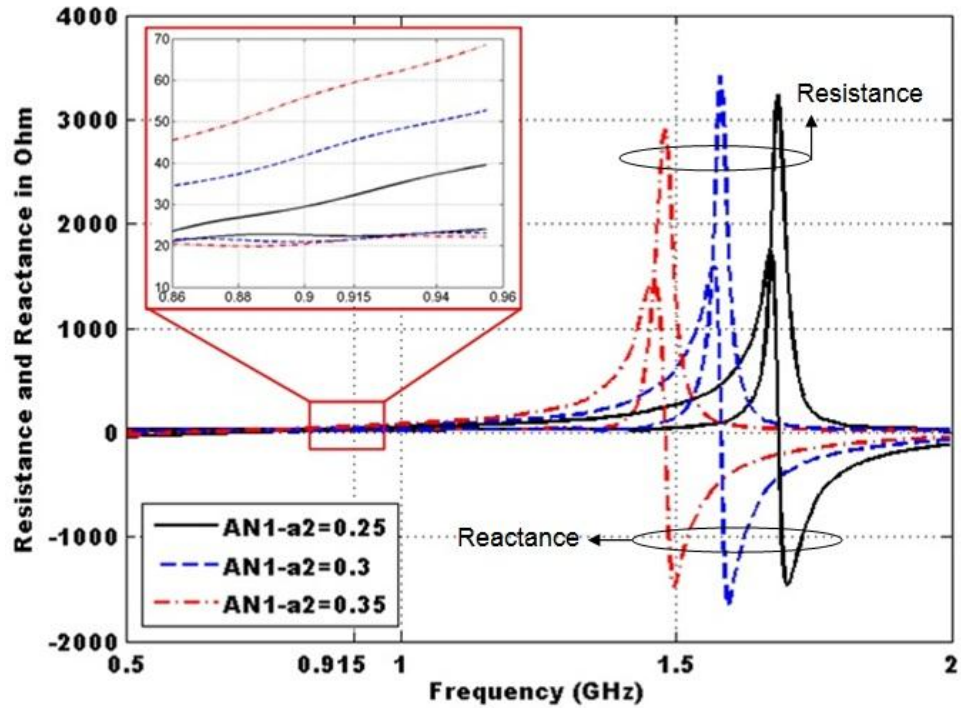
$$P_1 = (1 + 2a_2)P_0 = (1 + 2 \times 0.3)336 = 537.6 \text{ mm} \quad (4.2)$$

$P_1$  is 60% ( $2 \times 0.3$ ) longer than  $P_0$  which actually means that the electrical length of the current path in the designed antenna is increased thereby decreasing the resonant frequency.

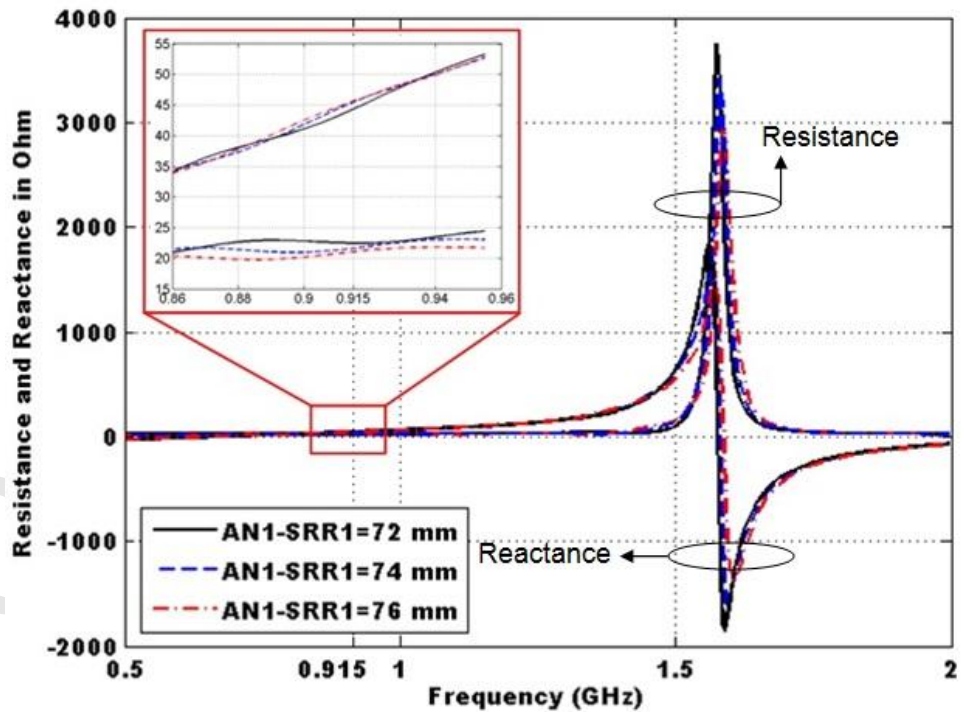
Figure 4.4 (c) shows the simulated results of the input impedances of ANI with different values of SRR lengths ( $SRR_l$ ). From the figure, it is clear that the larger SRR length results in lower antenna self-resonant frequency that is achieved by increasing the antenna reactance due to the added capacitance ( $C_s$ ) from the SRR as discussed in Chapter 3, Section 3.3. Figure 4.4 (c) also shows that a considerable change of the square SRR size results into a small change in the antenna self-resonance frequency. This feature may be useful in antenna fine tuning.



(a)



(b)



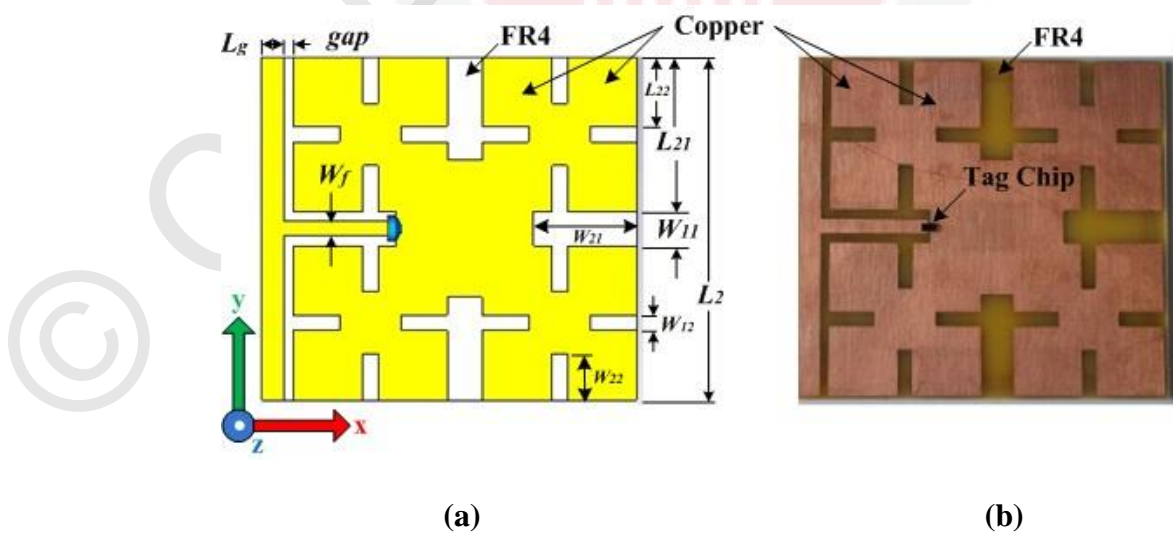
(c)

Figure 4.4. Simulation Results of Antenna AN1 Input Impedances with Different Values of: (a) Fractal Patch Length  $L_1$ , (b) Indentation Factor  $a_2$  and (c) SRR Outer Square Side Length ( $SRR_1$ ) ( $L_1$  and  $SRR_1$  are as Denoted in Figure 4.3)

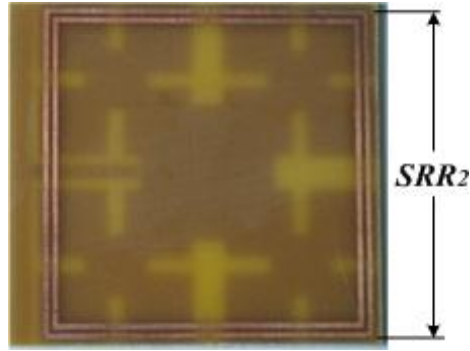
#### 4.2.2 Asymmetrical Antenna 2 (AN2)

The second asymmetrical antenna is designed using the second iteration as shown in Figure 4.5(a). This asymmetrical tag antenna design is named as (AN2). The antenna structure consists of a second iteration modified Minkowski microstrip fractal patch as a signal metallization and a T-shaped microstrip ground plane on the same side of an FR4 substrate. The antenna size is  $72 \times 78.59 \times 1.6 \text{ mm}^3$ .

Dimensions labeled on Figures 4.5(a) and (c) are given in Table 4.2. The design was also based on setting  $a_1$  and  $a_2$  to be equal to 0.1 and 0.3 respectively. Since this antenna design is based on the 2<sup>nd</sup> iteration fractal shape, its fractal patch perimeter  $P_2$  (discussed in Chapter 3, Equation 3.8) is more than that of AN1 ( $P_1$ ), thus verifying the concept of antenna size reduction. Design parameters show that antenna AN2 has a size reduction of 22% from that of antenna AN1. Photograph of the assembled RFID tag AN2 is shown in Figure 4.5(b).







(c)

Figure 4.5. (a) Layout of Antenna AN2, (b) its Photograph with Tag Chip and (c) Photograph of SRR<sub>2</sub>

Table 4.2: Dimensions of antenna AN2

Parameter	Dimension (mm)
Total square side length ( $L_2$ )	72
First iteration square side length ( $L_{21}$ )	32.4
Second iteration square side length ( $L_{22}$ )	14.58
First iteration slot width ( $W_{11}$ )	7.2
Second iteration slot width ( $W_{12}$ )	3.24
First iteration slot indentation ( $W_{21}$ )	21.6
Second iteration slot indentation ( $W_{22}$ )	9.72
Gap between T-shape and fractal shape ( $gap$ )	2
Feed element width ( $W_f$ )	3
T-shape length ( $L_g$ )	4.59
SRR outer square side length ( $SRR_2$ )	70

Figures 4.6 (a), (b) and (c) shows the simulated responses of the input impedances of AN2 with different values fractal patch lengths ( $L_2$ ), indentation factor ( $a_2$ ) and the SRR outer square side length ( $SRR_2$ ). Figure 4.6(a) clearly shows that by increasing patch length, antenna resonant frequency is lowered. This is because of the well known feature of antenna design in terms of the relation between size and resonant frequency. Figure 4.6(b) shows the antenna impedance simulation results for different values of indentation factor ( $a_2$ ). For this antenna, and assuming that a

square patch of length  $L_0=72$  mm without fractalation, its perimeter will be as shown in Equation 4.4:

$$P_0 = 4L_0 = 4 \times 72 = 288 \text{ mm} \quad (4.3)$$

By applying the 1<sup>st</sup> iteration of the modified Minkowski fractal structure and using Equation 3.8, the new perimeter will be as in Equation 4.5:

$$P_1 = (1 + 2a_2)P_0 = (1 + 2 \times 0.3)288 = 460.8 \text{ mm} \quad (4.4)$$

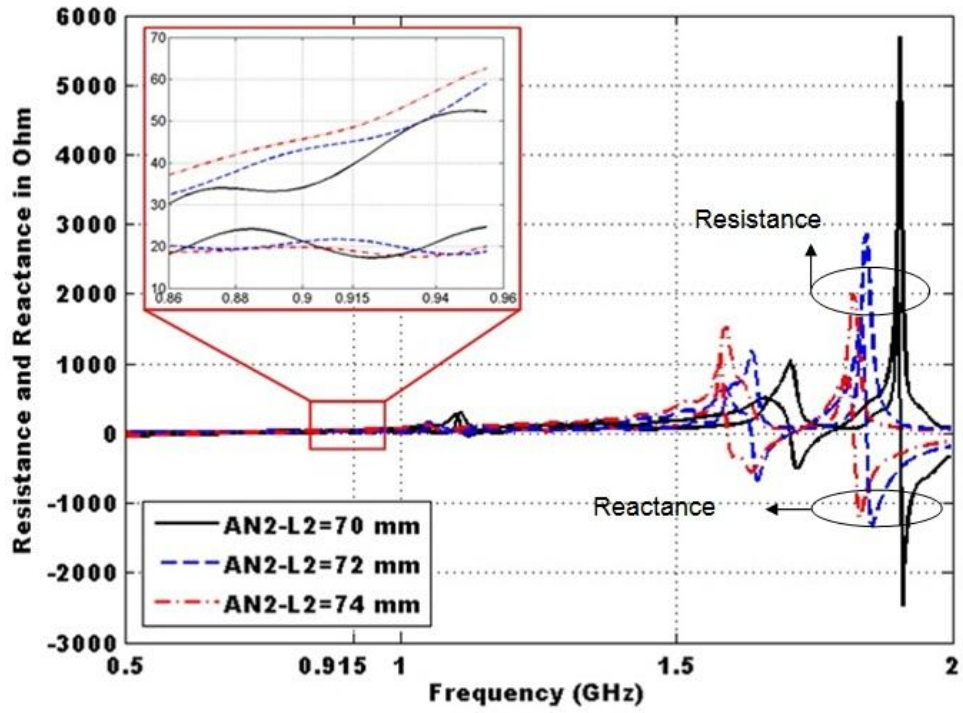
and after the 2<sup>nd</sup> iteration, the perimeter will be as in Equation 4.6:

$$P_2 = (1 + 2a_2)P_1 = (1 + 2 \times 0.3)460.8 = 737.28 \text{ mm} \quad (4.5)$$

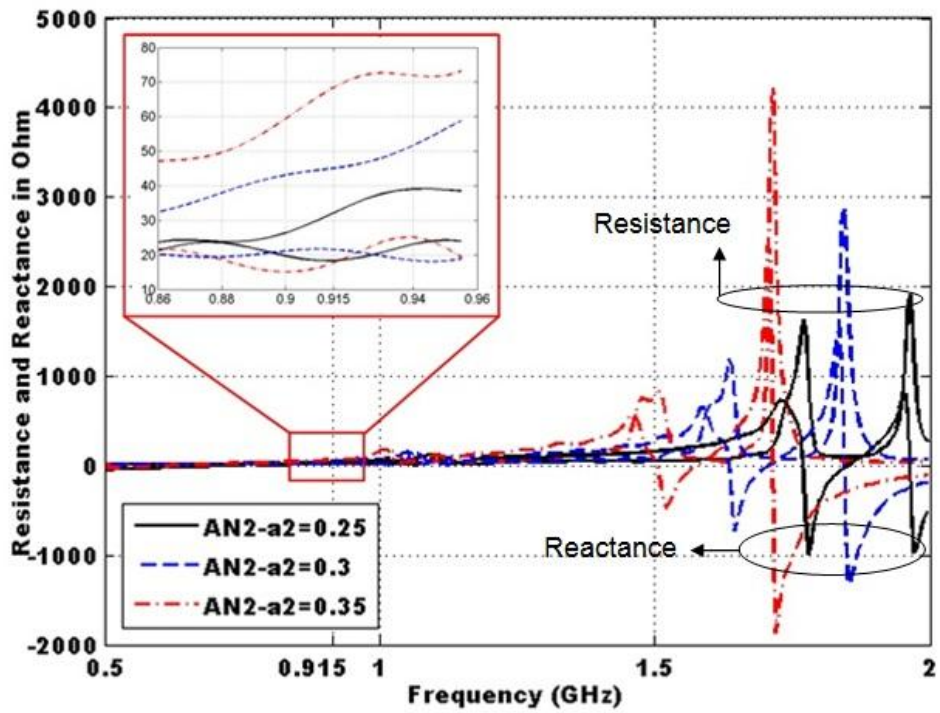
Again,  $P_1$  is 60% ( $2 \times 0.3$ ) longer than  $P_0$  and  $P_2$  is also 60% longer than  $P_1$  which means that  $P_2$  is 2.56 times longer than  $P_0$ . Hence, a further increase in the electrical length means a more decrease in the resonant frequency. By maintaining the same desired resonant frequency of 915 MHz, antenna miniaturization is obtained by decreasing the patch length  $L_2$  over  $L_1$ .

Figure 4.6 (c) shows the simulated results of the input impedances of AN2 with different values of SRR lengths ( $SRR_2$ ). From the figure, it is clear that the larger SRR length results in lower antenna self-resonant frequency that is achieved by increasing the antenna reactance due to the added capacitance ( $C_s$ ) from the SRR as discussed in Chapter 3, Section 3.3. Figure 4.6 (c) also shows that a considerable change of the square SRR size results into a small change in the antenna self-resonance frequency. This feature may be useful in antenna fine tuning.

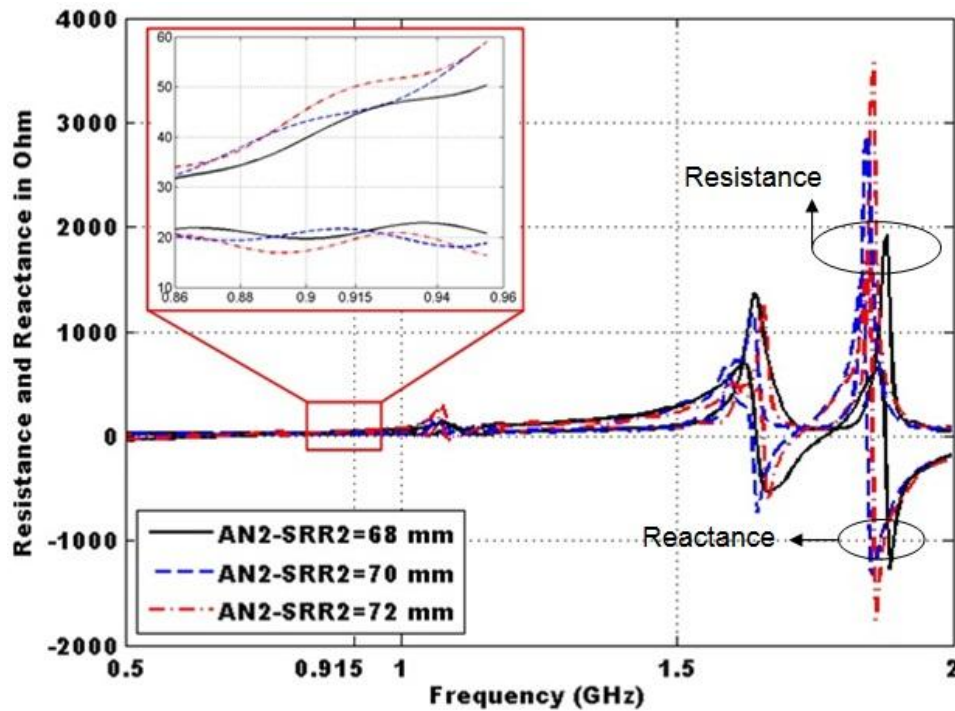




(a)



(b)



(c)

**Figure 4.6. Simulation Results of Antenna AN2 Input Impedances with Different Values of: (a) Fractal Patch Length  $L_2$ , (b) Indentation Factor  $a_2$  and (c) SRR Outer Square Side Length ( $SRR_2$ ) ( $L_2$  and  $SRR_2$  are as Denoted in Figure 4.5)**

### 4.2.3 Asymmetrical Antenna 3 (AN3)

In an attempt for further miniaturization, a third iteration asymmetrical antenna is also designed as shown in Figure 4.7(a). This asymmetrical tag antenna design is named as (AN3). The antenna structure consists of a 3<sup>rd</sup> iteration modified Minkowski microstrip fractal patch as a signal metallization and a T-shaped microstrip ground plane on one side of an FR4 substrate. The antenna size is  $66.5 \times 73.09 \times 1.6 \text{ mm}^3$ . Dimensions labeled on Figures 4.7(a) and (c) are given in Table 4.3. The design was also based on setting  $a_1$  and  $a_2$  to be equal to 0.1 and 0.3. As in AN2 design, and since AN3 design is based on 3<sup>rd</sup> iteration, the fractal patch perimeter ( $P_3$ ) is more than  $P_2$  and  $P_1$ , thus yielding to more antenna size reduction.

Design parameters show that antenna AN3 has a size reduction of 14% from that of antenna AN2 and 32% over that of AN1 for the same resonance frequency.

Photograph of the assembled RFID tag AN3 is shown in Figure 4.7(b).

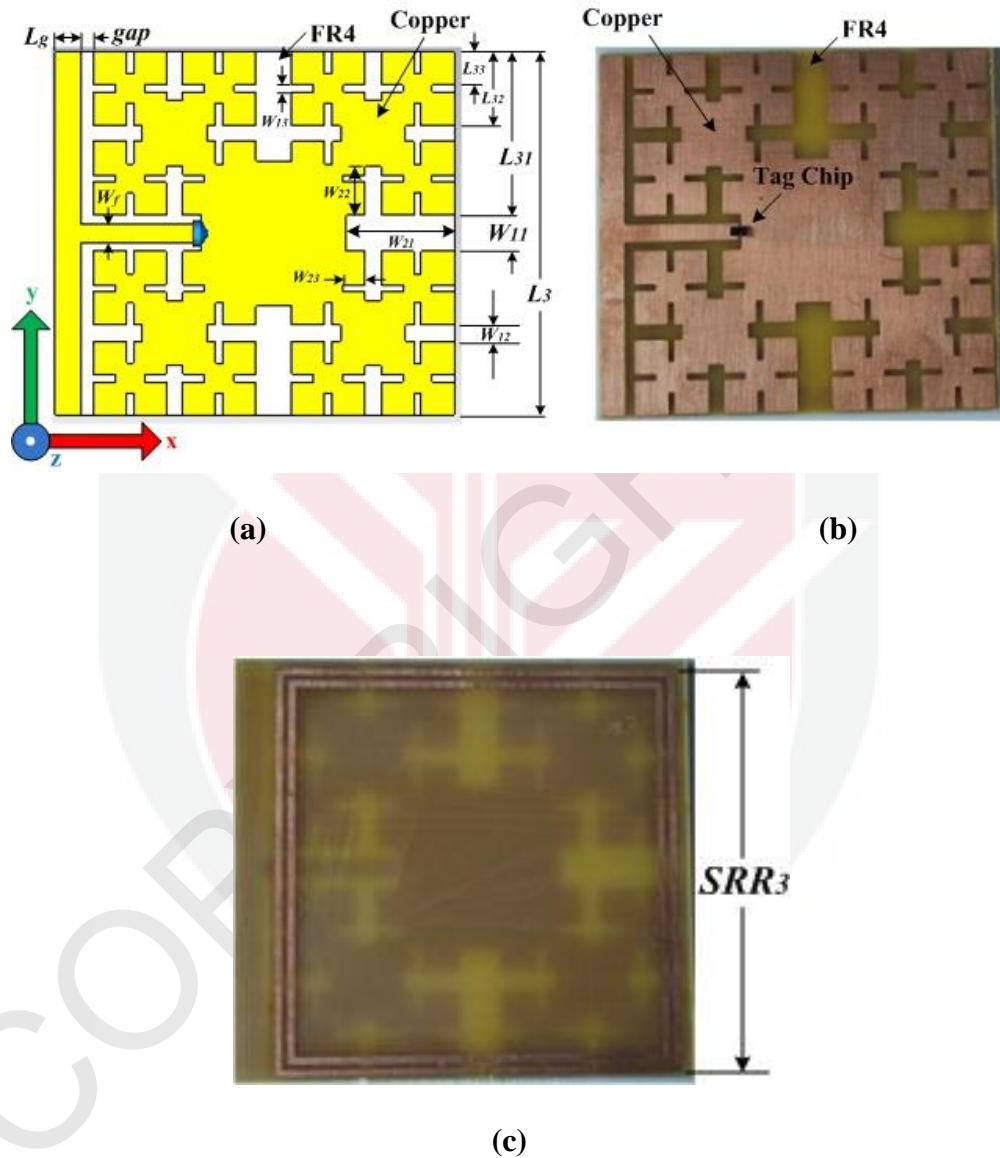


**Figure 4.7. (a) Layout of Antenna AN3, (b) its Photograph with Tag Chip and (c) Photograph of  $SRR_3$**

**Table 4.3: Dimensions of antenna AN3**

Parameter	Dimension (mm)
Total square side length ( $L_3$ )	66.5
First iteration square side length ( $L_{31}$ )	29.925
Second iteration square side length ( $L_{32}$ )	13.46625
Third iteration square side length ( $L_{33}$ )	6.059813
First iteration slot width ( $W_{11}$ )	6.65
Second iteration slot width ( $W_{12}$ )	2.9925
Third iteration slot width ( $W_{13}$ )	1.346625
First iteration slot indentation ( $W_{21}$ )	19.95
Second iteration slot indentation ( $W_{22}$ )	8.9975
Third iteration slot indentation ( $W_{23}$ )	4.039875
Gap between T-shape and fractal shape ( $gap$ )	2
Feed element width ( $W_f$ )	3
T-shape length ( $L_g$ )	4.59
SRR outer square side length ( $SRR_3$ )	65

Figures 4.8 (a), (b) and (c) shows the simulated responses of the input impedances of AN3 with different values fractal patch lengths ( $L_3$ ), indentation factor ( $a_2$ ) and the SRR outer square side length ( $SRR_3$ ). Figure 4.8(a) clearly shows that by increasing patch length, antenna resonant frequency is lowered. Figure 4.7(b) shows the antenna impedance simulation results for different values of indentation factor ( $a_2$ ). For this antenna, and assuming that a square patch of length  $L_0=66.5$  mm without fractalation, its perimeter will be as shown in Equation 4.7:

$$P_0 = 4L_0 = 4 \times 66.5 = 266 \text{ mm} \quad (4.6)$$

By applying the 1<sup>st</sup> iteration of the modified Minkowski fractal structure and using Equation 3.8, the new perimeter will be as in Equation 4.8:

$$P_1 = (1 + 2a_2)P_0 = (1 + 2 \times 0.3)266 = 425.6 \text{ mm} \quad (4.7)$$

and after the 2<sup>nd</sup> iteration, the perimeter will be as in Equation 4.9:

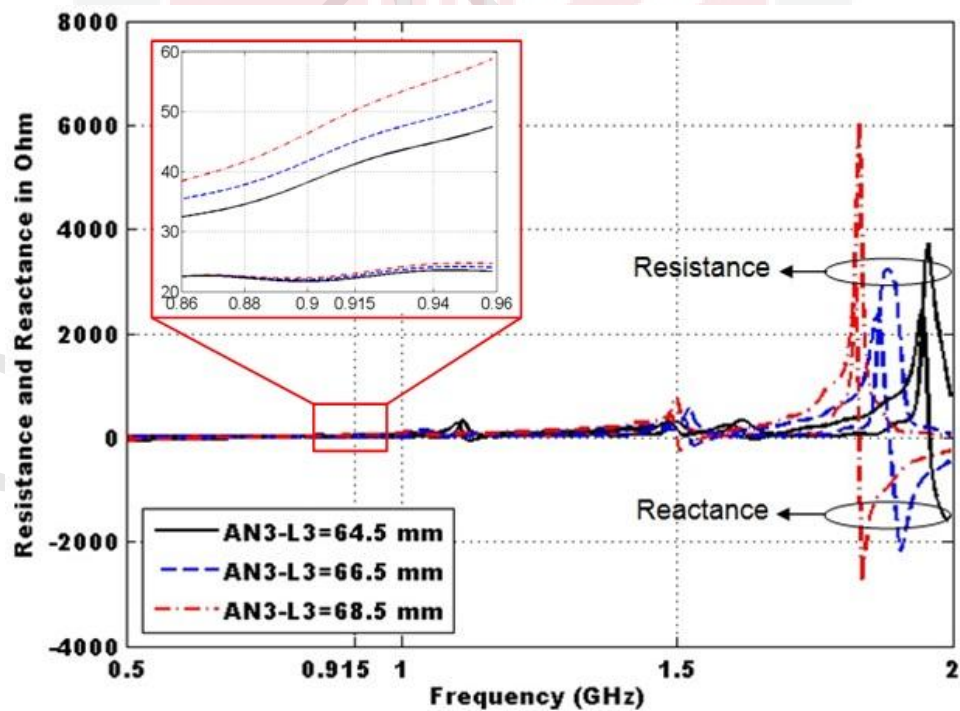
$$P_2 = (1 + 2a_2)P_1 = (1 + 2 \times 0.3)425.6 = 680.96 \text{ mm} \quad (4.8)$$

Performing the 3<sup>rd</sup> iteration, the perimeter  $P_3$  will be as in Equation 4.10:

$$P_3 = (1 + 2a_2)P_2 = (1 + 2 \times 0.3)680.96 = 1089.636 \text{ mm} \quad (4.9)$$

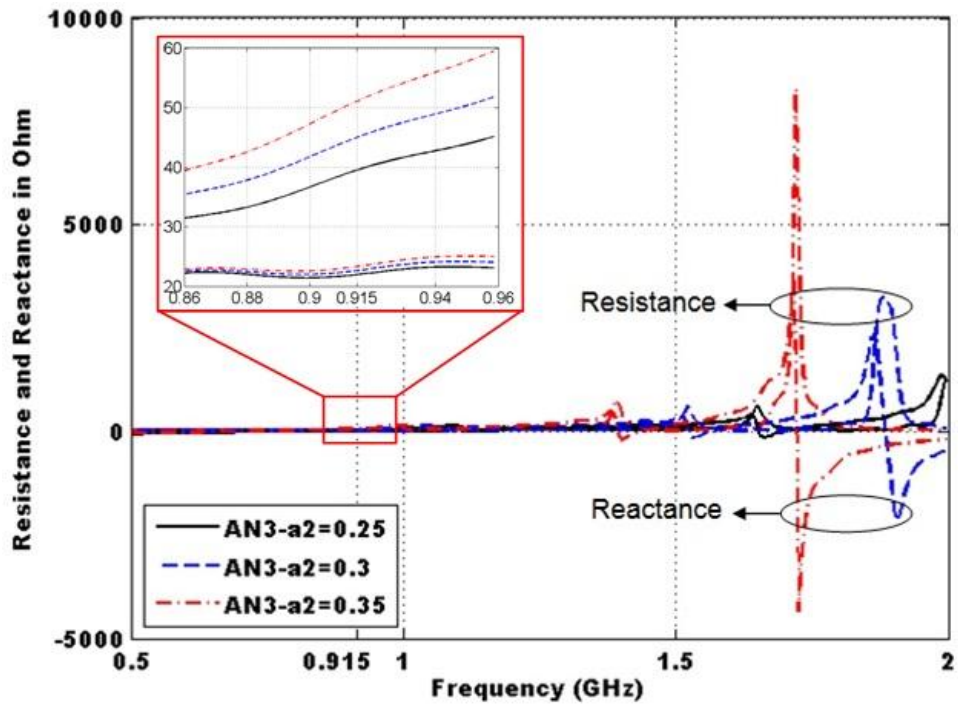
After each iteration ( $n$ ), the perimeter of the fractal patch ( $P_n$ ) is 60% longer than the perimeter of the previous ( $P_{n-1}$ ). In total,  $P_3$  is more than 4 times longer than  $P_0$  for AN3. Hence, a further increase in the electrical length for AN3 over AN2 and AN1 which means more decrease in the resonant frequency. By maintaining the same desired resonant frequency of 915 MHz, more antenna miniaturization is obtained by decreasing the patch length  $L_2$  over  $L_1$  and  $L_2$ .

Figure 4.8 (c) shows the simulated results of the input impedances of AN3 with different values of SRR lengths ( $SRR_3$ ). From the figure, it is clear that the larger SRR length results in lower antenna self-resonant frequency that is achieved by increasing the antenna reactance due to the added capacitance ( $C_s$ ) from the SRR as discussed in Chapter 3, Section 3.3.

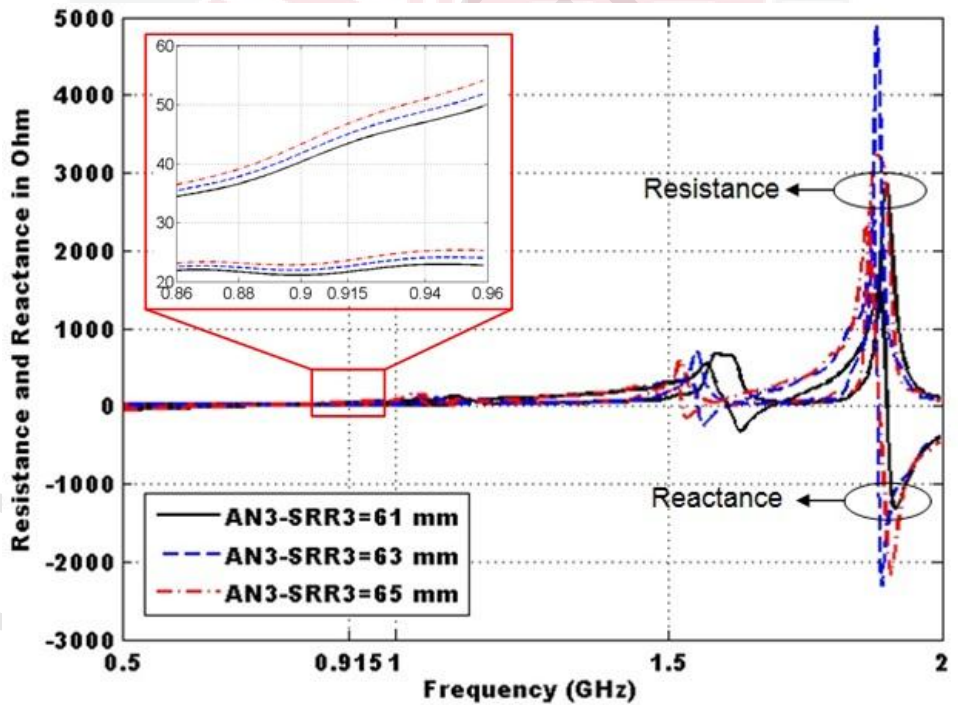


(a)





(b)



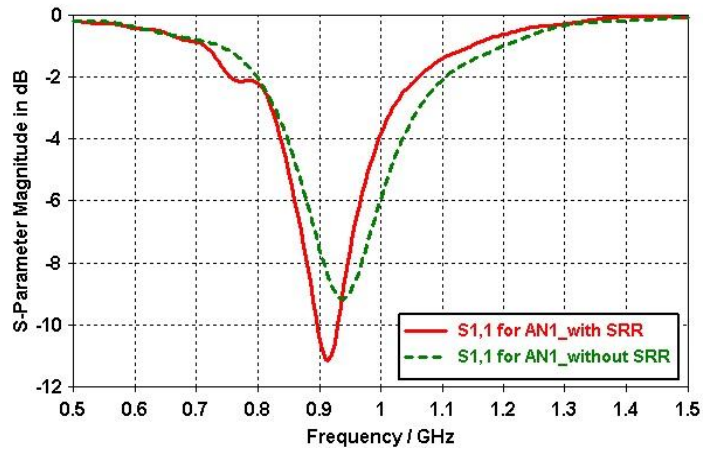
(c)

Figure 4.8. Simulation Results of Antenna AN3 Input Impedances with Different Values of: (a) Fractal Patch Length  $L_3$ , (b) Indentation Factor  $a_2$  and (c) SRR Outer Square Side Length ( $SRR_3$ ) ( $L_3$  and  $SRR_3$  are as Denoted in Figure 4.7)

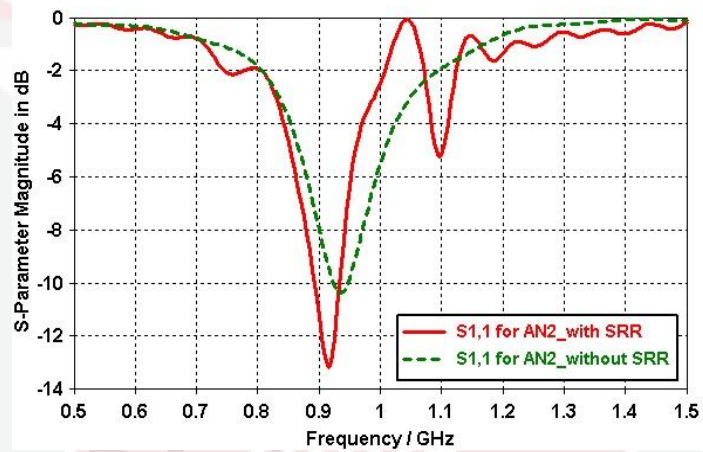
### 4.3 Results and Discussion

The geometry of the three antenna designs is etched on an epoxy FR4 substrate with thickness,  $h = 1.53$  mm, dielectric constant  $\epsilon_r = 4.4$ , copper thickness on each side  $t=0.035$  mm and loss tangent of 0.02.

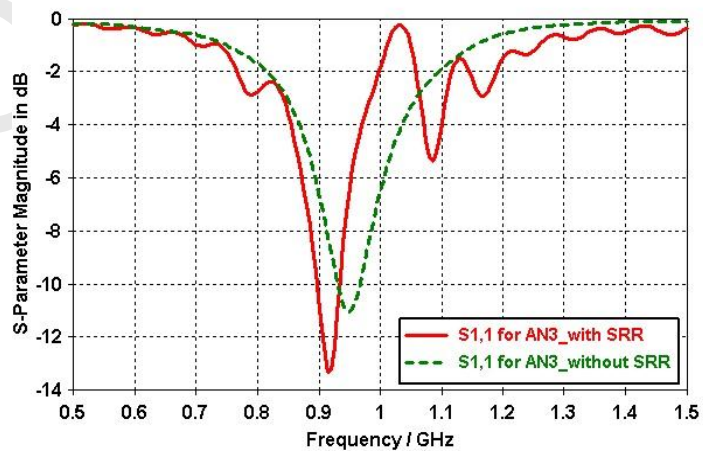
The three designed RFID tag antennas were modeled and simulated using full-wave electromagnetic simulator (CST Microwave Studio, 2010). The antennas were simulated with and without the SRR loading. Figure 4.9 (a), (b) and (c) shows  $S_{11}$  of the three antennas  $AN1$ ,  $AN2$  and  $AN3$  respectively; simulated by considering chip impedance lumped-element values of  $(25-j45) \Omega$  in CST Microwave Studio. It is clear from Figure 4.9 that the antennas present different values of  $S_{11}$  when simulated without SRR in the same frequency range (0.5-1.5 GHz). Antenna  $AN1$  resonates at around 940 MHz with  $S_{11} = -9.0$  dB without SRR loading, while it performs better with  $S_{11} = -11.0$  dB at the operating frequency of 915 MHz with SRR. Antenna  $AN2$  resonates at around 935 MHz with  $S_{11} = -10.2$  dB without SRR loading, while it performs better with  $S_{11} = -12.5$  dB at the operating frequency of 915 MHz with SRR. Antenna  $AN3$  resonates at around 950 MHz with  $S_{11} = -11.0$  dB without SRR loading, while it performs better with  $S_{11} = -13.2$  dB at the operating frequency of 915 MHz with SRR. Consequently, and according to the previous discussion on the SRR's square side length effect ( $SRR_n$ ) in Section 4.2 which is based on Section 3.3 in the design methodology, it is clearly shown that the advantage of integrating SRRs to the antenna designs is to further decrease the resonant frequency over that obtained from fractalation, hence offering more size reduction and enhances the return loss due to the added reactance from SRRs.



(a)



(b)

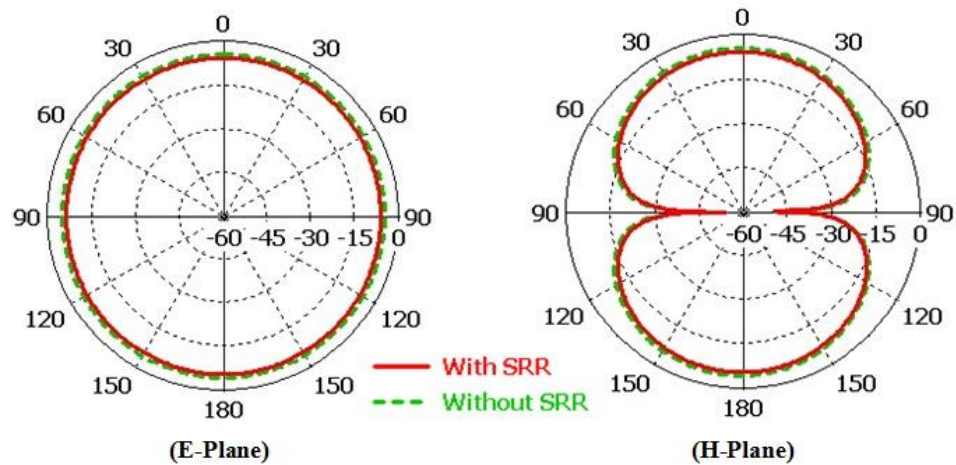


(c)

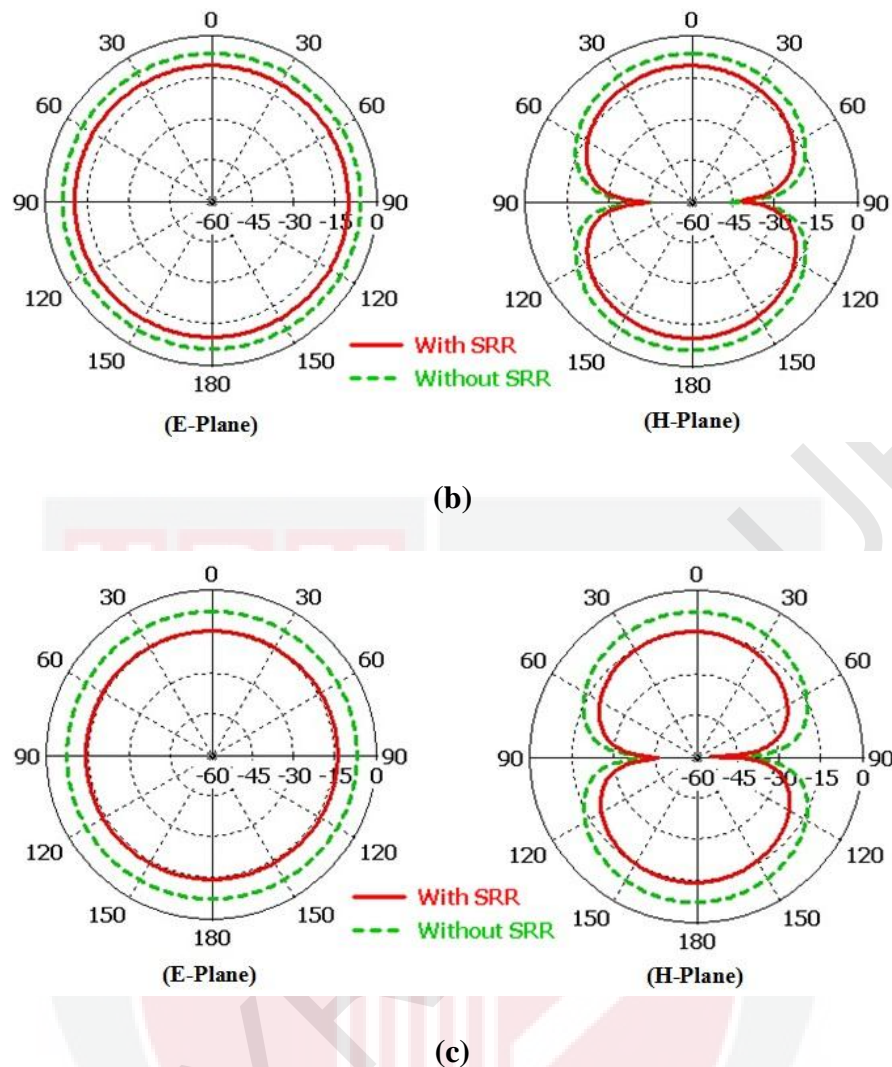
**Figure 4.9. Simulated  $S_{11}$  of the Three Antennas with and without SRR for: (a) Antenna AN1, (b) Antenna AN2 and (c) Antenna AN3**



Figure 4.10(a), (b) and (c) plots both E- and H-plane simulated radiation patterns of the three tag antennas' gains. As the results revealed, the integration of SRR structures has degraded antennas' gains compared to that without SRRs, because of the further size reduction achieved by the added capacitance ( $C_s$ ) from the SRR. The gain of the designed tag antenna is a trade off with its miniaturized structure. However, a good improvement is achieved in terms of the return loss, as well as the resonant frequency down shift which should have been done by increasing the antenna size. Since the input impedance of the tag antenna cannot match a 50-coaxial line, it is difficult to accurately measure the radiation patterns of the tag antenna by using a conventional far-field measurement system. The three antennas also exhibit omnidirectional radiation patterns in both the E- and H-plane.



(a)



**Figure 4.10. Simulated Far Field Radiation Patterns for: (a) Antenna AN1, (b) antenna AN2 and (c) Antenna AN3**

Next, the three designed asymmetrical fractal antennas with SRR were fabricated and measured, then compared to the simulation results. A differential probe reported in (Palmer et al., 2006; Kuo et al., 2008; Qing et al., 2009; Kim et al., 2009), which has a symmetrical structure, was employed as part of our measurement method to verify the tag antenna impedance (Section 2.6, page 32). The differential probe is constructed by using two semirigid coaxial cables with a length of 120 mm and an outer conductor diameter of 3 mm as shown in Figure 4.11(a). One end of the two semirigid coaxial cables is soldered together on their outer conductors to form the

common virtual ground (Figure 4.11(b)), while the inner conductors are open-ended and partially extended to be soldered to the antenna under test at the chip position. The other end of the probe is with two subminiature version A (SMA) connectors and connected to a Vector Network Analyzer, (VNA model: Anritsu 37347D) through the test cables. The measurement setup was performed in an ordinary room environment as shown in Figure 4.11(c) and (d).

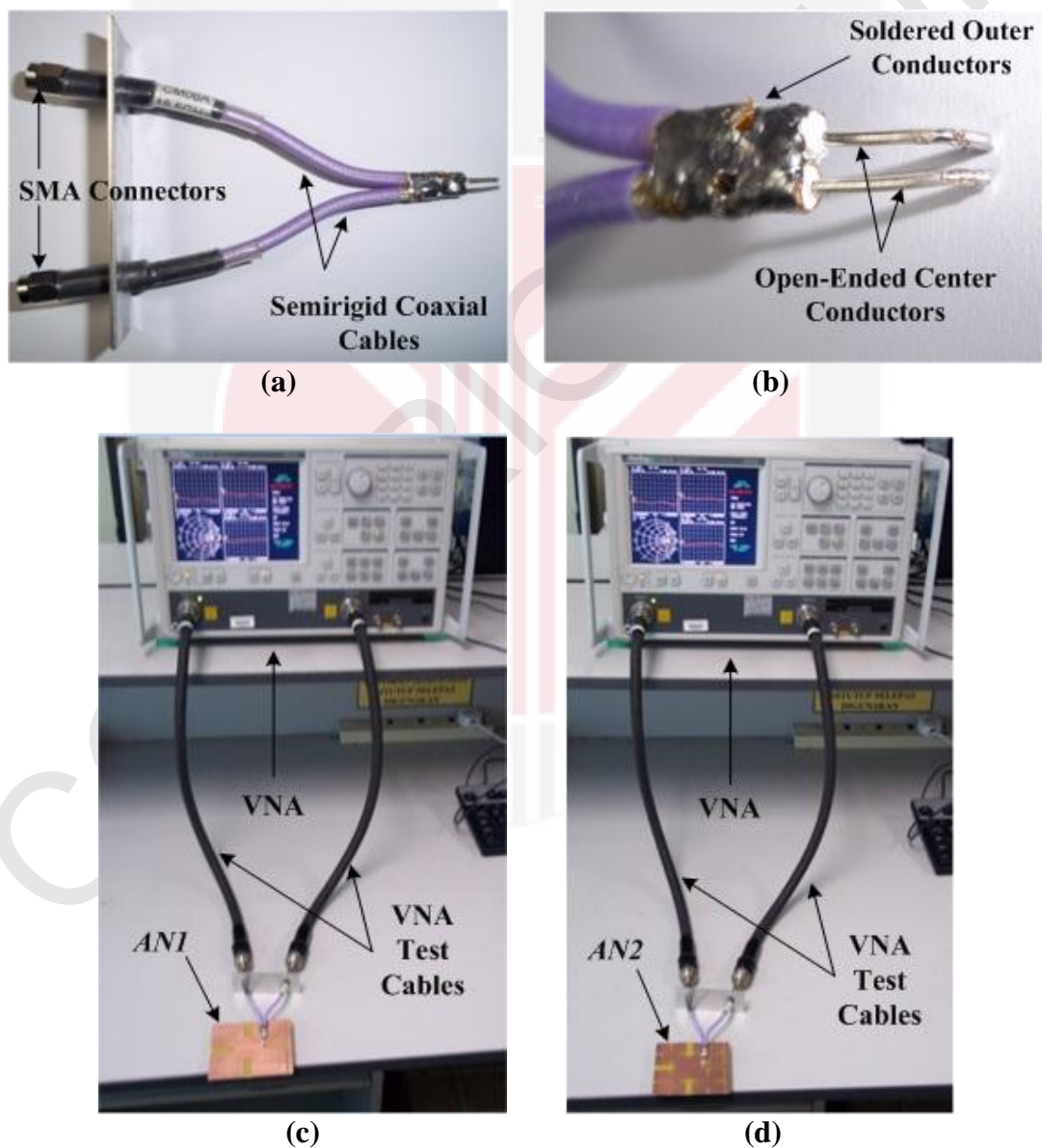


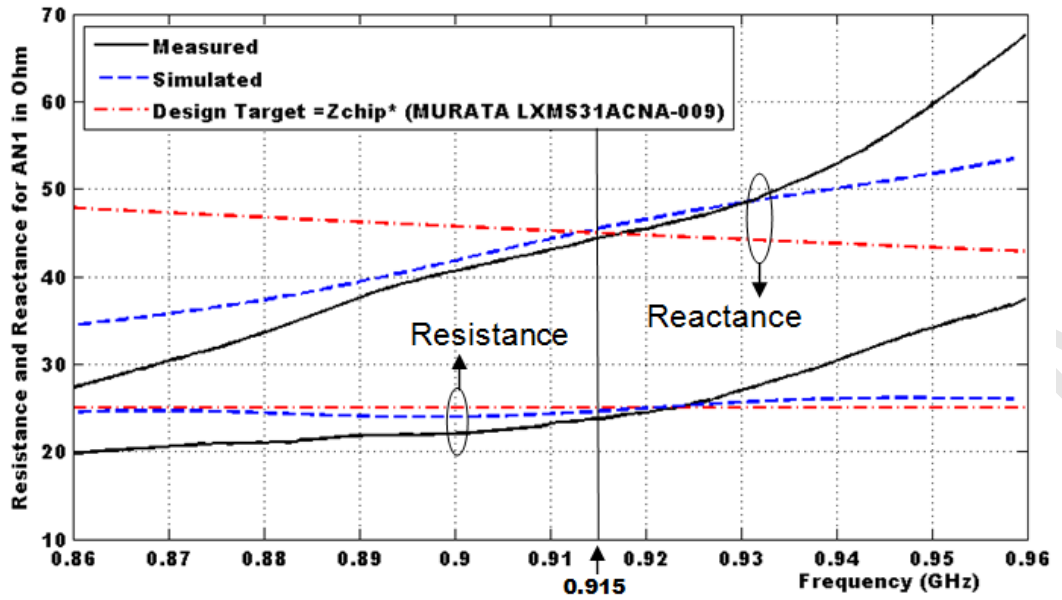
**Figure 4.11. (a) Differential Probe, (b) Open-Ended Side of Semirigid Cables, (c) Measurement Setup of Antenna AN1 and (d) Measurement Setup of Antenna AN2**

The simulation results of the proposed tag antennas were obtained using (CST Microwave Studio, 2010), while the measured results were obtained from a Vector Network Analyzer, VNA (Anritsu 37347D). For comparison purposes, the simulated and measured results of antenna impedances are shown in Figure 4.12. The measured results were obtained after deembedding the influence of the semirigid cables from the two-port  $S$ -parameters ( $S_{11}$ ,  $S_{12}$ ,  $S_{21}$ , and  $S_{22}$ ).

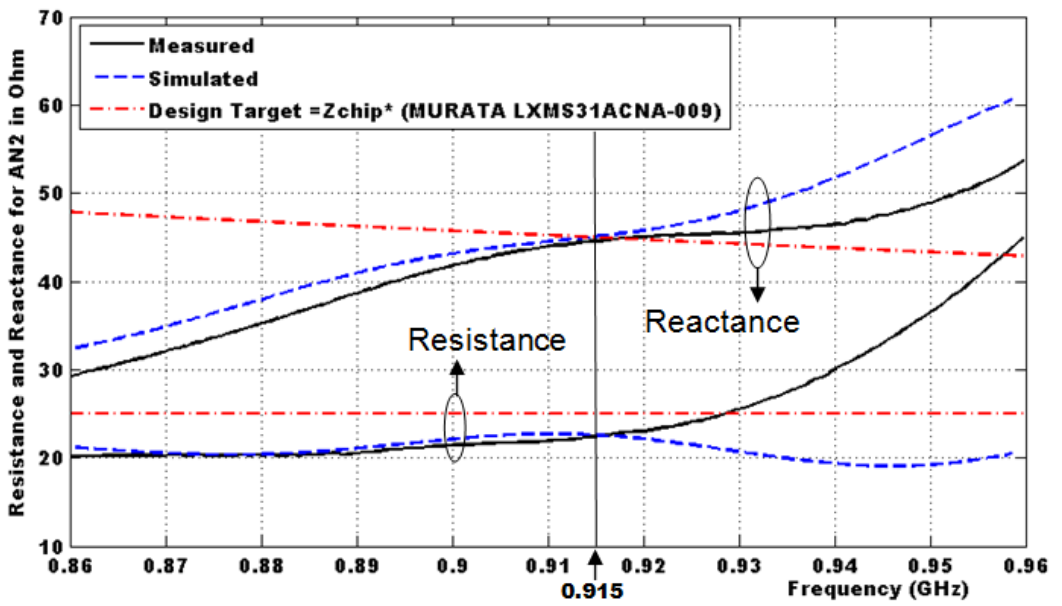
Figure 4.12(a), (b), and (c) shows that the measured and simulated impedances for antennas  $AN1$ ,  $AN2$ , and  $AN3$  respectively are in good agreement, thus verifying the design process. However, the measured reactance and resistance of the antennas are deviated from the simulated values at frequencies higher than 0.93 GHz. The small deviations between the measured and simulated results is from the mismatch between the feeding line and subminiature version A (SMA) connector, as well as imperfectness of the standard printed circuit board (PCB) fabrication process. Table 4.4 shows the simulated and measured impedances of the three proposed antennas  $AN1$ ,  $AN2$ , and  $AN3$  taken from Figures 4.12(a), (b), and (c). It is clear from the table that the measured and simulated antenna resistance and reactance are in good agreement with the design target of the chip impedance ( $25-j45 \Omega$ ) at the design frequency of 915 MHz, which validates the antenna design.

**Table 4.4: Simulated and measured antenna impedances**

Antenna impedance ( $\Omega$ )					
$AN1$		$AN2$		$AN3$	
Simulated	Measured	Simulated	Measured	Simulated	Measured
24+j46	23+j44	22+j45	22+j44	23+j46	23+j44

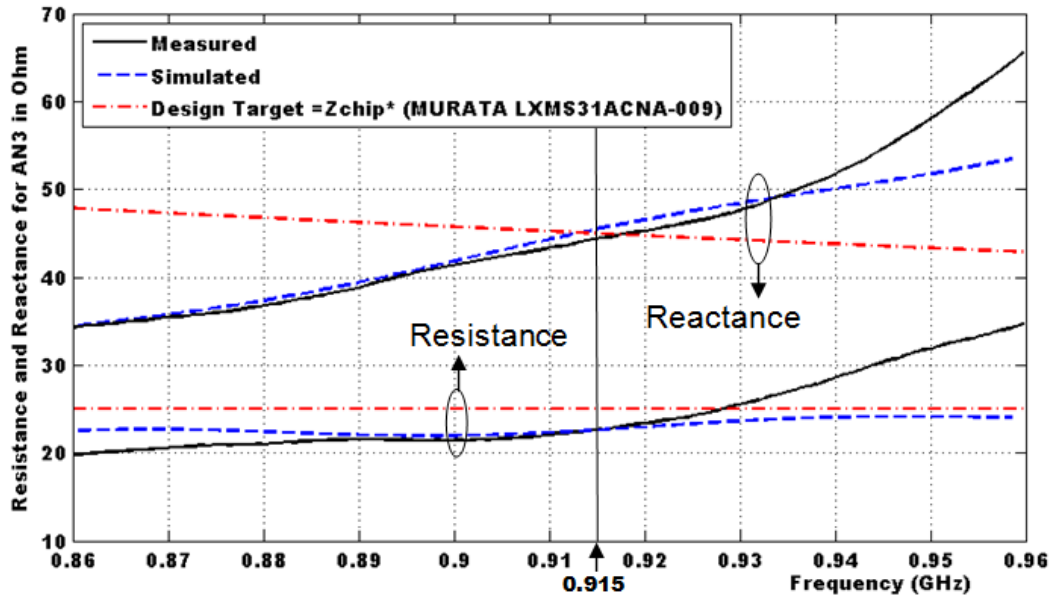


(a)



(b)





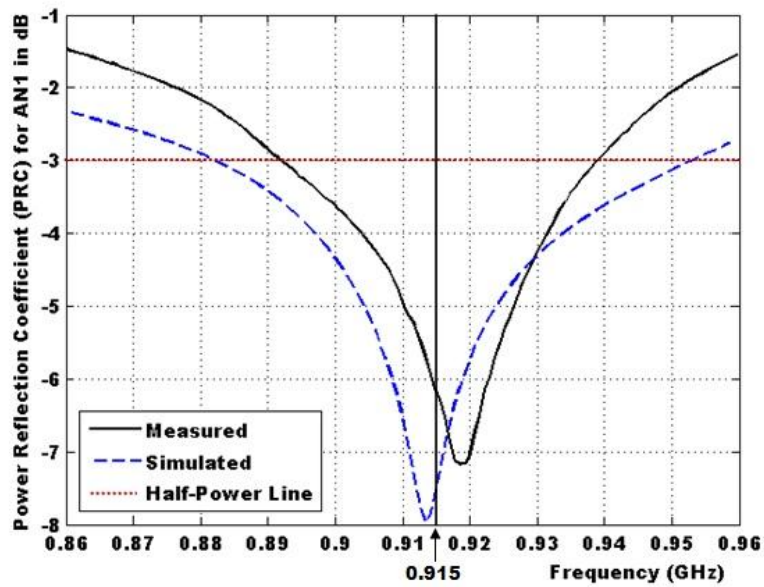
(c)

**Figure 4.12. Impedance Simulation and Measurement Results of the Proposed Antennas: (a) Antenna AN1, (b) Antenna AN2 and (c) Antenna AN3**

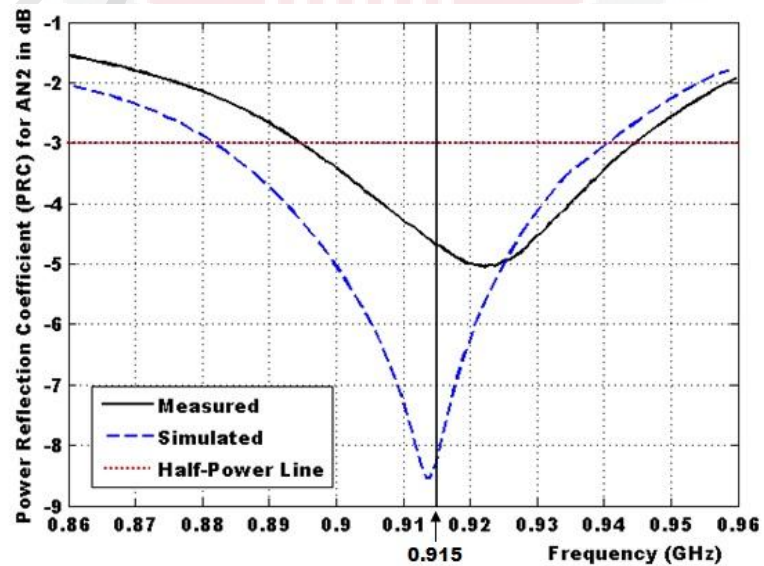
Power Reflection Coefficient (PRC)  $\Gamma$  analysis used by (Nikitin et al., 2005) is adopted here as discussed in Chapter 2, Section 2.5.6. Each tag antenna design is required to provide impedance matching between two impedance components with complex values. The measured and simulated PRC curves of the three implemented antennas with half-power bandwidth are depicted in Figure 4.13(a), (b) and (c). The curves are based on the assumption that the real part of the chip impedance is not changing with frequency. Figures 4.13(a), (b), and (c) show good agreement between the simulated and measured PRC curves for the three antennas; however it shows some variation in the bandwidth, due to the variation of the measured and simulated reactance and resistance curves below and above resonance. The half-power bandwidths of the three antennas are summarized in Table 4.5 based on the criterion  $\Gamma < -3$  dB.

**Table 4.5: Simulated and measured half-power bandwidths of the three antennas**

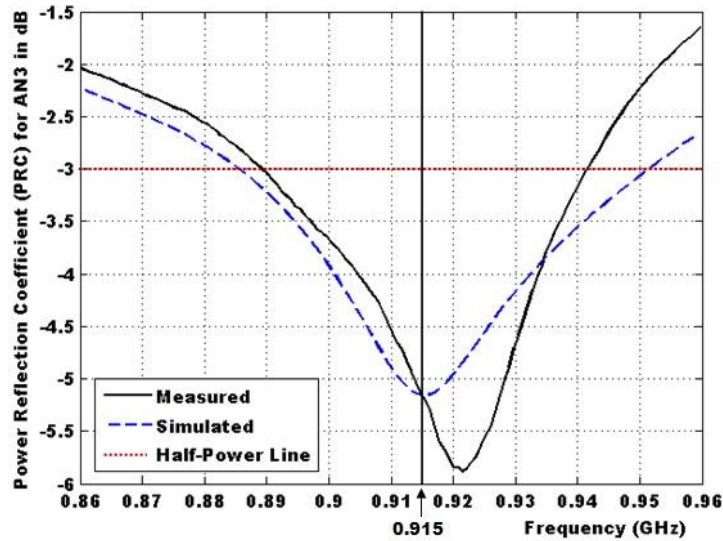
	AN1		AN2		AN3	
	Simulated	Measured	Simulated	Measured	Simulated	Measured
Center Frequency (MHz)	913	918	913	923	915	921
-3 dB Bandwidth (MHz)	882-953	892-938	882-941	895-944	885-951	899-941
-3 dB Bandwidth (%)	7.77	5.01	6.46	5.31	7.21	4.56



(a)



(b)



(c)

**Figure 4.13. Simulated and Measured PRC of the Proposed Tag Antennas: (a) Antenna AN1, (b) Antenna AN2 and (c) Antenna AN3**

A MURATA RFID magicstrap LXMS31ACNA-009 chip (Murata MAGICSTRAP® Application Note, 2012), with input impedance of  $(25-j45) \Omega$  at 915 MHz was used for the three tag antenna designs. The minimum operating power of the MURATA RFID magicstrap is -8 dBm ( $160 \mu\text{W}$ ). Each tag antenna was tuned to the desired resonant frequency by adjusting its physical dimensions in terms of patch length ( $L$ ), indentation factor ( $a_2$ ) and the side length of the square SRR ( $SRR$ ); until its inductance provides conjugate impedance matching to the used RFID chip.

The maximum theoretical read range of each proposed RFID tag antenna ( $r_{\max}$ ) is calculated using Friis free-space formula (Equation 2.16, Section 2.5.7) (Balanis et al., 2005; Rao et al., 2005b). The calculated and measured read ranges of the three antennas are summarized in Table 4.6. It is clear from the table that the measured and calculated read ranges for the three antennas good agreement which validates



the antenna design. The read range is measured using the ATid (AT-870) handheld reader. The reader's output power is set to 4.0 W EIRP. The variation between the measured and calculated read ranges is due to that the measurement was conducted in an ordinary room environment. The antennas feature a lower read range because of the high threshold power required to turn on the MURATA chip (-8 dBm). The read ranges can be improved, even tripled, depending on the chip that is used. Some chips may offer lower minimum threshold power required to turn it on (e.g. -18 dBm) (Alien Higgs-3, 2012).

**Table 4.6: Calculated and measured read range of the three antennas**

	AN1		AN2		AN3	
	Calculated	Measured	Calculated	Measured	Calculated	Measured
$r_{\max}$ (m)	2.17	2.10	1.23	1.10	0.82	0.75

#### 4.4 Summary

In this chapter, three new types of compact Minkowski-like fractal RFID tag antennas have been presented for RFID applications in the 915 MHz frequency band with adequate read range, better return loss when integrated with SRRs, as well as their Omni-directional radiation pattern. Each of the antenna structures showed high degree of self-similarity and space-filling properties. The antenna designed with the 2<sup>nd</sup> iteration AN2 is more compact than that designed with the 1<sup>st</sup> iteration AN1, with a size reduction of about 22%. A further size reduction of 14% is obtained with a 3<sup>rd</sup> iteration antenna (AN3) over that of AN2, and 32% over that of AN1 for the same resonance frequency. A complete design procedure is provided for both the SRR and the antennas. AN1 and AN2 were designed for consistency and validation in terms of

fabrication and measurement. *AN3* is the best in terms of size, however there is a tradeoff between antenna size and gain or read range. Further iterations (4<sup>th</sup>, 5<sup>th</sup> ...etc) of fractal antenna designs may also be done, but size reduction would not be significant at the expense of increased structure complexity which might be difficult to fabricate with traditional photolithography process. Experimental results showed that the maximum read range of the three antennas *AN1*, *AN2* and *AN3* with 4.0 W EIRP radiation power of the RFID reader is about 2.10 m, 1.10 m and 0.75 m respectively. *AN3* offers a small size of  $66.5 \times 73.09 \times 1.6 \text{ mm}^3$  with a good reading range although the chip used has a very high threshold of -8 dBm compared to those mentioned in Table 2.2, for example (Kimouche et al., 2011) with -10 dBm and (Rusu et al., 2008) of -18 dBm with read ranges of 5 m and 0.5 m respectively. The literature lack for RFID tag antenna designs based on the modified Minkowski fractal motivated the tag antenna designs in this chapter. Other fractal structures like Koch fractals, Sierpinski carpet and Hilbert curves may have been used for RFID tag antenna designs to some extent.

Simulations and measurements show that the integration of SRR is efficiently usable with antennas to shift their resonance frequency and further enhance the performance characteristics in terms of return loss. It has been shown that the simple design of SRR has been integrated with each antenna at a low fabrication cost on PCB substrates using inexpensive standard photolithography process. Accordingly, it also promises cheap costs if integrated with RFID chips to produce RFID tags. RFID tag antennas fabricated and measured in this chapter are designed for normal objects tagging other than metals. For this reason, the next chapter will show small size RFID tag antenna designs that are mountable on metallic objects.

## CHAPTER 5

### MINIATURIZED METAL MOUNT MINKOWSKI FRACTAL RFID TAG ANTENNAS WITH COMPLEMENTARY SPLIT RING RESONATOR

#### 5.1 Introduction

This chapter proposes two miniature RFID tag antennas designed to operate on metallic objects, in the UHF frequency band of 915 MHz, without significantly degrading the read range. The two tag antennas belong to the fractal family based on 1<sup>st</sup> and 2<sup>nd</sup> iteration of the modified Minkowski fractal structure discussed in Chapter 3, Section 3.3. The design is proposed since the three tag antennas that were designed and validated in Chapter 4 cannot be tagged on metallic objects. The antenna structures are inserted by an unconnected (floating) intermediate CSRR layer, rather than using SRR as in the previous antenna designs discussed in Chapter 4. The proposed antenna structures are comprised of two FR4 substrates sandwiched between three copper layers. The antennas were simulated and measured to verify their conjugate matching with chip impedance and validate their readability when placed on metallic objects.

#### 5.2 Antennas Design

In this chapter, the modified Minkowski fractal geometry is also used to design two fractal microstrip loop antennas operating in the 915 MHz frequency band for UHF RFID applications. The two antenna designs are based on the 1<sup>st</sup> and 2<sup>nd</sup> iteration of the modified Minkowski fractal shape shown in Figures 3.3 (c) and (d) respectively, discussed earlier in Chapter 3.

The two antenna structures consist of two fractal patches deposited on the upper layer and a ground plane at the bottom layer for metallic objects identification. The upper and bottom layers are electrically connected through vias to form a loop antenna structure. The structure is inserted with an unconnected (floating) intermediate CSRR layer to achieve further size reduction over fractalation and enhance the performance in terms of return loss and gain. The intermediate layer contains two CSRRs, each centered underneath one of the two patches. Figure 5.1 shows the layout of the square CSRR structure used as a floating layer in both tag designs.

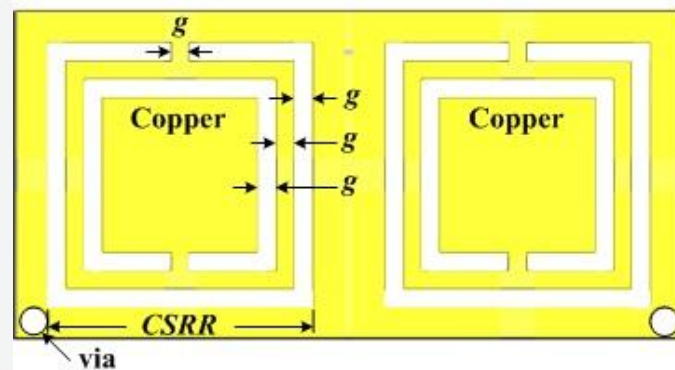


**Figure 5.1. Layout of the Two Square CSRR Design**

It consists of a rectangular copper sheet with 0.035 mm thickness having two pairs of concentric square slits with opposite discontinuities,  $g$  of 1 mm, in the  $x$ - $y$  plane. Both slits have equal widths and spacing of  $g$  which is also 1 mm. The side length of the outer slit is assigned as  $CSRR$ . The value of  $CSRR$  for each antenna is tuned such that it gives a better return loss as well as the shift of resonant frequency due to the added reactance. The CSRR structure offers more capacitive reactance than SRR and enhances the antenna performance better than using a full-copper layer as validated later in this chapter. The two antenna designs were simulated without

CSRR (full copper) intermediate layer and with CSRR layer to show its effect. Figure 5.2(a) and (b) depicts the lumped-element circuit diagrams of the proposed RFID tag antenna with and without the intermediate CSRR layer. Figure 5.2(b) illustrates that the capacitance considered in the model is doubled while the inductance is halved since two CSRRs are used in the inter-layer. Figure 5.2(c) illustrates the complete circuit model of the tag antenna.

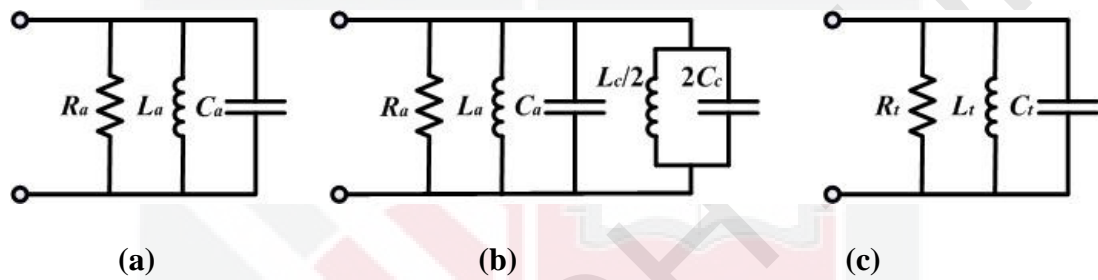


**Figure 5.2. Lumped-Element Circuit Model of (a) Proposed Tag Antenna, (b) Proposed Tag Antenna with an Inter-CSRR Layer and (c) the Proposed RFID Tag Antenna Overall Equivalent Lumped-Element Model**

The inductor  $L_a$  is basically from the loop formed by patches, vias, and ground; which can be adjusted by changing the patch length  $L$ . The intermediate CSRR layer increases the capacitance by  $2C_c$  to the antenna, thereby increasing the total capacitance  $C_t = (C_a + 2C_c)$  significantly rather than the added inductance  $L_c/2$ . Therefore, antenna resonance,  $f_c$  shifts down to the low-frequency band. The above mentioned analysis and lumped-element circuit models apply for both antenna designs in this chapter.

### 5.2.1 Antenna $NI$

This section presents a miniature RFID tag antenna design with two 1<sup>st</sup> iteration ( $NI$ ) modified Minkowski fractal structure patches deposited as an upper layer and a ground plane at the bottom layer for metallic objects identification. Figure 5.3 shows the layout of the tag antenna design.

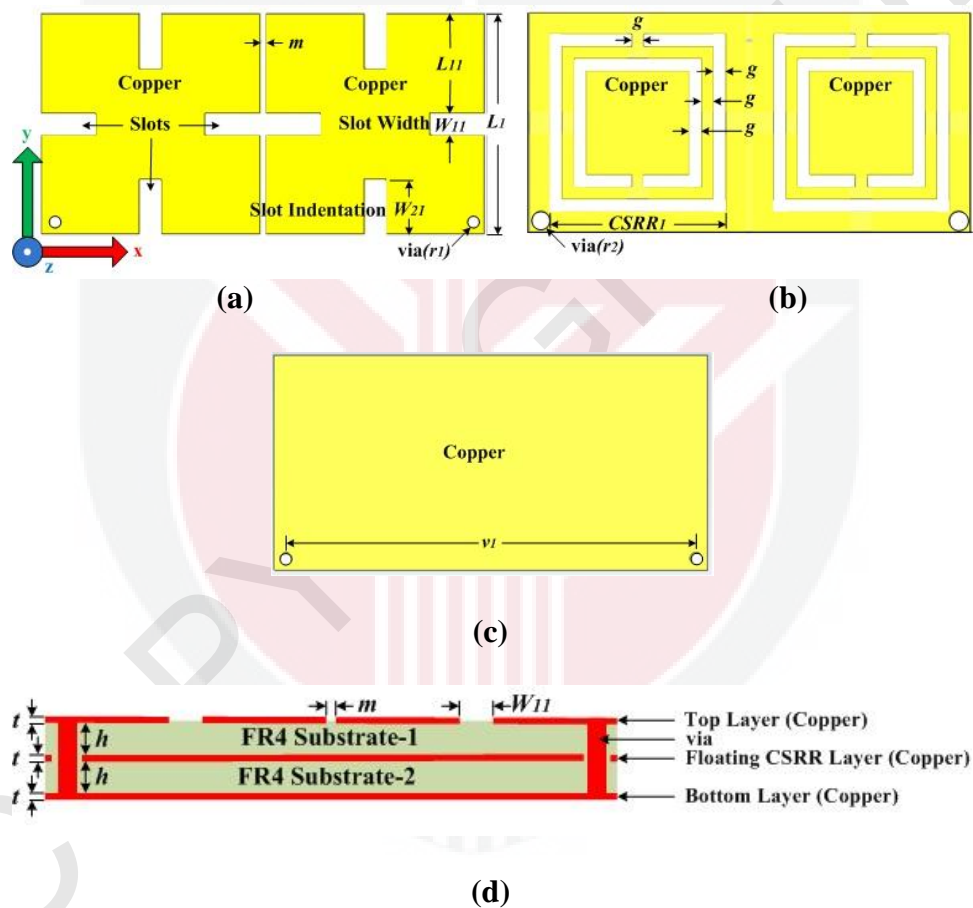


**Figure 5.3. Design Arrangement of the Proposed 1<sup>st</sup> Iteration ( $NI$ ) Fractal RFID Tag Antenna: (a) Top Layer, (b) Inter-CSRR Layer, (c) Bottom Layer and (d) Cross Section**

The top layer consists of two symmetrical square fractal patches of the modified Minkowski type (Figure 5.3(a)) with a gap  $m$  of 0.5 mm separating them for the RFID chip placement. The slot width and indentation factors of each patch is chosen

as  $a_1=0.1$  and  $a_2=0.25$  respectively for best design performance in terms of gain and return loss.

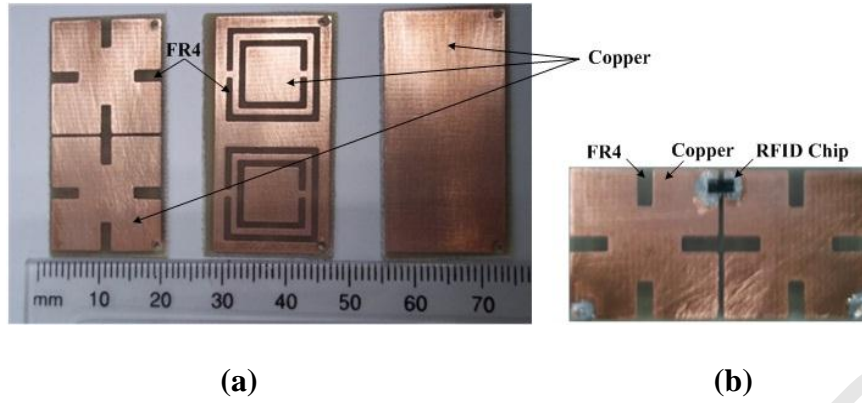
The fractal patches and ground plane are electrically connected to each other by two vias of 0.5 mm radius separated by a distance  $v_1$  as shown in Figure 5.3(c); the intermediate CSRR layer is unconnected to the top and bottom layers using a via hole of 0.75 mm radius. Figure 5.3(b) displays the intermediate layer containing two CSRRs, each centered underneath one of the two patches. The three copper layers shown in Figure 5.3(a), (b) and (c) are with thickness of 0.035 mm and separated by two FR4 substrates each of thickness 1.53 mm, dielectric constant  $\epsilon_r = 4.4$ , and loss tangent of 0.02.

Figure 5.4 shows a photograph of the three layers of the fabricated antenna *NI* as well as the assembled RFID tag where the chip is attached across the gap between the two fractal patches, opposite to the vias position, and connects to both of them. Proposed RFID tag antenna dimensions labeled on Figure 5.3 are given in Table 5.1. Antenna *NI* has an overall size of  $36.7 \times 18.1 \times 3.165 \text{ mm}^3$ .

**Table 5.1: Antenna *NI* dimensions**

Parameter	Dimension (mm)
Square fractal patch side length ( $L_1$ )	18.1
First iteration square side length ( $L_{11}$ )	8.145
First iteration slot width ( $W_{11}$ )	1.81
First iteration slot indentation ( $W_{21}$ )	4.525
Spacing between the two fractal patches ( $m$ )	0.5
Top and bottom layers via radius ( $r_1$ )	0.5
Intermediate (floating) layer via radius ( $r_2$ )	0.75
Outer square CSRR side length ( $CSRR_1$ )	14.6
Distance between via centers ( $v_1$ )	34.7
CSRR gap size, width, and spacing ( $g$ )	1





**Figure 5.4. (a) Photograph of the Three Layers of the Proposed 1<sup>st</sup> Iteration (NI) Fractal RFID Tag Antenna and (b) Photograph of the Assembled RFID Tag**

Figures 5.5 (a), (b) and (c) shows the simulated responses of the input impedances of NI with different values fractal patch lengths ( $L_1$ ), indentation factor ( $a_2$ ) and the CSRR outer square side length ( $CSRR_1$ ) respectively. Figure 5.5(a) clearly shows that the larger length of patch results in lower resonant frequency of the RFID tag antenna. This is because of the well known feature of antenna design in terms of the relation between size and resonant frequency. Figure 5.5(b) shows the antenna impedance simulation results for different values of indentation factor ( $a_2$ ). It is clear that by increasing  $a_2$ , the fractal patch perimeter ( $P_n$ ) increases too as discussed in Chapter 3, Section 3.2.2. Hence, by considering first a square patch of length  $L_0=18.1$  mm without fractalation, its perimeter will be as shown in Equation 5.2:

$$P_0 = 4L_0 = 4 \times 18.1 = 72.4 \text{ mm} \quad (5.1)$$

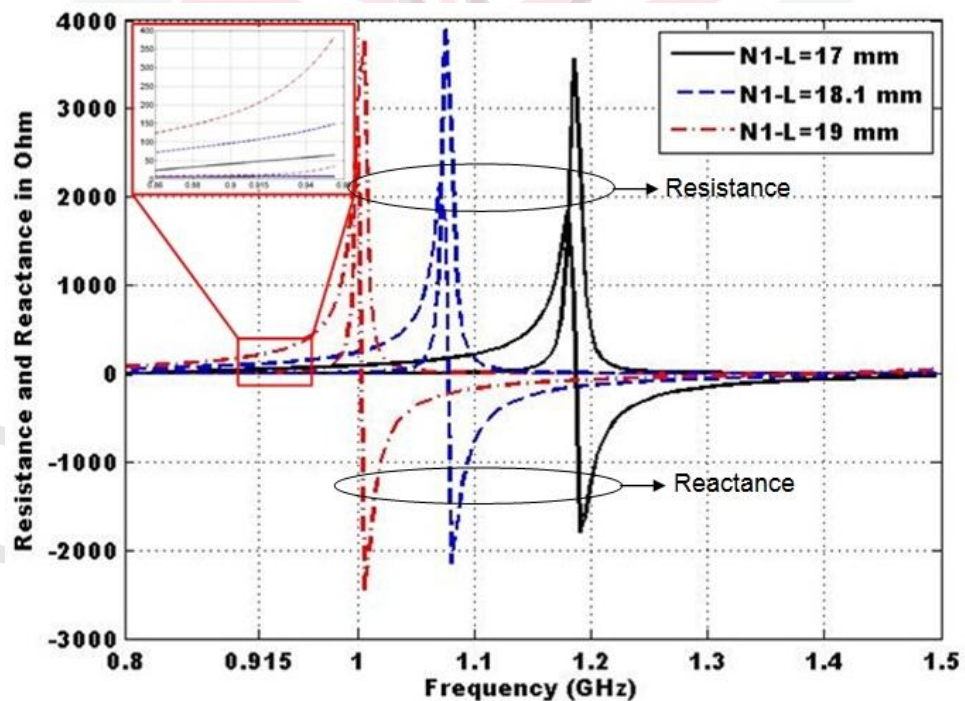
By applying the 1<sup>st</sup> iteration of the modified Minkowski fractal structure and using Equation 3.8 with  $a_2=0.25$  for NI, the new perimeter will be as shown in Equation 5.3:

$$P_1 = (1 + 2a_2)P_0 = (1 + 2 \times 0.25)72.4 = 108.6 \text{ mm} \quad (5.2)$$

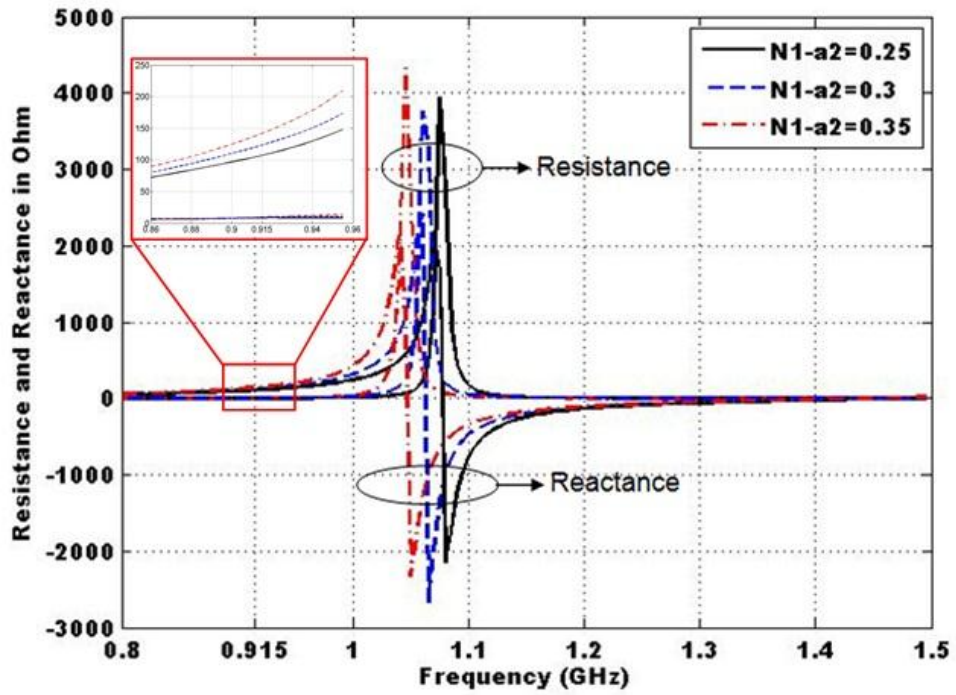


$P_1$  is 50% ( $2 \times 0.25$ ) longer than  $P_0$  for each fractal patch, and since there are two fractal patches in the antenna design, then the current path is actually twice as that of  $P_1$  obtained from Equation 5.2. Figure 5.5(b) also shows that any variation of  $a_2$  results into a small change in the antenna resonance frequency. This feature may be useful in antenna fine tuning.

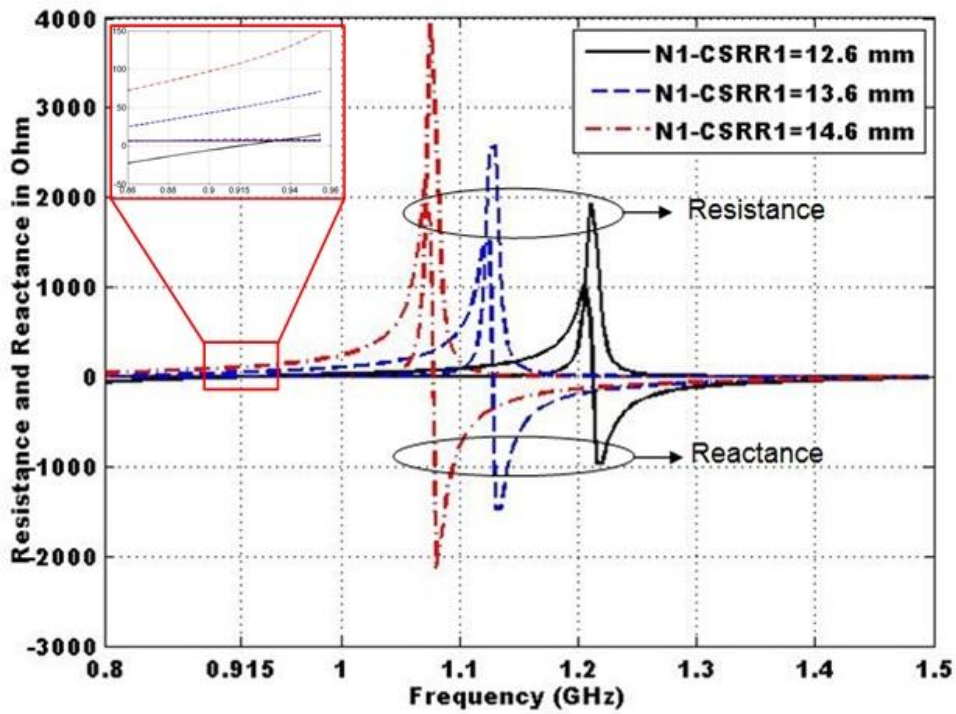
Figure 5.5(c) shows the simulated results of the input impedances of  $N1$  with different values of CSRR lengths ( $CSRR_l$ ). From the figure, it is clear that the larger  $SRR$  length results in lower antenna self-resonant frequency that is achieved by increasing the antenna reactance due to the added capacitance ( $2C_c$ ) from the CSRR as discussed in Chapter 3, Section 3.3.



(a)



(b)



(c)

Figure 5.5. Simulation Results of Antenna  $N1$  Input Impedances with Different Values of: (a) Fractal Patch Length  $L_1$ , (b) Indentation Factor  $a_2$  and (c) CSRR Outer Square Side Length ( $CSRR_1$ ) ( $L_1$  and  $CSRR_1$  are as Denoted in Figure 5.3)

### 5.2.2 Antenna $N_2$

A 2<sup>nd</sup> iteration ( $N_2$ ) modified Minkowski fractal structure is also designed in an attempt for more size reduction from  $N_1$ . It is also designed with two fractal structure patches deposited on an upper layer and a ground plane at the bottom layer for metallic objects identification. The structure is inserted with an unconnected (floating) intermediate CSRR layer. Figure 5.6 shows the layout of the tag antenna design.

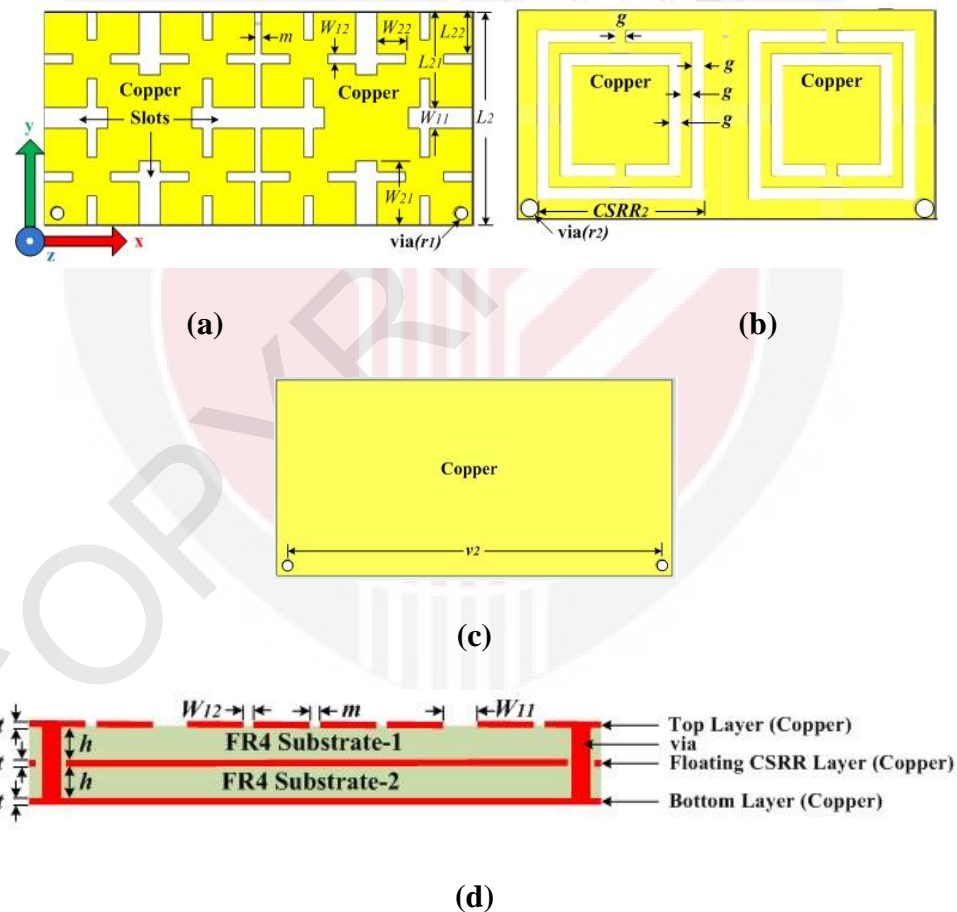


**Figure 5.6. Design Arrangement of the Proposed 2<sup>nd</sup> Iteration ( $N_2$ ) Fractal RFID Tag Antenna: (a) Top Layer, (b) Inter-CSRR Layer, (c) Bottom Layer, and (d) Cross Section**

Antenna  $N2$  also consists of two symmetrical square fractal patches of the modified Minkowski type (Figure 5.6(a)) with a gap  $m$  separating them for RFID chip placement. For this antenna design, the slot width factor and indentation factor of each patch are chosen as  $a_1=0.1$  and  $a_2=0.3$  respectively for best tag performance in terms of gain and return loss. The overall structure is similar to that of  $N1$  in terms of via connections and intermediate layer.

Figure 5.7 shows a photograph of the three layers of the fabricated antenna  $N2$  as well as the assembled RFID tag where the chip is attached across the gap between the two fractal patches, opposite to the vias, and connects to both of them. Proposed RFID tag antenna dimensions labeled on Figure 5.6 are given in Table 5.2. This tag antenna structure  $N2$  has an overall size of  $35.3 \times 17.4 \times 3.165 \text{ mm}^3$ . It performs a size reduction of 7.5 % over  $N1$ .

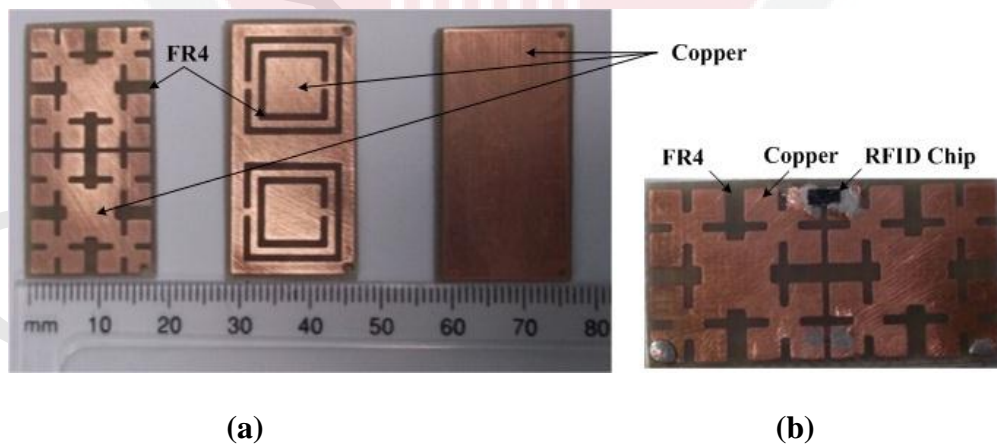


**Figure 5.7. (a) Photograph of the Three Layers of the Proposed 2<sup>nd</sup> Iteration ( $N2$ ) Fractal RFID Tag Antenna and (b) Photograph of the Assembled RFID Tag**

**Table 5.2: Antenna  $N2$  dimensions**

Parameter	Dimension (mm)
Square fractal patch side length ( $L_2$ )	17.4
First iteration square side length ( $L_{21}$ )	7.83
Second iteration square side length ( $L_{22}$ )	3.52
First iteration slot width ( $W_{11}$ )	1.74
Second iteration slot width ( $W_{12}$ )	0.783
First iteration slot indentation ( $W_{21}$ )	5.22
Second iteration slot indentation ( $W_{22}$ )	2.349
Spacing between the two fractal patches ( $m$ )	0.5
Top and bottom layers via radius ( $r_1$ )	0.5
Intermediate (floating) layer via radius ( $r_2$ )	0.75
Outer square CSRR side length ( $CSRR_2$ )	13.9
Distance between via centers ( $v_1$ )	33.3
CSRR gap size, width, and spacing ( $g$ )	1

Figures 5.8 (a), (b) and (c) shows the simulated responses of the input impedances of  $N2$  with different values fractal patch lengths ( $L_2$ ), indentation factor ( $a_2$ ) and the CSRR outer square side length ( $CSRR_2$ ). Figure 5.8(a) clearly shows that by increasing patch length, antenna resonant frequency is lowered. This is because of the well known feature of antenna design in terms of the relation between size and resonant frequency. Figure 5.8(b) shows the antenna impedance simulation results for different values of indentation factor ( $a_2$ ). For this antenna, and assuming that a square patch of length  $L_0=17.4$  mm without fractalation, its perimeter will be as shown in Equation 5.4:

$$P_0 = 4L_0 = 4 \times 17.4 = 69.6 \text{ mm} \quad (5.3)$$

By applying the 1<sup>st</sup> iteration of the modified Minkowski fractal structure and using

Equation 3.8 with  $a_2=0.3$  for  $N2$ , the new perimeter will be as in Equation 5.5:

$$P_1 = (1 + 2a_2)P_0 = (1 + 2 \times 0.3)69.6 = 111.36 \text{ mm} \quad (5.4)$$

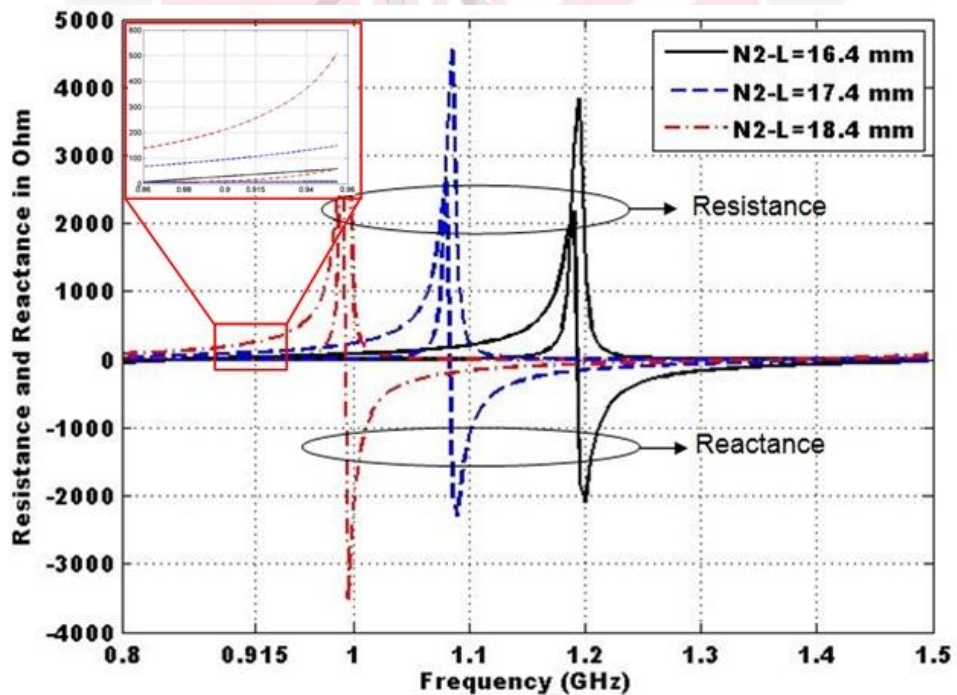
and after the 2<sup>nd</sup> iteration, the perimeter will be as in Equation 5.6:

$$P_2 = (1 + 2a_2)P_1 = (1 + 2 \times 0.3)111.36 = 178.176 \text{ mm} \quad (5.5)$$

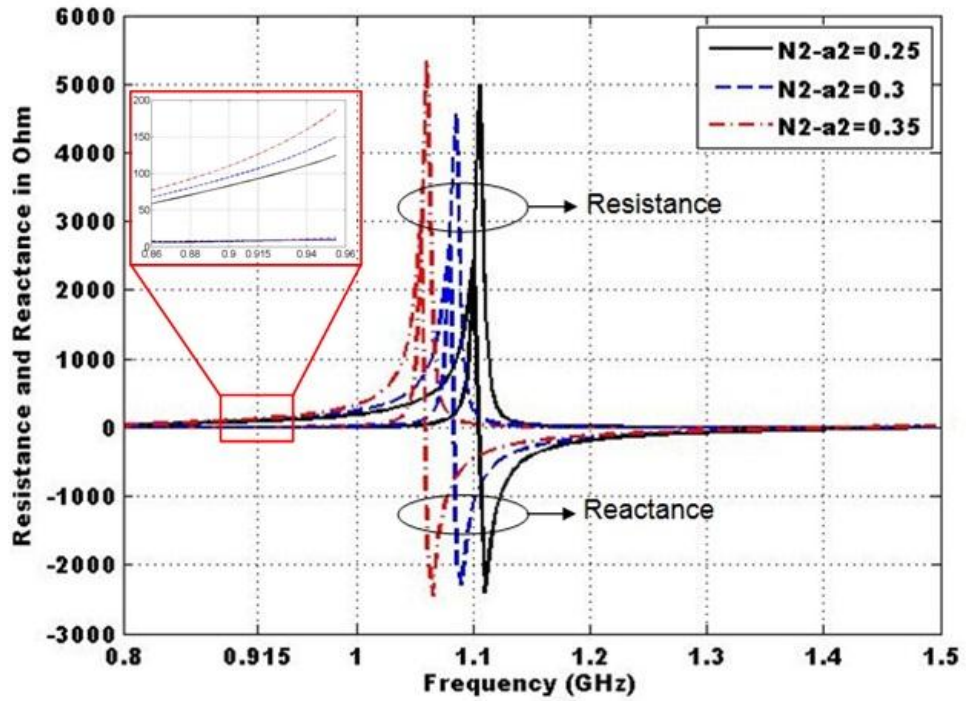


Here  $P_1$  is 60% ( $2 \times 0.3$ ) longer than  $P_0$  and  $P_2$  is also 60% longer than  $P_1$  which totally means that  $P_2$  is 2.56 times longer than  $P_0$  for each fractal patch. Hence, a further increase in the electrical length is achieved over  $NI$  meaning more decrease in the resonant frequency. By maintaining the same desired resonant frequency of 915 MHz, antenna miniaturization is obtained by decreasing the patch length  $L_2$  over  $L_1$ .

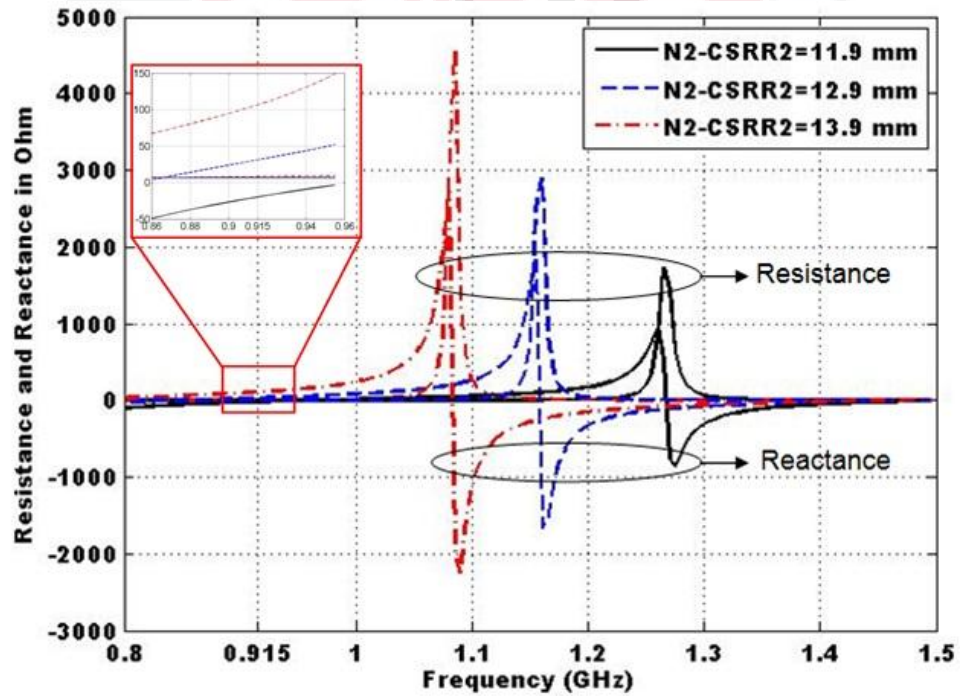
Figure 5.8 (c) shows the simulated results of the input impedances of  $N2$  with different values of CSRR lengths ( $CSRR_2$ ). From the figure, it is clear that the larger  $SRR$  length results in lower antenna self-resonant frequency that is achieved by increasing the antenna reactance due to the added capacitance ( $2C_s$ ) from the CSRR as discussed in Chapter 3, Section 3.3.



(a)



(b)

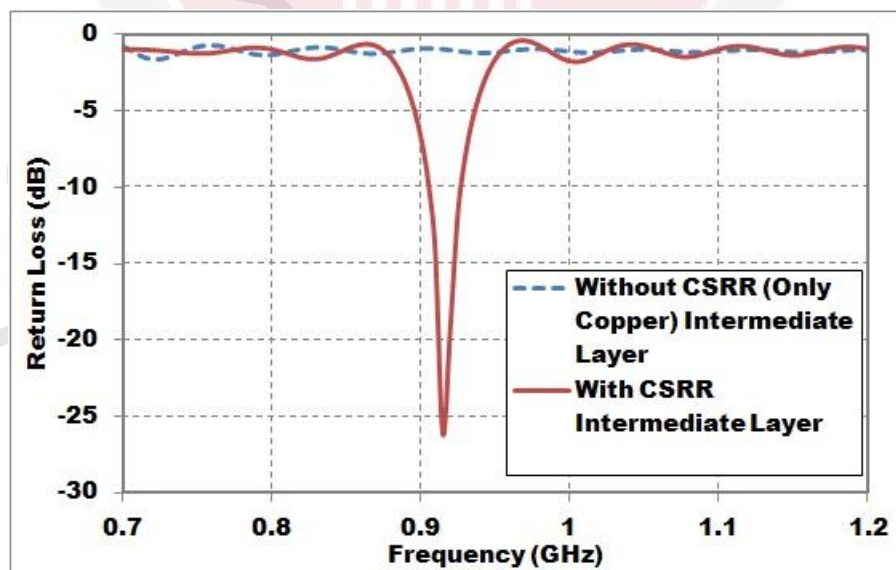


(c)

Figure 5.8. Simulation Results of Antenna  $N_2$  Input Impedances with Different Values of: (a) Fractal Patch Length  $L_2$ , (b) Indentation Factor  $a_2$  and (c) CSRR Outer Square Side Length ( $CSRR_2$ ) ( $L_2$  and  $CSRR_2$  are as Denoted in Figure 5.6)

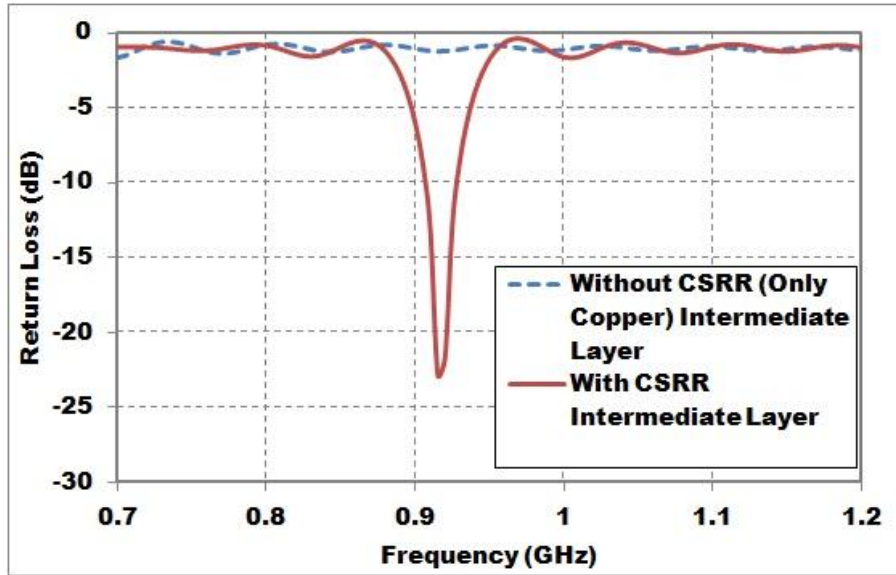
### 5.3 Simulation and Measurement Results

The designed RFID tag antennas were modeled and simulated using full-wave electromagnetic simulator (CST Microwave Studio, 2010). Tuning of the proposed RFID tag performance was simulated by considering a square sheet metal of  $0.5\lambda$  side length and  $0.006\lambda$  thickness as a background. Figure 5.9(a) and (b) shows the return loss of the two proposed tag antennas ( $N1$  and  $N2$ ) simulated by considering chip impedance lumped-element values in CST Microwave Studio. Good resonance is obtained for both antennas at the operating frequency of 915 MHz when the intermediate layer is comprised of two CSRR structures, one under each fractal patch. Figure 5.9 also demonstrates that the two antennas do not resonate if the intermediate CSRR layer is replaced by a full copper one, which verified the concept of frequency shift due to this layer.



(a)

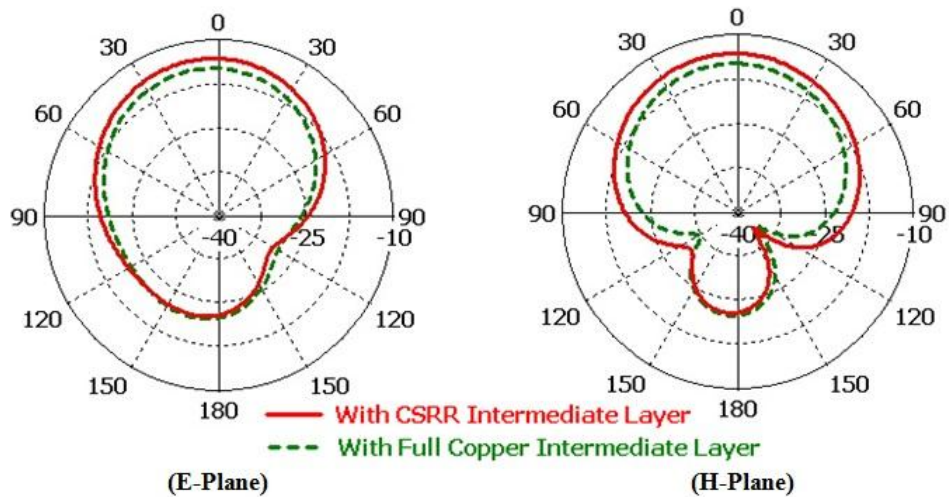




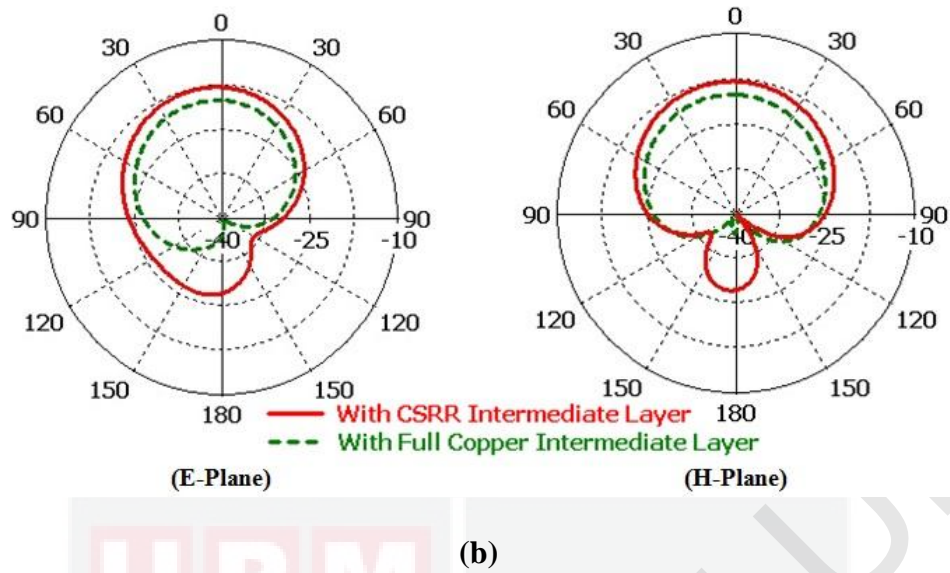
(b)

Figure 5.9. Simulated Return Loss for: (a) Antenna N1 and (b) Antenna N2

Figure 5.10(a) and (b) plots both E- and H-plane simulated radiation patterns of the two tag antennas. As the results revealed, the integration of a CSRR structure shows more significant anticipated improvement in directivity compared to the antenna with full copper intermediate layer. Both antennas also exhibit almost symmetric radiation patterns in both the E- and H-plane.



(a)



**Figure 5.10. Simulated Far Field Radiation Patterns: (a) for Antenna  $N1$  and (b) for antenna  $N2$**

The geometry of the two designed tag antennas was etched on an epoxy FR4 substrate with thickness,  $h = 1.53$  mm, dielectric constant  $\epsilon_r = 4.4$ , copper thickness  $t=0.035$  mm and loss tangent of 0.02.

The same differential probe reported in (Palmer et al., 2006; Kuo et al., 2008; Qing et al., 2009; Kim et al., 2009), which has been used for antenna measurements in Chapter 4 is employed here again as part of our measurement method to verify the tag antenna impedance (Section 2.6, page 32). The measurement setup was performed in an ordinary room environment as shown in Figure 5.11.

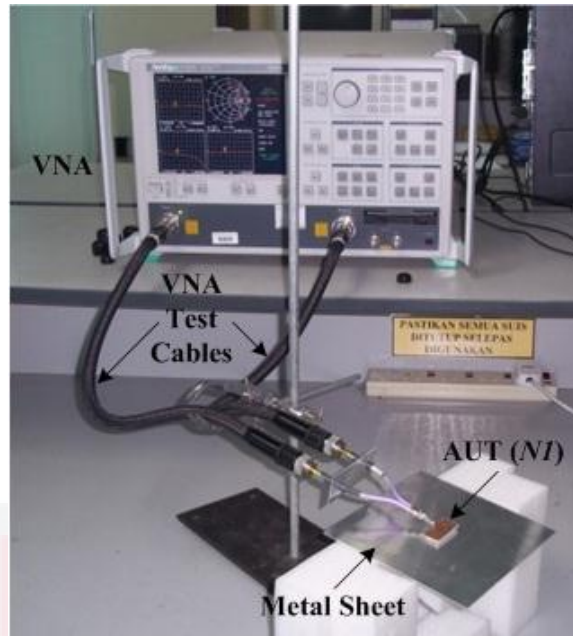
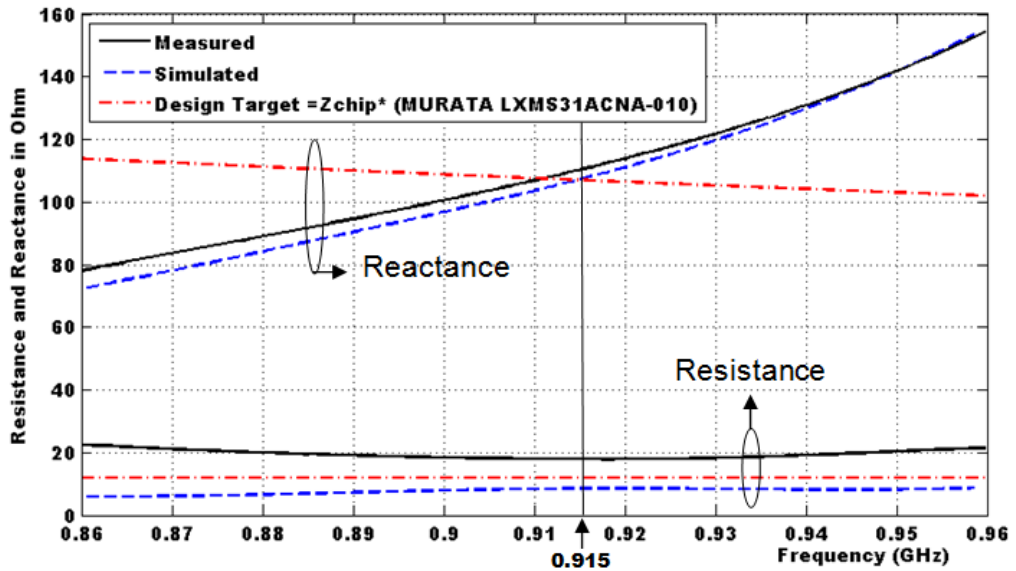


**Figure 5.11. Measurement Setup for Metal Mount Tag Antenna**

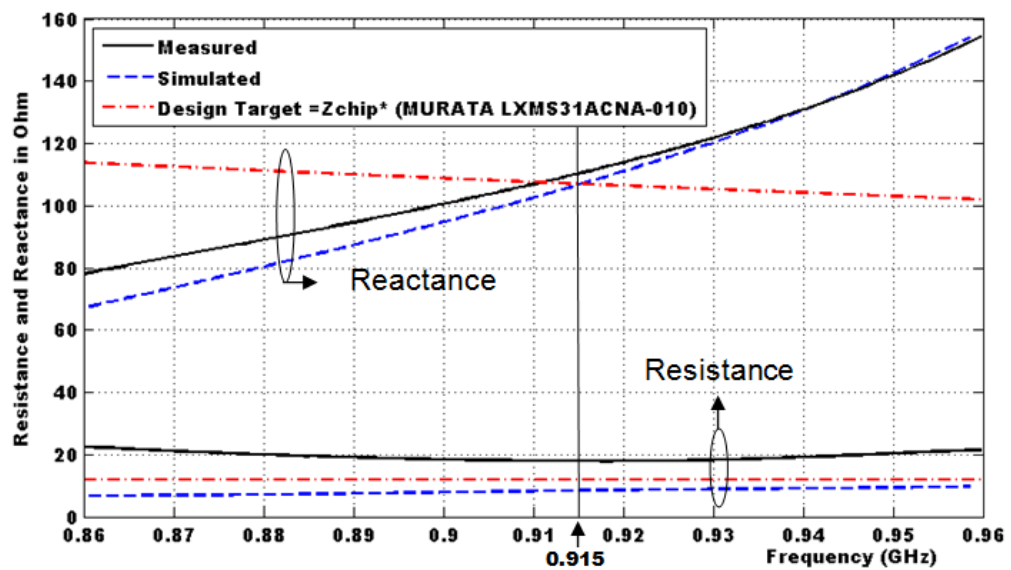
Figure 5.12(a) and (b) shows the simulated and measured results for the impedance of the designed tag antenna. The measured results were obtained after deembedding the influence of the semirigid cables from the two-port  $S$ -parameters ( $S_{11}$ ,  $S_{12}$ ,  $S_{21}$ , and  $S_{22}$ ) as discussed in section 2.6. From Figure 5.12, we observed that there is little difference between the simulated and measured resistance curves at the operating frequency. However, the simulated and measured reactance curves are in good agreement. The variation between these results may be originating from the non-ideal nature of the measurement probe; small mismatch between the feeding lines and SMA connectors, as well as defects of the Printed Circuit Board (PCB) fabrication process. Table 5.3 shows the simulated and measured impedances of the two proposed antennas  $N1$  and  $N2$  taken from Figure 5.14 at 915 MHz. The table clearly shows that there is good agreement between the measured and simulated antenna impedance with the design target ( $12-j107 \Omega$ ) at the design frequency of 915 MHz.

Table 5.3: Simulated and measured antenna impedances

Antenna impedance ( $\Omega$ )			
<i>N1</i>		<i>N2</i>	
Simulated	Measured	Simulated	Measured
9+j106	18+j110	9+j105	18+j109



(a)



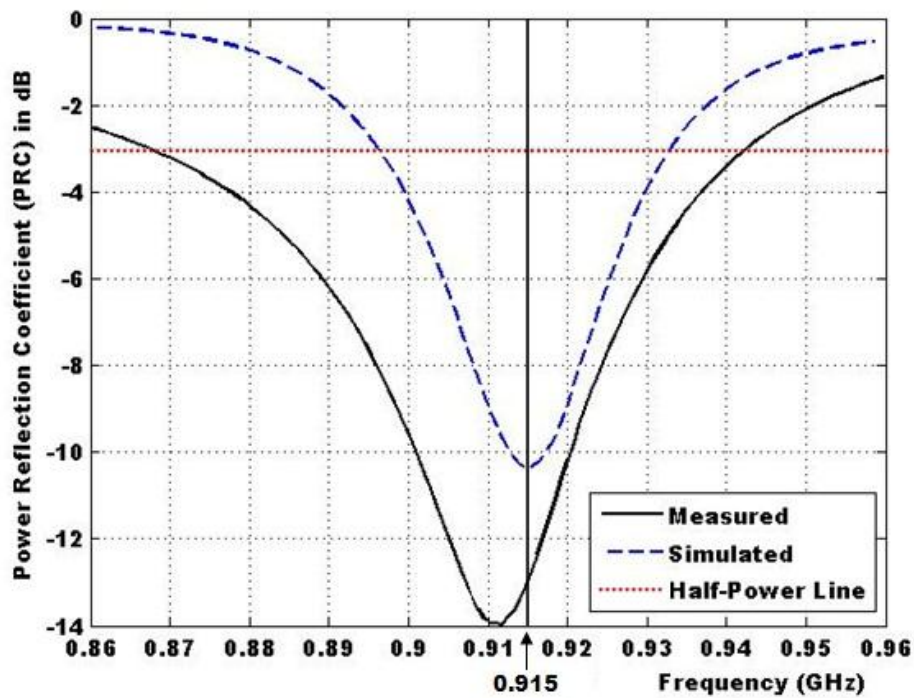
(b)

Figure 5.12. Impedance Simulation and Measurement Results of the Proposed Tag Antennas for: (a) Antenna *N1* and (b) Antenna *N2*

Power Reflection Coefficient (PRC)  $\Gamma$  analysis used by (Nikitin et al., 2005) is adopted here as discussed in Chapter 2, Section 2.5.6. The tag design is required to provide impedance matching between two components with complex values. The measured and simulated PRC curves of the two implemented antennas with half-power bandwidth are depicted in Figure 5.13(a) and (b). The curves are based on the assumption that the real part of the chip impedance is not changing with frequency. The half-power bandwidths of the two antennas are summarized in Table 5.4 based on the criterion  $\Gamma < -3$  dB.

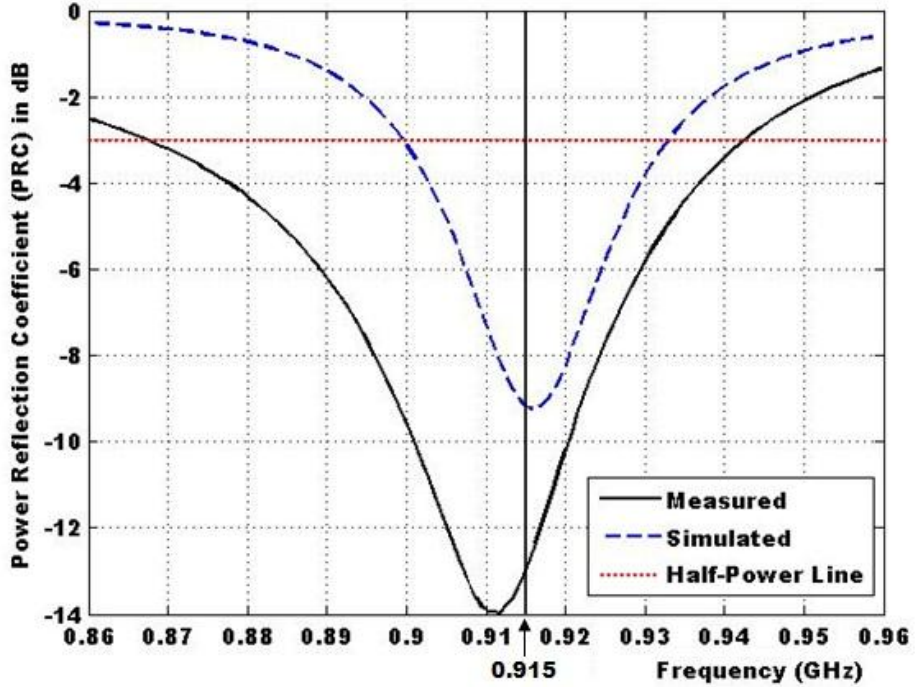
**Table 5.4: Simulated and measured half-power bandwidths of the two antennas**

	<i>N1</i>		<i>N2</i>	
	Simulated	Measured	Simulated	Measured
Center Frequency (MHz)	915	903	917	912
-3 dB Bandwidth (MHz)	896-933	867-943	899-933	866-943
-3 dB Bandwidth (%)	4.04	8.41	3.70	8.44



(a)





(b)

**Figure 5.13. Simulated and Measured PRC of the Proposed Tag Antennas: (a) for Antenna *N1* and (b) for Antenna *N2***

A MURATA magicstrap LXMS31ACNA-010 chip (Murata MAGICSTRAP® Application Note, 2012), with input impedance of  $(12-j107) \Omega$  at 915 MHz was used for the two tag designs. The minimum operating power of the RFID magicstrap is -8 dBm ( $160 \mu\text{W}$ ). The antenna parameter dimensions are adjusted until its inductance provides conjugate impedance matching to the RFID used chip, where the resonant frequency of the two antennas is accordingly determined.

The maximum theoretical read range of the proposed RFID tag antennas ( $r_{max}$ ) is calculated using Friis free-space formula of (Equation 2.16) (Balanis, 2005; and Rao et al., 2005a). The maximum theoretical read range for antenna *N1* is calculated as 0.93 m, while that of antenna *N2* is calculated as 0.53 m. The read range is also measured using the ATid (AT-870) handheld reader. The reader's output power is

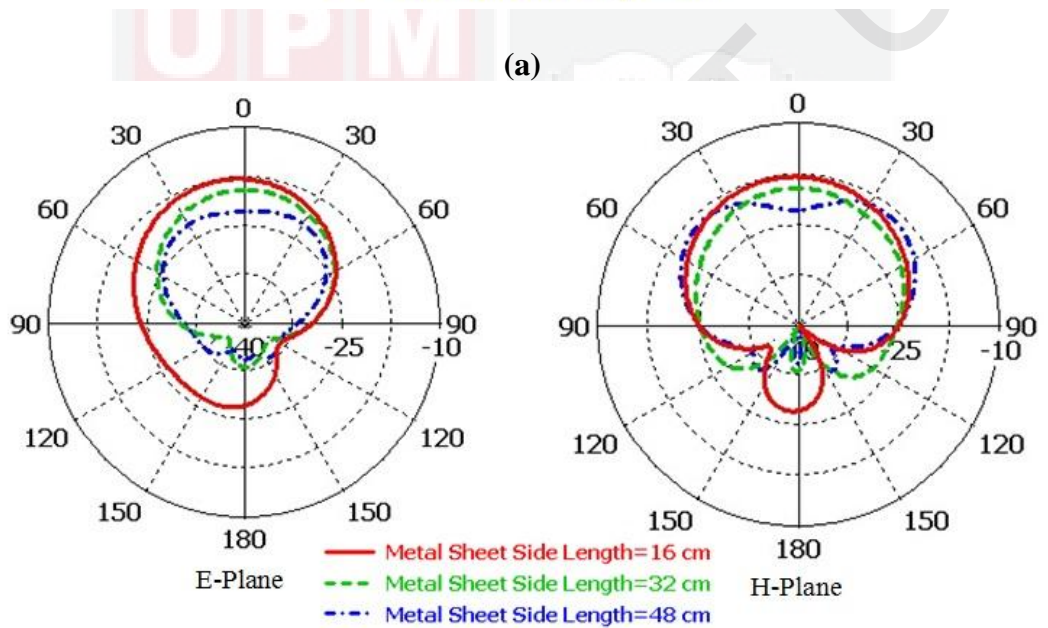
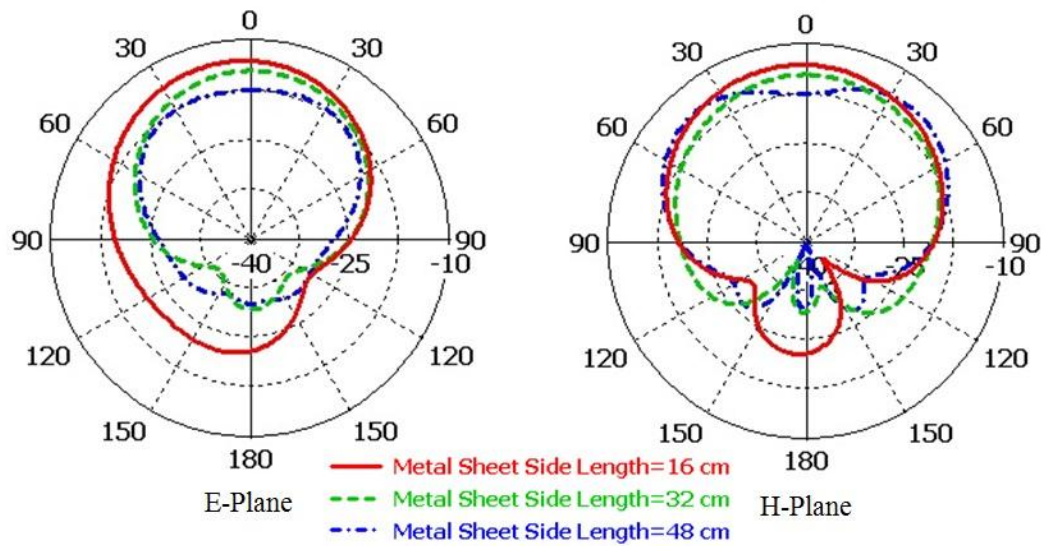
set to 4.0 W EIRP. The tag was mounted on a square sheet metal of  $0.5\lambda$  side length and  $0.006\lambda$  thickness spaced 1.0-mm beneath to account for RFID tag casing, while the operating frequency of the reader sweeps from 900 MHz to 930 MHz. The maximum measured read range was found to be 0.82 m for antenna *N1* and 0.48 m for antenna *N2*. The variation between the measured and calculated read ranges is due to that the measurement was conducted in an ordinary room environment. The gain of the designed tag antennas is a trade off with its miniaturized structure. The two antennas feature a lower read range because of the high minimum threshold power required to turn on the MURATA chip of -8 dBm (160  $\mu$ W). The read range can be improved, even tripled, depending on the chip that is used. Some chips may offer lower minimum threshold power required to turn it on (e.g. -18 dBm) (Alien Higgs-3, 2012).

Figure 5.14 shows the simulation results of the radiation pattern for the two antennas *N1* and *N2* at different values of the metal sheet side length in the background plain. It is clear from the figure that increasing the metal sheet size at the tag's background plane slightly decreases its gain and hence the read range. Table 5.5 summarizes the calculated and measured read range for different values of metal sheet size.

**Table 5.5: Variation of maximum read range for different values of metal sheet size**

Metal Sheet Side Length (cm)	$r_{max}$ (m)			
	<i>N1</i>		<i>N2</i>	
	Calculated	Measured	Calculated	Measured
16	0.93	0.82	0.53	0.48
32	0.82	0.72	0.47	0.43
48	0.77	0.68	0.42	0.39





**Figure 5.14. Simulation Results of Antenna Radiation Patterns with Different Values of Metal Sheet Side Length for: (a) Antenna  $N1$  and (b) Antenna  $N2$**

## 5.4 Summary

This chapter presented two miniaturized RFID tag antennas, in which their configuration is optimized specifically to be mountable on metallic objects. The small design is achieved by inserting a CSRR layer into the antenna structures,

which lowers their resonant frequency by increasing the capacitive reactance and allows high reactive impedance. Their fractal structure adds further miniaturization by increasing the electrical length of the antennas. The size of the proposed tag antennas is  $36.7 \times 18.1 \times 3.165 \text{ mm}^3$  for antenna *N1* and  $35.3 \times 17.4 \times 3.165 \text{ mm}^3$  for antenna *N2*. The three layers of each antenna are etched on two FR4 substrates with thickness of 1.53 mm each. The percentage size reduction achieved by *N2* over *N1* is 7.5 %. Further size reduction may also be done by considering a third iteration (*N3*), but it would not be significant at the expense of increased structure complexity and fabrication errors that might occur in miniature shapes. Very small and compact tag antennas are achieved with good agreement between measured and simulated results. The experiment attested that the maximum read range of the prototypes is about 0.82 m and 0.48 m, obtained when the two tags are placed on a metallic object, with 4.0 W EIRP radiation power of the RFID reader. The results show that the fabricated antennas are very compact. Compared to those reported in (Chen, 2009; Chen et al., 2010a; and Kimouche et al., 2011); the proposed antennas are more than 9%, 51%, and 74% smaller in size respectively. The proposed RFID tag antennas offer attractive design for metallic objects identification such as gas cylinders and oil barrels tagging in petroleum refineries.

## CHAPTER 6

### SUMMARY, CONCLUSIONS, CONTRIBUTIONS AND RECOMMENDATIONS FOR FUTURE WORK

#### 6.1 Summary and Conclusions

Summing up the entire work done throughout this thesis, it encompasses investigation of integrating SRRs and CSRRs into dipole and loop antennas with the sole aim of achieving overall performance improvement.

Three asymmetrical dipole fractal antennas (*AN1*, *AN2* and *AN3*) are presented in Chapter 4 for RFID applications using SRRs. It has been shown that the simple design of SRR has been integrated with each antenna at a low fabrication cost on PCB substrates using inexpensive standard photolithography process. Each antenna design was etched on FR4 epoxy substrate with an evident compact size. The antenna sizes are:  $82 \times 88.59 \times 1.6 \text{ mm}^3$  for *AN1*;  $72 \times 78.59 \times 1.6 \text{ mm}^3$  for *AN2* and  $66.5 \times 73.09 \times 1.6 \text{ mm}^3$  for *AN3*. The modified Minkowski fractal structure has been adopted to perform size reduction in three different iteration designs. The antenna designed with the second iteration *AN2* is more compact than that designed with the first iteration *AN1*, with a size reduction of about 22%. A further size reduction of 14% is obtained with a third iteration antenna (*AN3*) over that of *AN2*, and 32% over that of *AN1* for the same resonance frequency. Return loss simulations demonstrated that these antennas achieve better  $S_{11}$  when integrated with SRRs. Return loss results also show that the integration of SRRs with antennas performs a frequency down-shift of the antenna resonant frequency thereby achieving further size reduction over the original fractal structure that was aimed for size reduction and

better return loss. The impedance of the three designed antennas was measured to verify their impedance matching with tag chip. The measurement results show good agreement with those of simulations as well as good Omni-directional characteristics within its operating frequency. The experiment results showed that the maximum read range of the proposed tag antennas, *AN1*, *AN2* and *AN3* is about 2.10 m, 1.10 m and 0.75 m respectively with 4.0 W EIRP radiation power of the RFID reader. The proposed RFID Tag antennas are compact, with good reading range and suitable for RFID applications.

Chapter 5 presented two miniaturized RFID tag antennas, in which their configuration is optimized specifically to be mountable on metallic objects. The small design is achieved by inserting a CSRR layer into the antenna structures, which lowers their resonant frequency by increasing the capacitive reactance and allows high reactive impedance. Their fractal structure adds further miniaturization by increasing the electrical length of the antennas. The size of the proposed tag antennas is  $36.7 \times 18.1 \times 3.165 \text{ mm}^3$  for antenna *N1* and  $35.3 \times 17.4 \times 3.165 \text{ mm}^3$  for antenna *N2*. Two FR4 substrates each with thickness of 1.53 mm are sandwiched between the three copper layers of each antenna. The percentage size reduction achieved by *N2* over *N1* is 7.5 %. Further size reduction may also be done by considering a third iteration (*N3*), but it would not be significant at the expense of increased structure complexity and fabrication errors that might occur in the lithographic process of fabricating small structures. Very small and compact metal mount tag antennas are achieved with good agreement between measured and simulated results. The read range measurements showed that the maximum read range of *N1*, and *N2* is about 0.82 m and 0.48 m respectively, obtained when the two

tags are placed on a square metallic sheet of  $0.5\lambda$  side length and  $0.006\lambda$  thickness , with 4.0 W EIRP radiation power of the RFID reader. The designed antennas were also simulated and measured for two other different sizes of the metallic object in their background planes (square metallic sheet side lengths of  $\lambda$  and  $1.5\lambda$ ). The proposed RFID tag antennas offer attractive design for metallic objects identification such as gas cylinders and oil barrels tagging in petroleum refineries.

## 6.2 Contributions

The main contributions of this work include the following:

- New fractal tag antennas have been designed, fabricated, and measured for RFID applications in an effort towards size reduction. Moreover, a further size reduction is achieved by taking more fractal iterations as discussed earlier in Chapter 3 for the three antennas *AN1*, *AN2*, and *AN3*.
- Two new miniaturized metal-mount fractal tag antennas were designed, fabricated, and measured; namely *N1* and *N2*. The results show that the fabricated antennas are compact and compared to the ones reported in (Chen, 2009; Chen et al., 2010a; and Kimouche et al., 2011); the proposed antennas are more than 9%, 51%, and 74% smaller in size respectively.
- Successfully integrated SRRs and CSRRs with RFID tag antennas to enhance their performance characteristics in terms of gain and return loss. Moreover, a further size reduction is achieved due to these SRRs and CSRRs in addition to that obtained by the fractal structure.
- Antennas were fabricated at low cost using FR4 substrate and standard PCB lithographic fabrication process.

- The flexibility of antenna tuning with different parameters, rather than changing the overall size only, allows for a wide manipulation of its performance characteristics without considerable degradation.

### **6.3 Recommendations for Future Work**

The proposed RFID tag antennas integrated with SRRs and CSRRs were designed to function at the UHF frequency band with the capability to improve their performance as discussed throughout this thesis. Optimistically speaking, it has an appealing potential to be used for dielectric characterization of some materials of interest. Further work may consider the use of the Minkowski fractal technique or any other fractal structure towards the design and implementation of new printable chip-less RFID tag antennas for cost-effective and multi-resonance backscattering to achieve more tag-ID capacity. Moreover, the designed tag antennas may be used in sensors design for material characterization.



## REFERENCES

- Ali, J. K. (2007). A New Reduced Size Multiband Patch Antenna Structure Based on Minkowski Pre-Fractal Geometry. *Journal of Engineering and Applied Sciences*, 2, 1120-1124.
- Ali, J. K., and A. S. A. Jalal (2007). A miniaturized multiband Minkowski-like pre-fractal patch antenna for GPS and 3G IMT-2000 Handsets. *Asian J. Inform. Technol.*, AJIT, 6(5), 584-588.
- Alien Higgs-3, (2012). Online available: <http://www.prosign.dk/en/rfid-products/alien-technology/>, (accessed 20/4/2012).
- Ammam, M. (1997). Design of Rectangular Microstrip Patch Antennas for 2.4 GHz Band, *Applied Microwave and Wireless*.
- Angeles, R. (2005). RFID technologies: Supply-chain applications and implementation issues. *Information Systems Management*, 22(1), 51–65.
- Baena, J. D., J. Bonache, F. Martin, and R. M. Sillero (2005). Equivalent-circuit models for split-ring resonators and complementary split-ring resonators coupled to planar transmission lines. in *IEEE Transactions on Microwave Theory and Techniques*, 53(4), 1451-1461.
- Balanis, C. A. (2005). *Antenna Theory - Analysis and Design*. Third Edition, New York: John Wiley & Sons, Inc.
- Catarinucci, L., M. Cappelli, R. Colella, and L. Tarricone (2008). A Novel Low-Cost Multisensor-Tag for RFID Applications in Healthcare. *Microwave and Optical Technology Letters*, 50(11), 2877-2880.
- Catarinucci, L., R. Colella, and L. Tarricone (2012). Design, Development, and Performance Evaluation of a Compact and Long-Range Passive UHF RFID Tag. *Microwave and Optical Technology Letters*, 54(5), 1335-1339.
- Catarinucci, L., R. Colella, M. De Blasi, L. Patrono, and L. Tarricone (2011). Experimental Performance Evaluation of Passive UHF RFID Tags in Electromagnetically Critical Supply Chains. *Journal of Communications Software and Systems*, 7(2), 59-70.
- Catarinucci, L., R. Colella, M. De Blasi, L. Patrono, and L. Tarricone (2010). Improving Item-Level Tracing Systems through Ad Hoc UHF RFID Tags. *Proc. IEEE Radio and Wireless Symposium, RWW 2010*, 160-163.
- Chen, H.-D., and Tsao, Y.-H. (2010a). Low-Profile Meandered Patch Antennas for RFID Tags Mountable on Metallic Objects. *IEEE Antennas and Wireless Propagation Letters*, 9, 118-121.
- Chen, H.-D., and Tsao, Y.-H. (2010b). Low-Profile PIFA Array Antennas for UHF Band RFID Tags Mountable on Metallic Objects. *IEEE Transactions on Antennas and Propagation*, 58(4), 1087-1092.



- Chen, S.-L., S.-K. Kuo, and C.-T. Lin (2009). A metallic RFID tag design for steel-bar and wire-rod management application in the steel industry. *Progress In Electromagnetics Research*, 91, 195-212.
- Cole, P. H. (2002). A Study of Factors Affecting the Design of EPC Antennas & Readers for Computer Simulation Technology (CST) Microwave Studio, Version 2010.
- Congedo, F., G. Monti, L. Tarricone, and M. Cannarile (2011). Broad-Band Bowtie Antenna for RF Energy Scavenging Applications. *Proceedings of the 5th European Conference on Antennas and Propagation, EUCAP 2011*. 335-337.
- De Vita, G., and G. Iannaccone (2005). Design Criteria for the RF Section of UHF and Microwave Passive REID Transponders. *IEEE Transactions on Microwave Theory and Techniques*, 53(9), 2978-2990.
- Derneryd, A. (1976). Linearly Polarized Antennas. *IEEE Trans. on Antennas and Propagation*, AP-44, 846-851.
- Dobkin, D. M., and S. M. Weigand (2005). Environmental Effects on RFID Tag Antennas. *IEEE MTT-S Int. Microw. Symp. Dig.* 135 - 138.
- Drabowitch, S., and A. Papiernik, H. D. Griffiths, and J. Encinas (2005). *Modern Antennas*, 2nd edition, New York: Springer.
- Esposito, A., L. Tarricone, M. Zappatore, L. Catarinucci, and R. Colella (2010). A framework for contextaware home-health monitoring. *International Journal of Autonomous and Adaptive Communications Systems*, 3(1), 75-91.
- Falconer, K. (2003). *Fractal Geometry; Mathematical Foundations and Applications*. 2nd Edition, John Wiley and Sons Ltd.
- Falcone, F., T. Lopetegui, M. A. G. Laso, J. D. Baena, J. Bonache, M. Beruete, R. Marqués, F. Martín and M. Sorolla (2004). Cabinet principle applied to metasurface and metamaterial design. *Phys. Rev. Lett.*, 93, 197 401(1)–197 401(4).
- Finkenzeller, K. (2003). *RFID Handbook*. Wiley & Sons, 2nd edition.
- Frickey, D. A., (1994). Conversions between S, Z, Y, H, ABCD, and T parameters which are valid for complex source and load impedances. *IEEE Trans. Microw. Theory Tech.*, 42(2), 205–211.
- Gay-Balmaz, P., and O. J. F. Martina (2002). Electromagnetic resonances in individual and coupled split-ring resonators. *Journal of Applied Physics*, 92(5), 2929-2936.
- Gianvittorio, J.P., and Y. Rahmat-Samii. (2002). Fractal Antennas: A Novel Antenna Miniaturization Technique, and Applications. *IEEE Antennas and Propagation Magazine*, 44: 20-35.

- Hidayath, M., A. R. Islam, and S. Ali (2007). On the Design Considerations and Limitations of Passive RFID Tag Antennas. *Proceedings of ISAP2007*. 1138-1141.
- Imping Monza RFID Products, <http://www.impinj.com/>, (accessed 25/5/2012).
- Jalal, A. S. A. (2008). A New Compact Patch Design for Circular Polarization Application Based on Third Iteration Minkowski-Like Pre Fractal Geometry. *Journal of Engineering and Applied Sciences*, 3(9), 729-734.
- Kim, D, and Yeo, J. (2012). Dual-Band Long-Range Passive RFID Tag Antenna Using an AMC Ground Plane. *IEEE Transactions on Antennas and Propagation*. 60(6), 2620-2626.
- Kim, D., T. W. Koo, J.-I. Ryu, J.-G. Yook, and J. C. Kim (2009). Accurate Impedance Measurement and Implementation of a Folded Dipole Antenna for RFID Tags. In *The 2009 International Symposium on Antennas and Propagation (ISAP 2009)*, pp. 93-96.
- Kimouche, H. and H. Zemmour (2011). A Compact Fractal Dipole Antenna for 915 MHz and 2.4 GHz RFID Tag Applications. *Progress In Electromagnetics Research Letters*, 26, 105-114.
- Konya, S., T. Sasamori, T. Tobana, and Y. Isota (2011). Wideband Impedance Measurement of Balanced Antenna Using the S-Parameter Method. in *Proceedings of the Asia-Pacific Microwave Conference*, 717-720.
- Kossel, M., Benedickter H, and W. Baechtold. (1999). An active tagging system using circular polarization modulation. in *IEEE Trans. Microwave Theory Tech.*, 47(12), 2242–2248.
- Kraus, J. de, and R. J. Marhefka (2001). *Antennas for All Applications*. 3rd edition, New York: McGraw-Hill Science/Engineering/Math.
- Kuo, S.-K., S.-L. Chen, and C.-T. Lin (2008). An accurate method for impedance measurement of RFID tag antenna. *Progress In Electromagnetics Research, PIER* 83, 93–106.
- Kurokawa, K. (1965). Power waves and the scattering matrix. *IEEE Trans. Microw. Theory Tech.*, 13(3), 194–202.
- Kwon, H., and B. Lee (2005). Compact slotted planar inverted-F RFID tag mountable on metallic objects. *Electron. Lett.*, 41(24), 1308-1310.
- Landt, J. (2001). Shrouds of Time: The History of RFID. *AIM Inc., White Paper*, Online available at: <https://ewhdbks.mugu.navy.mil/iff.htm>, (accessed 3/10/2012).
- Lee, Y.-C., and J.-S. Sun (2008). Dual-Band Dipole Antenna for RFID Tag Applications. *Proceedings of the 38th European Microwave Conference*, (2008 EuMA), 995-997.
- Leong, K. S., and M. L. Ng, and P. H. Cole (2007). Investigation of RF cable effect on RFID tag antenna impedance measurement. *IEEE Antennas and Propag. Symp.*, 573-576.

- Libbrecht, K.G. (2003). *The Snowflake*. Voyageur Press, USA.
- Lin, B., J. Zhou, B. You, and W. Xu, (2008). A dual-frequency ceramic spiral antenna with rectangle PBG structure array used for modern RFID System. *Proceeding of 2nd IET Int Conf on Wireless, Mobile and Multimedia*, 94–97.
- Liu, Y., K. M. Luk, and H. C. Yin (2010). A RFID tag metal antenna on a compact HIS substrate. *Progress in Electromagnetics Research Letters*, 18, 51-59.
- Loebbecke, C. (2005). RFID Technology and Applications in the Retail Supply Chain: The Early Metro Group Pilot. in *18th Bled e-Conference: e-Integration in Action*.
- Mandelbort, B. B. (1983). *The Fractal Geometry of Nature*, W.H. Freeman and Company, New York.
- Marques R., F. Medina and R. Rafii-El-Idrissi (2002). Role of bianisotropy in negative permeability and left handed metamaterials. *Phys. Rev. B*, 65, 144 440(1)–144 440(6).
- Marques R., F. Mesa, J. Martel and F. Medina (2003). Comparative Analysis of Edge- and Broadside-Coupled Split Ring Resonators for Metamaterial Design-Theory and Experiment. *IEEE Transactions on Antennas and Propagation*, 51(10), 2572–2581.
- Marrocco, G. (2008). The art of UHF RFID antenna design: Impedance-matching and size-reduction techniques. *IEEE Antennas Propagation Mag.* 50(1), 66-79.
- Marrocco, G. and S. Caizzone (2012). Electromagnetic models for passive RFID tag-to-tag communications. *IEEE Transactions on Antennas and Propagation*. 60(11), 5381 – 5389.
- Meys, R., and F. Janssens (1998). Measuring the impedance of balanced antennas by an S-parameter method. *IEEE Ant. and Prop. Magazine*, 40(6), 62-65.
- Mitra, R. (2007). Challenges in antenna designs and some novel techniques for meeting them. *Loughborough Antennas and Propagation Conference*. 1-4.
- Monti, G., L. Catarinucci, and L. Tarricone (2009). Compact microstrip antenna for RFID applications. *Progress In Electromagnetics Research Letters*. 8, 191-199.
- Monti, G., L. Catarinucci, and L. Tarricone (2010). Broad-band dipole for RFID applications. *Progress In Electromagnetics Research C*, 12, 163-172.
- Murata MAGICSTRAP® Application Note (2012). Online available: <http://www.murata.co.jp/products/rfid/index.html>, (accessed 17/5/2012).
- Ngai, E. W. T., T. C. E. Cheng, S. Au, and K.-h. Lai (2007). Mobile commerce integrated with RFID technology in a container depot. *Decision Support Systems - Mobile Commerce: Strategies, Technologies, and Applications*, 43(1), 62–76.

- Nikitin, P. V., K. V. S. Rao, S. F. Lam, V. Pillai, R. Martinez and H. Heinrich (2005). Power reflection coefficient analysis for complex impedances in RFID tag design. *IEEE Transactions on Microwave Theory and Techniques*, 53(9), 2721–2725.
- Nikitin, P. V., and K. V. S. Rao (2008). Antennas and Propagation in UHF RFID Systems. In *Proceedings of 2008 IEEE International Conference on RFID*, 277-288.
- Occhiuzzi, C., C. Paggi, and G. Marrocco (2011). Passive RFID strain-sensor based on meander-line antennas. *IEEE Trans. Antennas Propagat.*, 59(12), 4836-4840.
- Or, Y. C., K. W. Leung, R. Mittra, and K. V. S. Rao (2009). Analysis on the platform-tolerant radio-frequency identification tag antenna. *IET Microw. Antennas Propagation*. 3(4), 601-606.
- Palmer, K. D. and M. W. Rooyen (2006). Simple broadband measurements of balanced loads using a network analyzer. *IEEE Transactions on Instrumentation and Measurement*, 55(1), 266–272.
- Pendry, J. B., A. J. Holden, D. J. Robbins, and W. J. Stewart (1999). Magnetism from conductors and enhanced nonlinear phenomena. *IEEE Trans. Microwave Theory Tech.*, 47, 2075–2084.
- Plessky, V. P., and Leonhard M. Reindl (2010). Review on SAW RFID Tags. In *IEEE Transactions on Ultrasonics, Ferroelectrics, and Frequency Control*, 57(3), 654 - 668.
- Powell K. (2003). Passive Radio Frequency Identification – A Primer for New RF Regulations. *Matrics*.
- Qian, Y., R. Cocciali, D. Sievenpiper, V. Radisic, E. Yablonowtch, and T. Itoh (1999). Microstrip patch antenna using novel photonic band-gap structures. *Microwave Journal*, 42 66–76.
- Qing, X., C. K. Goh, and Z. N. Chen (2009). Impedance characterization of RFID tag antennas and application in tag co-design. *IEEE Trans. on Microwave Theory and Techniques*, 57(5), 1268-1274.
- Rao, K. V. S., P. V. Nikitin, and S. F. Lam (2005a). Impedance matching concepts in RFID transponder design. *IEEE Workshop on Automatic Identification Adv. Tec.*, 39- 42.
- Rao, K. V. S., P. V. Nikitin, and S. F. Lam (2005b). Antenna design for UHF RFID tags: A review and a practical application. *IEEE Trans. Antennas Propagation*. 53(12), 3870-3876.
- Roberti, M. (2006). The History of RFID Technology. Available online: <http://www.rfidjournal.com/article/articleview/1338/1/129>, (accessed 10/4/2012).
- Roberts, C. M. (2006). Radio frequency identification (RFID). *Computers & Security*, 25(1), 18-26.

- Rusu, M., M. Hirvonen, H. Rahimi, P. Enoksson, C. Rusu, N. Pesonen, O. Vermesan, and H. Rustad (2008). Minkowski Fractal Microstrip Antenna for RFID Tags. *Proceedings of the 38th European Microwave Conference*, (2008 EuMA), 666-669.
- Sadat, S., M. Fardis, G. Dadashzadeh, and R.K. Bae (2005). Proximity coupled microstrip patch antenna miniaturization using new fractal geometry. in *Proceedings of AP-S Int. Symp. Dig. 3A*, 262–265.
- Salama, A., and K. M. Quboa (2008). A New Fractal Loop Antenna for Passive UHF RFID Tags Applications. *3rd International Conference on Information and Communication Technologies: From Theory to Applications*, (ICTTA 2008), 1-6.
- Sarma, S., and Engels, D. W. (2003). On the future of RFID tags and protocols. *White paper, Auto-ID Center, Massachusetts Institute of Technology*.
- Sarma, S., D. Brock, and D. Engels (2001). Radio frequency identification and the electronic product code. *IEEE Micro*, 21(6), 50–54.
- Sasamori, T., T. Tobana, and Y. Isota (2012). A Study on Jig Fabricated by Microstrip Line for S-Parameter Method. In *Proceedings of ISAP2012*, 1007-1010.
- Seshagiri, K. V., and P. V. Nikitin (2005). Antenna Design for UHF RFID Tags: A Review and a Practical Application. In *IEEE Trans. on Antenna and Propagation*, 53(12), 3870-3876.
- Smith, D. R., W. J. Padilla, D. C. Vier, S. C. Nemat-Nasser, and S. Schultz (2000). Composite Medium with Simultaneously negative Permeability and Permittivity. *Physical Review Letters*, 84(18).
- Smith, H., and B. Konsynski (2003). Developments in Practice X: Radio Frequency Identification (RFID)-an Internet for Physical Objects. in *Communications of the Association for Information Systems*, 12, 301–311.
- Stockman, H. (1948). Communication by means of reflected Power. in *Proc. Of the IRE*, 1196-1204.
- Stutzman, W. L., and G. A. Thiele (1998). *Antenna Theory and Design*. John Wiley & Sons.
- Temes, G. C., and J. W. LaPatra (1977), *Introduction to Circuit Synthesis and Design*. New York: McGraw-Hill, 1977, p. 327.
- Turcu, C. (2009). *Development and Implementation of RFID Technology*. I-Tech Education and Publishing KG, Vienna, Austria.
- Uddin, J., M. B. I. Reaz, M. A. Hasan, A. N. Nordin, M. I. Ibrahimy, M. A. M. Ali (2010). UHF RFID antenna architectures and applications. *Scientific Research and Essays*. 5(10), 1033-1051.



- Vaz, A., A. Ubarretxena, I. Zalbide, D. Pardo, H. Solar, A. Garcia-Alonso, and R. Berenguer (2010). Full passive UHF tag with a temperature sensor suitable for human body temperature monitoring. *IEEE Trans. Circuits Syst. II*, 57(2), 95-99.
- Vinoy, K.J., and A. Pal (2010). Dual-Frequency Characteristics of Minkowski-Square Ring Antennas. *IET Microwaves, Antennas & Propagation*, 4(2), 219-2.
- Wei, T., Bin, L., Jian-hua, Z., and Bai-qiang, Y. (2008). Design and simulation of a minimized RFID tag antenna. *J Xiamen University*, 47, 50-54.
- Werner, D. H., and Ganguly, S. (2003). An Overview of Fractal Antenna Engineering Research. *IEEE Antennas Propagation Mag.*, 45, 38-53.
- Wilding, R., and T. Delgado (2004). RFID - Applications within the Supply Chain. *Supply Chain Practice*, 6(2).
- Wu, N. C., M. A. Nystrom, T. R. Lin, and H. C. Yu (2006). Challenges to global RFID adoption. *Technovation*, 26(12), 1317-1323.
- Yeager, D., P. Powledge, R. Prasad, D. Wetherall, and J. Smith (2008). Wirelessly-charged UHF tags for sensor data collection. *IEEE Proceeding of RFID International Conference*, 320-327.
- Yu, B., S. J. Kim, B. Jung, F. J. Harackiewicz, and B. Lee (2007). RFID tag antenna using two-shortened microstrip patches mountable on metallic objects. *Microwave and Optical Technology Letters*, 49(2), 414-416.
- Zhou, J., Luo, Y., You, B., and Lin B. (2010). Three to Two Curve Fractal Folded Dipole Antenna for RFID Applications. *Microwave and Optical Technology Letters*. 52(8), 1827-1830.
- Zhu, H., Y. C. A. Ko, and T. T. Ye (2010). Impedance Measurement for Balanced UHF RFID Tag Antennas. in *Radio and Wireless Symposium (RWS)*, 128 – 131.

## APPENDICES

### Appendix A

#### Derivation of the Common Mode and Differential Mode Impedance as Seen by a Two-Port Network Analyzer

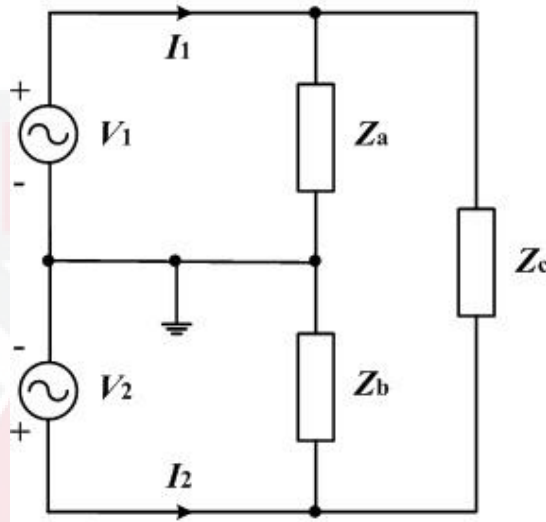


**Figure A.1. Circuit Model for a Complex Antenna Load when Both Ports of the Network Analyzer are Connected**

Using Y-parameters in Figure A.1, the two-port network equations are

$$I_1 = Y_{11}V_1 + Y_{12}V_2 \quad (\text{A.1})$$

$$I_2 = Y_{21}V_1 + Y_{22}V_2 \quad (\text{A.2})$$

To find  $Y_{11}$ , source  $V_2$  is short circuited

$$Y_{11} = \left. \frac{I_1}{V_1} \right|_{V_2=0} \quad (\text{A.3})$$

which yields to

$$Y_{11} = \frac{1}{Z_a \parallel Z_c} \quad (\text{A.4})$$

Similarly,  $Y_{22}$  can be found by short-circuiting source  $V_1$



$$Y_{22} = \left. \frac{I_2}{V_2} \right|_{V_1=0} = \frac{1}{Z_b \parallel Z_c} \quad (\text{A. 5})$$

$$Y_{21} = \left. \frac{I_2}{V_1} \right|_{V_1=0} = \frac{-1}{Z_c} \quad (\text{A. 6})$$

which yields

$$Z_c = \frac{-1}{Y_{22}} \quad (\text{A. 7})$$

Now substituting A.7 into A.4 and solving for  $Z_a$  we obtain

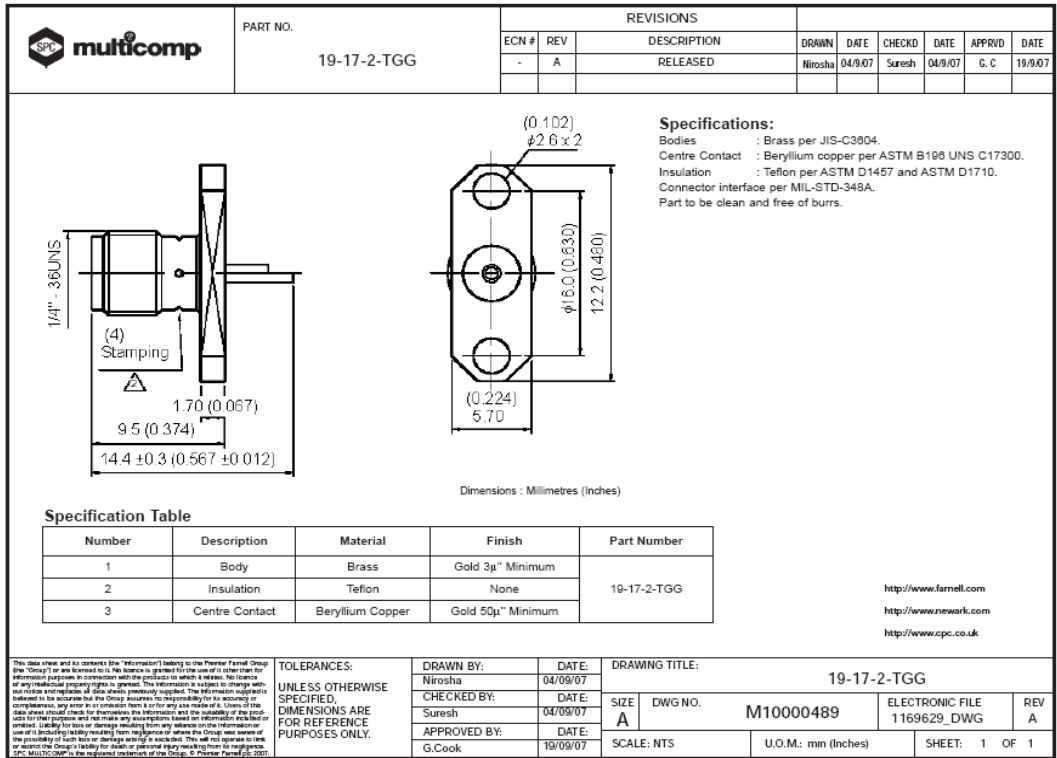
$$Z_a = \frac{1}{Y_{22} + Y_{21}} \quad (\text{A. 8})$$

Similarly, substitute A.7 into A.5 and solve for  $Z_b$  yielding

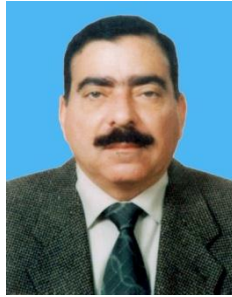
$$Z_b = \frac{1}{Y_{11} + Y_{21}} \quad (\text{A. 9})$$

## Appendix B

### 50 Ω SMA Connector Specifications



## BIODATA OF STUDENT



**Ali Sadeq Abdulhadi Jalal** was born in 1958 in Baghdad – the capital city of the Republic of Iraq. His schooling started in his very own vicinity up to secondary school level. Later, he furthered his dream bachelor degree of Electrical Engineering in Al-Rasheed College for Engineering and Science, University of Technology, Baghdad, Iraq within 1976–1980.

Feeling insufficient of his zeal to master his field through working had compelled him to continue his postgraduate study. At the start of 1984, he registered himself as a master student specialized in Communication Engineering at Al-Rasheed College for Engineering and Science, University of Technology, Baghdad, Iraq, and graduated in 1986.

From that date, he was appointed as an assistant lecturer in the field of Electronics and Communication Engineering in the same college he graduated from. He was awarded the lecturer and assistant professorship chairs in 1994 and 2009 respectively. After a long academic work journey, he carried on to the doctorate level at Universiti Putra Malaysia (UPM) in 2010. His main research interests are in Antennas and Microwave devices.

## LIST OF PUBLICATIONS

1. **Ali S. A. Jalal**, Alyani Ismail, Adam R. H. Alhawari, Mohd F. A. Rasid, Nor K. Noordin, and Mohd A. Mahdi, “Miniaturized Metal Mount Minkowski Fractal RFID Tag Antenna with Complementary Split Ring Resonator,” *Progress In Electromagnetics Research C*, Vol. 39, 25-36, 2013.
2. **Ali S. A. Jalal**, Alyani Ismail, Adam R. H. Alhawari, Mohd F. A. Rasid, Nor K. Noordin, and Mohd A. Mahdi, “Minkowski Fractal Asymmetrical RFID Tag Antenna with Split Ring Resonator,” *Submitted to Microwave and Optical Technology Letters*.
3. **Ali S. A. Jalal**, Alyani Ismail, Adam R. H. Alhawari, Mohd F. A. Rasid, Nor K. Noordin, and Mohd A. Mahdi, “Metal Mount Fractal RFID Tag Antenna with Complementary Split Ring Resonator,” in *Proceeding of the 2013 IEEE International Conference on RFID Technologies and Applications*, 04–05 September 2013 Johor Bahru, Malaysia.